Open Research Online

The Open University's repository of research publications
and other research outputs

Nephrotic Syndrome and Glomerular Basement Membrane: Genetic Defect of the Laminin 5 Chain

Thesis

How to cite:

Falcone, Sara (2018). Nephrotic Syndrome and Glomerular Basement Membrane: Genetic Defect of the Laminin 5 Chain. PhD thesis The Open University.

For guidance on citations see FAQs.

© 2018 The Author

Version: Version of Record

Copyright and Moral Rights for the articles on this site are retained by the individual authors and/or other copyright owners. For more information on Open Research Online's data policy on reuse of materials please consult the policies page.

oro.open.ac.uk

Nephrotic Syndrome and Glomerular Basement Membrane: Genetic Defect of the Laminin α5 Chain

Sara Falcone

Mammalian Genetics Unit, Medical Research Council Harwell Institute, Harwell, UK

The Open University

Discipline: Life and Biomolecular Sciences

Supervisors: Dr Paul K Potter (MGU, MRC Harwell)

Prof Fred Tam (Renal Unit, Imperial College London)

A thesis submitted for the degree of Doctor of Philosophy

April 2018

Abstract

Nephrotic syndrome is a heterogeneous group of disorders characterised by renal and extra-renal manifestations. Classic symptoms of nephrotic syndrome include severe proteinuria, hypoalbumiaemia, oedema and hyperlipidaemia.

Genetic studies of hereditary forms of nephrotic syndrome have led to the identification of proteins playing a crucial role in slit diaphragm signalling, regulation of actin cytoskeleton dynamics and cell-matrix interactions.

The laminin α5 chain is a 404 kDa protein essential for embryonic development and, in association with laminin β2 and laminin γ1, it is a major component of the glomerular basement membrane. Mutations in *LAMB2* are associated with Pierson's syndrome and mutations in *LAMA5* have recently been identified in paediatric patients affected by nephrotic syndrome.

As part of the MRC Harwell Ageing Screen, a large-scale ENU mutagenesis screen, a novel missense mutation (E884G) was identified in the gene *Lama5*. Homozygous mice showed a nephrotic phenotype including a severe proteinuria that preceded histological and ultrastructural changes. Further investigation using *in vitro* studies, extensive proteomics analysis and investigation of integrin activation, revealed a possible impact of the causative mutation on protein folding. Data suggest that changes in protein structure lead to a reduced secretion, integrin β1 activation, and agrin expression ultimately resulting in possible instability of the podocyte actin cytoskeleton.

Contributions

Routine animal husbandry was undertaken by the ward 3 staff at the Medical Research Council (MRC) Mary Lyon Centre.

The MRC Harwell bioinformatics team performed mapping and sequencing data analysis.

Routine genotyping analysis were carried by the MRC Harwell Genotyping and Mutation Detection Screens (GEMS) core facility.

Embedding, cutting and mounting of wax sections, and cutting and mounting of cryo-sections were performed by the histology core services group at MRC Harwell.

Proteomics core facility at the University of Manchester and Dr Michael Randles, De Montfort University performed mass spectrometry experiments, data and network analysis.

Abbreviations

ALP	Alkaline Phosphatase
ALT	Alanine Transaminase
ANOVA	Analysis of Variance
AST	Aspartate Aminotransferase
BSA	Bovine Serum Albumin
CKD	Chronic Kidney Disease
CTGF	Connective Tissue Growth Factor
DMEM	Dulbecco's Modified Eagle's Medium
DNA	Deoxyribonucleic Acid
dNTP	Nucleoside Triphosphate
ECM	Extracellular Matrix
EDTA	Ethylenediaminetetraacetic Acid
EGF	Epidermal Growth Factor
ENU	N-Ethyl-N-Nitrosourea
ER	Endoplasmic Reticulum
ERAD	Endoplasmic Reticulum associated degradation
ERES	Endoplasmic Reticulum Exit site
ES	Embryonic Stem
ESRD	End Stage Renal Disease
FSGS	Focal Segmental Glomerulosclerosis
FBS	Foetal Bovine Serum
GAG	Glycosaminoglycan

GAP	GTPase-Accelerating Protein
GBM	Glomerular Basement Membrane
GDI	Guanine Nucleotide Dissociation Inhibitor
GDP	Guanosine Diphosphate
GEF	Guanine Nucleotide Exchange Factor
GEMS	Genotyping and Mutation Detection Screens
GFB	Glomerular Filtration Barrier
GIT	G protein-coupled receptor kinase- interacting protein
GFR	Glomerular Filtration Rate
GTP	Guanosine triphosphate
H&E	Haematoxylin and Eosin
HEK293	Human Embryonic Kidney Cells
HDL	High-Density Lipoprotein
HSPGs	Heparin Sulphate Proteoglycans
IGF	Insulin-Like Growth Factor
IMN	Idiopathic Membranous Glomerulopathy
IMPC	International Mouse Phenotyping Consortium
IVF	*In Vitro* Fertilization
LB	Luria-Bertani
LDH	Lactate Dehydrogenase
LDL	Low-Density Lipoprotein
LDS	Lithium Dodecyl Sulphate
LG	Laminin globular
LN	Laminin N-terminal

MCD	Minimal Change Disease
MHC-I	Major Histocompatibility Class I
MPC	MUTA-PED-C3pde
MRC	Medical Research Council
mRNA	Messenger Ribonucleic Acid
MS	Mass Spectrometry
MS/MS	Tandem Mass Spectrometry
MT	Masson's Trichrome
nDNA	Nuclear Deoxyribonucleic Acid
OPPF	Oxford Protein Production Facility
PAS	Periodic acid-Schiff
PBS	Phosphate Buffered Saline
PCR	Polymerase Chain Reaction
PDGF	Platelet-Derived Growth Factor
PKD	Polycystic Kidney Disease
QTL	Quantitative Trait Loci
RAAS	Renin-Angiotensin-Aldosterone System
RIPA	RadioImmunoPrecipitation Assay
RNA	Ribonucleic Acid
RT-qPCR	Quantitative Reverse Transcription PCR
SDS-PAGE	Sodium Dodecyl Sulfate Polyacrylamide Gel Electrophoresis
SEM	Scanning Electron Microscope
SEM	Standard Error of the Mean
SNP	Single Nucleotide Polymorphism

SOC	Super Optimal Broth
TEM	Transmission Electron Microscopy
TGF-β1	Transforming Growth Factor β1
TUDCA	TauroUrsoDeoxyCholic Acid
UPR	Unfolded Protein Response
VEFG	Vascular Endothelial Growth Factor
VLDL	Very Low-Density Lipoproteins
WGS	Whole Genome Sequencing
XLAS	X-Linked Alport Syndrome

Table of Contents

List of Figures

List of Tables

CHAPTER 1

Introduction

1. Introduction

1.1 The Kidney

The kidneys have essential roles in keeping the chemical-physical components of the interior milieu (plasma and interstitial fluid) constant, including the removal of catabolites and exogenous substances from the circulation, the control of the extracellular fluid and regulation of the pH of the blood and of the concentration of the ions.

The functional unit of the kidney is the nephron composed of: a blood-filtering component, the renal corpuscle, consisting of the glomerulus (a capillary network) and a capsule (Bowman's capsule) that encapsulates the capillary tuft; and a tubular network (divided in the segments proximal convoluted tubule, loop of Henle, distal convoluted tubule and connecting tubule) containing the tubular fluid filterated in the glomerulus (Figure 1.1).

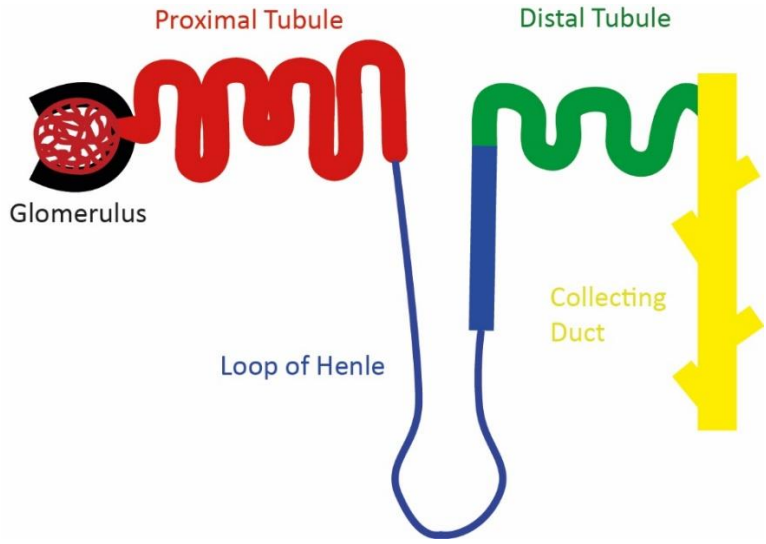

Figure 1.1. A schematic representation of the nephron. In black the glomerulus, the filtering unit of the kidney. In red the proximal tubule, in blue the loop of Henle, in green the distal tubule and in yellow the collecting duct: in these structures, the pre-urine is concentrated based on the needs of the bodies. The collecting duct terminates in the bladder where urine is collected.

Blood enters the glomerulus via the afferent arteriole and flows into the glomerulus where it is filtered, producing the ultrafiltrate that accumulates in the Bowman's space. Filtered blood exits the glomerulus via the efferent arteriole while the ultrafiltrate progresses through the tubular network where it is modified and concentrated becoming urine. In a healthy human kidney, the average nephron number is approximately 900,000 to 1 million per kidney[1] and about 20% of the total cardiac output (filtration fraction) will enter the kidneys to undergo filtration[2].

Additionally, the kidneys also have important endocrine functions, secreting hormones with systemic actions such as renin and erythropoietin and activating calcitriol. Renin is involved in the renin-angiotensin-aldosterone signalling axis that controls blood pressure. Calcitriol, the active metabolite of vitamin D, is involved in the reabsorption of calcium in the intestine and the kidney and the release of calcium from the bone, increasing the blood calcium levels. Erythropoietin stimulates erythropoiesis in the bone marrow. Impairment of the kidney function during disease compromises all these vital processes.

1.1.2 The glomerular Filtration Barrier: constituents and function

The glomerular filtration barrier (GFB) is a layered structure between the vasculature and Bowman's space that functions as a barrier between the bloodstream and the urine. Small solutes (e.g. urea, mineral ions) and water can easily traverse the highly permselective GFB whilst high molecular weight components of the plasma, like albumin and circulating cells, are retained in the blood, making the resulting urine virtually free of protein[2].

Three layers form the GFB (Figure 1.2): the two cellular layers, fenestrated endothelial cells and epithelial podocyte, are separated by a specialized extracellular matrix (ECM), the glomerular basement membrane (GBM), with the properties of a viscous gel, originating from the fusion of a basement membrane synthesized by the podocytes and the one synthesized by the endothelial cells [3-5].

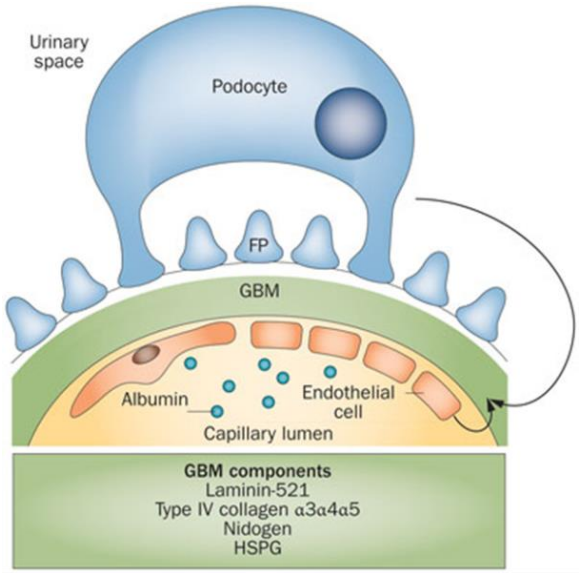

Figure 1.2. A diagram representing the three different layers of the GFB. From the capillary lumen to the urinary space (or Bowman space), the blood is filtered passing through the endothelium, the GBM (produced by both endothelial cells and podocytes and composed primarily of type IV collagen and laminin) and the space between interdigitating podocyte foot processes. Figure adapted from Suh *et al.*[6].

1.1.2.1 *Glomerular Endothelial cells*

The glomerular endothelium is the first layer of the GFB to act as a barrier to the passage of fluid and macromolecules. The glomerular endothelium has the peculiar aspect of being perforated with transcellular pores, *fenestrae*, of ~60 nm in diameter that allow the passage of fluid across the cell layer [2, 5] and constitute 20-50% of the entire

endothelial surface [7]. The fenestrations are too large to influence blood filtration as albumin, which is restricted by the glomerular wall, is only 3.6 nm in diameter [5]. However, the glomerular endothelium still plays an active role in renal filtration due to the presence of the glycocalyx on their luminal face, a 200 nm thick extracellular structure consisting of glycosaminoglycans, sialic acids and hyaluronan [8]. It has previously been hypothesised that the negative charge of the glycocalyx would electrically repel the negatively charged albumin [8], however, more recent studies have since challenged this hypothesis [9]. More likely, the glycocalyx components (glycosaminoglycans or GAGs), form a broader coat called the endothelial surface layer and bind plasma proteins, creating steric hindrance to protein filtration [8] and making the pores narrower and more restrictive.

1.1.2.2 *Glomerular Basement Membrane*

The ECM is a non-cellular component that provides structural and biochemical support to cell layers (in organs and tissues) in the form of a basement membrane, and single cells as substrate for cell mobility [10]. In the glomerulus, the GBM is synthesized by both podocytes and endothelial cells, with mesangial cells playing a role in turnover [11]. Unlike the other basement membranes, GBM is thicker and constantly exposed to flow and pressure, hence it needs to maintain its structural integrity [12]. The main components are the same as found in all the other basement membranes, but some of the isoforms of its macromolecules are specific to individual types of basement membrane [3]. The GBM contains:

Type IV Collagen. The collagen IV family is the major structural component of basement membranes and consists of six homologous α-chains (α1-α6) encoded by six different

genes COL4A1-COL4A6 [13]. Each α-chain contains a long collagenous region of repeated Gly-Xaa-Yaa amino acid triplets, which give the chains stability, but with numerous interruptions that provide flexibility to the protomers. The protomers are linked to each other by cysteine and lysine-rich 7S domain (non-collagenous NH2-terminal domain) and NC1 (non-collagenous COOH-terminal domain) [3]. The six α-chains can create only three types of network because of the information present within the NC1 domain sequence [14]: α1α1α2, α3α4α5 and α5α5α6. The distribution of the networks differs according to the developmental stage and organ: during embryogenesis the α1α1α2 network is ubiquitous and expressed in all basement membranes of immature nephrons [15] but in infancy it is replaced by the α3α4α5 network in kidney (glomerular basement membranes), cochlea, eye, lung and testis, and by α5α5α6 in skin, smooth muscle, oesophagus and Bowman's capsule[16].

Mutations in any of the genes that encode for a chain of the α3α4α5 network (*COL4A3*, *COL4A4*, *COL4A5*) arrest its normal maturation resulting in the incorrect assembly of the monomers and the related pathological condition arising from it is known as Alport's syndrome. This disease is characterised by a renal component consisting of haematuria, proteinuria, progressive kidney failure, and extrarenal phenotypes, primarily hearing loss and ocular disorders [17, 18].

Laminin. Laminins are a family of self-assembling glycoproteins made up of at least 15 different αβγ heterometric macromolecules [4]. The major laminin heterotrimer in the mature GBM is laminin α5β2γ1 and it is secreted by podocytes and endothelial cells [3]. Most laminin heterotrimers are cross-shaped macromolecules; the "long arm" is formed by the association of the α, β and γ chains via coiled-coil interaction and disulphide bonding [3], the three "short arms" contain LN domains (NH_2-terminal globular domains)

which mediate the trimer-trimer interactions [3]. The α-subunit is largely responsible for the cell surface adhesion and receptor interaction as well as contributing to self-assembly, while the β- and γ- subunits play a structural role and modulate receptor-binding [19]. Laminins serve as major adhesive proteins and mediate cell adhesion to basement membranes [20].

Mutations in the *LAMB2* gene, encoding the laminin β2 chain, cause disorders with a vast clinical spectrum. Truncating mutations lead to Pierson syndrome, characterized by microcoria, congenital nephrotic syndrome, muscular hypotonia and neurodevelopmental defects [21-23], whilst missense variants cause a much milder variant of Pierson syndrome or isolated congenital nephrotic syndrome [24].

Additional components. Laminin and collagen IV are linked in an indirect fashion via heparin sulphate proteoglycans (HSPGs) [25] and nidogens [26]. The matrix consists of a protein core with covalently linked glycosaminoglycan side chains that are frequently modified by sulfation, giving an anionic charge to the proteoglycan and consequently to the basement membrane [3]. Unlike all the other basement membranes where the most common HSPG is perlecan, the human GBM contains primarily agrin [27], deletion of which in mice significantly reduces the negative charge in the GBM but does not cause proteinuria, suggesting that the GBM has a limited role in charge selection during filtration [28]. Nidogen-1 and nidogen-2 are two proteins bound to the laminin γ1 chain short arm as well as to type IV collagen [26]. Double nidogen knock-out causes perinatal lethality in mice [29], however, it does not lead to defects of the GBM suggesting that nidogens are not crucial for its formation, but might increase its strength against mechanical stress.

Basement membranes self-assemble in a multi-step process that is initiated by the binding of laminin to a competent cell surface through the anchoring of the laminin LG domains to integrins and dystroglycan. This interaction promotes laminin polymerization through its LN domain[19]. The initial laminin-cell interaction enables the accumulation of other ECM components with nidogens binding and forming a stabilizing bridge between laminins and type IV collagen and giving input for the polymerization of the latter [19]. In the kidney, an *in vivo* Stochastic Optical Reconstruction Microscopy (STORM) study showed the presence of two layers of laminin-521, one on the endothelium side and one on the podocyte side. In each layer, the proteins are oriented with their C-terminal LG domains close to the cell membrane, while the LN domains and short arm are localised toward the middle of the GBM as is type IV collagen [30].

1.1.2.3 *Podocytes*

As highly specialized epithelial cells, podocytes encapsulate the outer aspect of the glomerular capillaries facing the Bowman's capsule. The cell body is detached from the underlying GBM and is made of an actin-cytoskeleton organised into stress fibres that control mobility and contraction. From the cell body start long primary processes (major processes) reinforced by microtubules and intermediate filaments [2, 31], and the secondary foot processes which emerge at right angles to the primary processes and mediate the adhesion with the GBM [32].

Foot processes are actin-rich projections that are embedded into and bind the GBM via cell surface focal adhesion proteins, like α3β1 integrin and α-/β-dystroglycans, to guarantee the stability of the podocyte [2, 33]. The foot process cytoskeleton is structured so it can oppose the high pressure in the capillary wall; the actin network is made of

contractile, highly ordered parallel filament bundles that change the morphology of the foot processes modulating the permeability of the GFB [34] and are regulated by synaptopodin[35].

Actin stress fibres of the cell body and actin filament bundles of the foot process are regulated respectively by tropomyosin and synaptopodin and are both modulated by small GTPases protein of the Rho family and calcium levels [35].

Adjacent podocytes foot processes interdigitate with those of neighbouring podocytes and form a tight junction, called the slit diaphragm, that maintains a specific pore size such that only molecules smaller than 50 kDa can traverse the filtration barrier and enter the urinary space [36]. The extracellular segment of the slit diaphragm is made up of rod-like units connected to the central linear bar so to form a zipper-like substructure with pores [34]. In addition to the slit diaphragm, the foot processes have two other functional membrane domains; the apical membrane domain and the basal membrane domain, or sole plate, which associates with the GBM. As with the slit diaphragm, these other two domains are also physically associated with the foot process actin bundles [34].

Any interference with any of the membrane domains perturbs the actin cytoskeleton, actively changing the organised parallel and contractile bundles into a dense network. The manifestation of these modifications is foot process effacement and related proteinuria.

1.1.3 Other Cells of the Glomerulus

1.1.3.1 *Mesangial Cells*

The mesangial cells are specialised pericytes, contractile cells that wrap around the endothelial cells, which constitute ~30% of all glomerular cells, and play a central role in stabilizing and maintaining the structural architecture of the glomerulus forming a central stalk [37]. They are embedded in their own extracellular matrix, the mesangium that differs in composition from the glomerular basement membrane. The main constituents of the mesangium are α1α1α2 type IV collagen, α5β1γ1 laminin, fibronectin, HSPGs and nidogen. The glomerular vascular structure is maintained with a cross-talking between mesangial cells and endothelial cells via platelet-derived growth factor (PDGF) signalling as indicated by the lack of mesangial cells and abnormal glomerular structure in knock-out mice of PDGF and its receptor PDGFR-β [38-40].

Given their contractile proprieties, mesangial cells can regulate capillary flow and ultrafiltration surface and, consequently, glomerular filtration rate [41] producing factors like vascular endothelial growth factor (VEFG) [42], transforming growth factor β1 (TGF-β1) [43] and connective tissue growth factor (CTGF) [44].

In a number of glomerulopathies, the mesangial cells tend to proliferate and the mesangium expands as is typically seen during diabetic nephropathy [45]. A similar finding is also seen during lupus nephritis and mesangioproliferative glomerulonephritis [46] like IgA nephropathy, a disease caused by the deposition of aberrant glycosylated IgA in the mesangium causing proteinuria [47].

1.1.4 Filtration models

In a lifetime, humans produce more than 4 million litres of virtually protein-free urine thanks to the sieving process of the glomeruli. How the GFB manages to clear more than 250,000 kg of plasma proteins without clogging even in old age is still unknown [48]. Understanding the filtration mechanism is necessary to understand the pathogenesis of proteinuria, the hallmark of glomerular diseases.

Several hypotheses have been suggested to explain the sieving function of the glomerulus. The main models are the pore model, the gel permeation hypothesis and the albumin retrieval hypothesis.

1.1.4.1 *The pore model*

It is well established that for neutral solutes, the glomerular sieving coefficients become smaller with increasing molecular size [5]. The simplest model, the "pore model", describes the GFB as a passive mechanical sieve consisting in a series of pores, with the podocyte slit diaphragm acting as the main size excluding layer, given the small size of its pores [49]. However, it was further observed that when the renal plasma flow is arrested, albumin is found in the Bowman space, but the glomerular architecture is preserved [50]. Since it was then clear that haemodynamics plays a role in glomerular filtration, the pore model included convection as a major force responsible for albumin sieving. The convective flux is driven by the drag of the flow of water across the GFB and it is proportional to the hydraulic pressure difference [48]. When the flow stops, diffusion of albumin is driven by the concentration difference within the capillary and the primary

filtrate in the Bowman's space [48]. However, the pore model does not explain why the GFB does not clog.

1.1.4.2 T*he gel permeation hypothesis*

In this model, the GBM is assumed to be very similar to a gel and it is almost exclusively acting as the selectively filtrating layer of the kidney [51]. As in the pore model, convection and diffusion are the two main forces responsible for the albumin flux, and proteinuria occurs when the filtration rate of water is reduced, while the diffusive flux of albumin remains constant [48]. However, this model does not explain why podocytopathies and/or endothelial alterations lead to proteinuria.

1.1.4.3 *The albumin retrieval hypothesis*

Some researchers have suggested that the GFB is more permeable to albumin than previously proposed [52]. The larger amounts of albumin (about 8% instead of 0.02-0.06%) would actually pass the filter and be reabsorbed (i.e. retrieved) by tubular cells [48, 53]. Proteinuria would, therefore, be considered a symptom of tubulopathy. This hypothesis is very controversial and not widely accepted [48].

1.1.4.4 *The electrokinetic model*

Based on the measurement of an electric field of –0.045 mV per 10 cm water cross the GFB of *Necturus maculosus* (common mudpuppy) [54], this recently proposed model suggests the existence of an electric field (also called filtration-dependent potential or

streaming potential), generated across the GFB. This electric field is produced by the forced filtration of plasma, which is an ionic solution containing small cations (sodium, potassium and calcium) and anions (chloride and bicarbonate), through an electrically charged barrier such as the GFB [48]. The streaming potential, that has an extrapolated measurement of 0.1-0.5 mV at 5mmHg effective filtration pressure in mammalian kidneys [55], influences the passage of albumin (negatively charged) across the GFB, dragging it towards the capillary lumen by electrophoresis, preventing the clogging [48]. Any insult that impairs homogeneous filtration will interfere with the generation of a homogeneous streaming potential and result in proteinuria [56].

1.2 Nephrotic Syndrome

Nephrotic syndrome is a heterogeneous group of disorders characterized by renal and extrarenal manifestations. Of all the symptoms, a severe proteinuria (greater than 3.5 g/24h) is the cornerstone reflecting a dysfunction of the normally highly permselective GFB. The other cardinal alterations of nephrotic syndrome include hypoalbuminemia, oedema, hyperlipidemia and lipiduria. Hypercoagulability is also frequently associated with nephrotic syndrome.

1.2.1 Pathophysiology of Nephrotic Syndrome

Proteinuria. Under normal circumstances, the GFB of the glomerular capillary wall prevents the passage of larger plasma components, in particular albumin, into the urine. A proteinuric disease is usually associated with a structural or functional defect of this barrier; in most nephrotic diseases, the major defect is associated with podocyte injury and dysfunction and/or loss of anionic charge in the GBM (loss of charge selectivity).

Hypoalbuminemia. Hypoalbuminaemia is predominantly due to the of loss protein in the urine. In response, the liver increases albumin production, but this is insufficient to prevent the fall in serum albumin concentration. The liver also responds by increasing the hepatic protein production in a non-specific way (producing proteins other than albumin) and therefore the serum concentration of total proteins in patients with nephrotic syndrome may be normal or increased. The consequences of this non-specific protein production include other typical alterations of nephrotic syndrome, hypercholesterolaemia and hypercoagulability.

Oedema. The physiopathology of oedema in nephrotic syndrome is not clear yet. There are two main theories, the “underfill model” and the “overfill model”. In the underfill model, the hypoalbuminaemia results in reduced plasma oncotic pressure and promotes the translocation of fluid from the vascular compartment into the extracellular fluid compartment. The activation of the renin-angiotensin-aldosterone system and the inhibition of secretion of the atrial natriuretic peptide (ANP), leads to secondary renal sodium retention that complicates oedema. According to the “overfill model”, the oedema is due to an intrinsic defect of the kidney affected by nephrotic syndrome leading to a primary renal sodium retention, which in turn causes expansion in plasma volume.

Hyperlipidaemia. The plasma levels of cholesterol, triglycerides and different lipoproteins (very low-density lipoproteins – VLDL, low-density lipoproteins – LDL, high-density lipoproteins – HDL) can be elevated in nephrotic patients. These abnormal concentrations result from impaired clearance of cholesterol and lipoproteins due to the increased expression and activity of acyl-CoA cholesterol acyltransferase-2 in the liver. This results in enhanced esterification of cholesterol and reduction of intracellular free cholesterol and by a deficiency of LDL receptor leading to a reduction in cholesterol uptake [57].

1.2.2 Classification of Nephrotic Syndrome

Nephrotic syndrome is a nonspecific kidney disorder caused by a damage to the glomeruli and has many causes, which can be limited to the kidney (primary nephrotic syndrome), or a systemic condition that affects the kidney (secondary nephrotic syndrome). Among secondary causes, type I and II diabetes are the most frequent

aetiology in adults. Other systemic diseases such as lupus erythematosus, amyloidosis, hepatitis B and C, HIV and systemic amyloidosis can also be associated with glomerular disorders causing nephrotic syndrome [58].

It is possible to classify nephrotic syndrome using several methodologies such as histopathological criteria, time of onset and response to pharmacological therapy.

Based on histopathological criteria, nephrotic syndrome is classified by the three most common histopathological patterns:

Minimal change disease (MCD). MCD is characterised by the presence of normal-appearing glomeruli on light microscopy whilst electron microscopy shows effacement and detachment of the foot processes [59]. It is the most common cause of primary nephrotic syndrome in children accounting for 70-90% of nephrotic syndrome cases in patients under 10 years old and 50% in children older than 10 years [60]. However, MCD is also an important cause of disease in adults, accounting for 10-15% of all nephrotic syndrome in older patients [60].

Focal Segmental Glomerulosclerosis (FSGS). FSGS is characterised by involvement of less than 50% of the glomeruli (focal) with sclerotic segments that affect only part of the glomerulus (segmental) and usually contain IgM and C3 deposits [59]. Primary FSGS is usually idiopathic although 20% of cases are familial with a significant racial/ethnic predilection. In the USA incident rates, expressed as patients per million, were 6.8 in African Americans, 3.7 in Hispanics, and 1.9 in Caucasians [61]. Secondary FSGS can have several causes including HIV infection, heroin use or obesity.

Idiopathic Membranous Glomerulopathy (IMN). IMN is characterised by histopathological features of subepithelial immune-complex deposits and subsequent

thickening of glomerular basement membrane with IgG and C3 deposits. [62]. It is more common in males with an incidence that peaks at 30-50 years of age [59].

Based on the age of disease onset, nephrotic syndrome can be classified as congenital (if the disease manifests itself within the first 3 months of life), infantile (if the presentation occurs between 4 or 12 months of age) and late-onset (or acquired, when the onset is after the first year of life, more frequently during adolescence or adulthood). Although the majority of congenital and infantile nephrotic syndrome cases are due to genetic defects in the components of the GFB, the disease could also be secondary to viral infection, maternal systemic lupus erythematosus or maternal steroid-chlorpheniramine treatment [63].

Based on the response to pharmacological therapy based on glucocorticoids, nephrotic syndrome can be classified as steroid-sensitive (the most common eventuality, the use of glucocorticoids will induce disease remission, hence the prognosis for the patient is favourable) or steroid-resistant (patients are more prone to complications and more likely to progress to ESRD).

1.2.3 Genetics of Nephrotic Syndrome

Genetic studies of hereditary forms of nephrotic syndrome have led to the identification of a number of proteins playing a crucial role in slit diaphragm signalling, regulation of actin cytoskeleton dynamics and cell-matrix interactions. A genetic cause is often found in cases of congenital, infantile and steroid-resistant nephrotic syndrome, but more rarely found in steroid-sensitive forms. The causative mutations are high-penetrance

variants that manifest with either Mendelian inheritance, for nuclear genes, or maternal inheritance, for genes encoded by mitochondrial DNA (Figure 1.3).

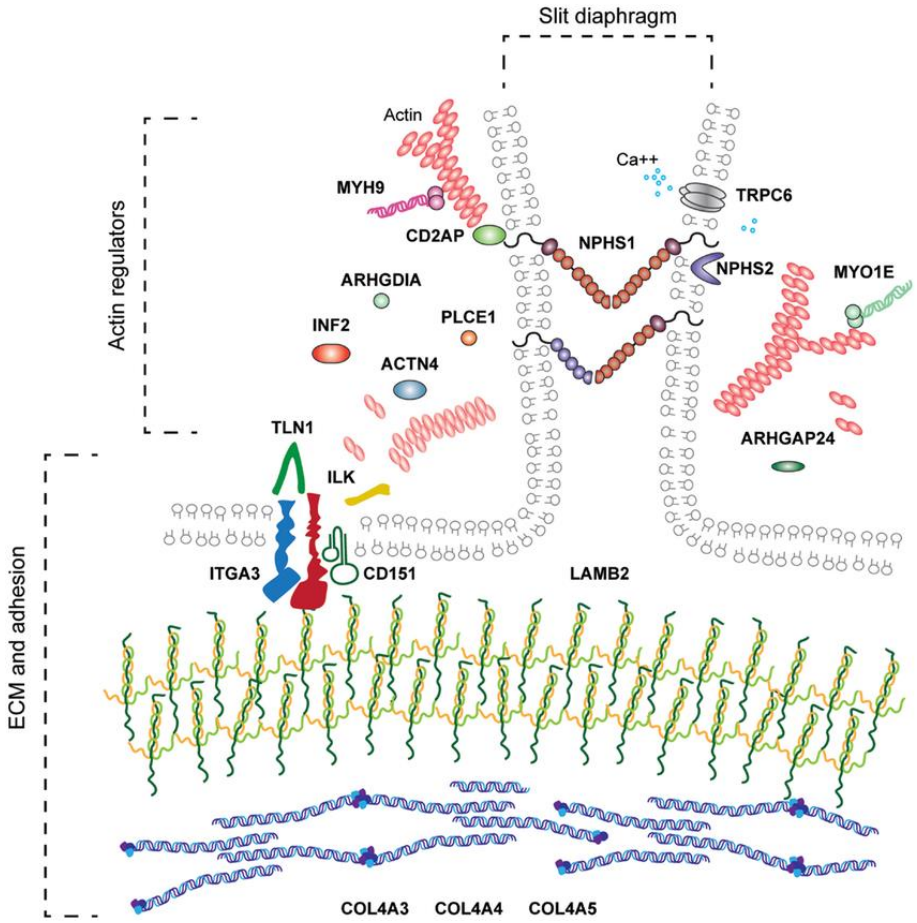

Figure 1.3. Genes known to be the cause of nephrotic syndrome in humans and distribution of their encoded proteins in the GFB. These include components of the GBM and ECM adhesion, proteins that regulate F-actin network, transcription factors and components of the slit diaphragm. Image adapted from Lennon *et al.* [64].

The majority of causative mutations responsible of congenital or infantile nephrotic syndrome occur in one of these five genes: nephrin (*NPHS1*), podocin (*NPHS2*), Wilms' tumour 1 (*WT1*), laminin β2 chain (*LAMB2*) and phospholipase C epsilon-1 (*PLCE1*). Of these main genes, *NPHS1* is the most commonly implicated in congenital nephrotic syndrome and it is the cause of autosomal recessive of the Finnish type, a very aggressive form that manifests with massive proteinuria and rapid deterioration of

kidney function leading to end stage renal disease (ESRD) [65]. Rarer hypomorphic mutations in this gene are associated with a milder phenotype and later onset [66]. Mutations in *NPHS2* are the most common cause of autosomal recessive nephrotic syndrome in older paediatric patients, with an average age of onset of 6 years old. [67, 68]. Mutations in *PLCE1* are also a relatively common cause of infantile nephrotic syndrome, presenting severe proteinuria and rapid progression to ESRD [66].

Autosomal dominant mutations in α-actinin 4 (*ACTN4*,) inverted formin 2 (*INF2*,) and transient receptor potential cation channel (*TRPC6*) are the main causes of late-onset FSGS [66].

Mutations in other genes associated with nephrotic syndrome can also result in extra-renal manifestations. *WT1* is a gene relatively commonly involved in congenic and infantile nephrotic syndrome, but mutations resulting in splice insertion and missense variants in exons 8 and 9, lead respectively to Frasier syndrome and Denys-Drash syndrome (nephrotic syndrome associated with male-to-female sex reversal, gonadoblastoma) [69]. Mutations in LIM homebox transcription factor 1 β (*LMX1B*) are responsible for isolated nephrotic syndrome as well as Nail-Patella syndrome (poor development of nails, kneecaps, elbows and pelvis) [70, 71]. Nephrotic syndrome can also be a manifestation of mutations in mitochondrial or nuclear-encoded mitochondrial proteins as part of a wider symptomatology like MELAS (myopathy, encephalopathy, lactic acidosis and stroke-like episodes) caused by mutations in mitochondrially encoded tRNA leucine 1 (*MTTL1),*. Coenzyme Q10 deficiency caused by mutations in coenzyme Q2 and Q6 polyprenyltransferase (*COQ2* and *COQ6)*, or Leigh syndrome caused by mutations in *PDSS2*, can result in nephrotic syndrome also as an isolated phenotype [66].

Lastly, some patients are associated with variants in susceptibility genes, the most common of which being apolipoprotein L1 (*APOL1*) [72, 73]. Two risk alleles in the coding-region of *APOL1*, called G1 and G2, have been indicated as being FSGS-associated and are common in countries with individuals of West African descent, who have a 3–5-fold increased risk of developing chronic kidney disease (CKD) and ESRD [72].

1.3 Diseases of the glomerular basement membrane

Inherited abnormalities of the GBM proteins often result in renal diseases demonstrating the importance of the GBM in maintaining the health of the kidney. Different diseases affect the GBM directly or indirectly. Type III collagen accumulates in the GBM in rare glomerulopathies such as nail-patella syndrome and collagenofibrotic glomerulopathy [74], and in Goodpasture syndrome, a rare autoimmune disease where the type IV collagen α3 chain is the target of antibodies in lung and kidneys [75, 76]. Very rarely, abnormal deposition of fibronectin occurs in fibronectin glomerulopathy [77]. However, the better characterised GBM diseases are probably Alport syndrome and Pierson syndrome "spectrum".

1.3.1 Alport Syndrome

Described for the first time in 1927 by Cecil Alport, Alport syndrome is a hereditary progressive nephropathy associated with ocular disorders (anterior lenticonus, abnormal pigment of the retina, cataracts), deafness (caused by abnormalities of the cochlea) and rarely with mental retardation and leiomyomatosis [16, 18].

In patients affected by Alport syndrome, one of the genes that encode for a chain of the α3α4α5 network, *COL4A3*, *COL4A4*, *COL4A5*, carries a mutation that arrests its normal maturation, resulting in the incorrect assembly of the monomers. The α3α3α5 network is then rapidly degraded, and the normal "isotype switching" between the normal network and the embryonic α1α1α2 network cannot take place in Alport patients.

The syndrome is classified into three types depending on the gene affected by the mutation. Approximately 85% of Alport patients are affected by X-linked Alport Syndrome (XLAS) and carry a mutation in the X-linked *COL4A5* gene that encodes for the α5(IV) chain of type IV collagen. About 500 mutations affecting *COL4A5* have been described in humans [78] and include missense mutations, splice variants, deletions and nonsense mutations. The effects on the α5(IV) chain vary and can result in a reduction, distortion or loss of the α3α4α5 network. In female patients, the penetrance of the disease is variable and depends also on the degree of mosaicism following lyonization of the X chromosome [16]. If a mutation in the *COL4A6* gene encoding the α6 type IV chain occurs simultaneously, leiomyomatosis could be associated [79].

The remaining 15% of patients are affected by the autosomal recessive or, very infrequently, by a dominant type of Alport syndrome and carry a mutation in either *COL4A3* or *COL4A4*. In the recessive form, homozygous or compound heterozygous nonsense mutations, missense mutations, frameshifts, small deletions or splice variants that lead to a loss of the α3α4α5 network [16]. In the dominant form, which has only been described in a few families, the mutations produce aberrations in the α3α4α5 network and are missense mutations carried on *COL4A4* or shortened signal-peptide sequences in the *COL4A3* gene [80].

Missense mutations in the *COL4A3* and *COL4A4* genes are also related to the thin glomerular basement membrane nephropathy: approximately 40% of patients with thin glomerular basement membrane nephropathy carry heterozygous missense mutation in *COL4A3* and *COL4A4*, producing aberrations in the α3α4α5 network (while autosomic AS is caused by homozygous or compound heterozygous mutations) [81, 82].

1.3.2 Pierson Syndrome

Identified for the first time in the 1960s in two patients from the same family with a microcoria and congenital nephrotic syndrome by M. Pierson, Pierson syndrome is a rare genetic disorder resulting from mutations in the *LAMB2* gene encoding the laminin β2 chain found in the GBM, structures of the eye and neuromuscular junction [21-23]. Truncating and nonsense mutations leading to Pierson syndrome result in the lack of laminin β2 chain and, consequently, of the whole laminin-521 network.

Lamb2 knockout mice recapitulate the human phenotype exhibiting congenital nephrotic syndrome and die at about three weeks of age with severe proteinuria and neuromuscular defects [83, 84]. Interestingly, at earlier time points the mice still exhibit proteinuria, but without foot process damage [85]. This observation suggests that the GBM is a key filtration barrier for albumin. Moreover, *Lamb2*$^{-/-}$ mice show accumulation of ectopic laminins in the GBM such as laminin β1, laminin α1 and α2 as an attempt to compensate the lack of laminin-521, but it is not sufficient to restore a normal renal function [85].

Missense mutations, primarily in the LN domain, result in a much milder disease and patients normally exhibit a later onset nephrotic syndrome, with or without extra-renal

symptoms like microcoria [24, 86-88]. The milder phenotype is also recapitulated by mouse models [89-91]. A study of two mutations found in humans (R246Q [89] and C321R [90]) through the creation of transgenic mice, showed a reduced secretion of LAMB2 with consequent endoplasmic reticulum (ER) stress in podocytes resulting in ER distention and podocyte injury [89, 90]. The use of chemical chaperones rescued the *in vitro* phenotype [90].

The laminin β2-associated phenotype can also result from defective polymerization but normal secretion, like in the case of the mutation S80R [92]. An *in vitro* study by Purvis *et al.* showed how the mutation S68R in the β1 chain (which corresponds to the S80R mutation in the closely related β2 chain that causes Pierson syndrome) affected laminin polymerization without perturbing the LN domain structure and the chain secretion [93].

1.4 The Laminin α5 Chain

Among the major basement membrane proteins, laminins have been shown to be essential for the formation of the basement membrane itself by regulating cell adhesion, migration and differentiation [94]. Identified in 1979 as a large molecular weight non-collagenous glycoprotein isolated from Engelbreth-Holm-Swarm sarcoma, there are currently five α, four β, and three γ chain genes that have been described in vertebrates and the chains can assemble into at least 16 different heterotrimers [95-97].

The laminin α5 chain was first cloned in a study by Miner and colleagues in 1995 [98]. Using polymerase chain reaction (PCR), the group was able to identify 3610 amino acids of the full 3718. The sequence was eventually completed in 2002 [99]. Based on predicted secondary structure and homology with the already known laminin α1, eight different

domains were identified, including a large G domain on the C-terminal half of the protein, three sets of epidermal growth factor (EGF)-like repeats and two globular regions on the N-terminal half that are peculiar of the laminin α chains. A study of laminin α5 expression by Nothern Blot analysis with a α5 cDNA, showed a high level of mRNA expression in heart, lung and kidney but also in brain, muscle, testis, liver, gut and skin suggesting that laminin α5 is a major α chain of adult epithelial and/or endothelial basal laminae.

The α5 chain combines with the β chains 1 and 2, and the γ chain 1 and 3, to form three different cross-shaped trimers: laminin-511 (α5β1γ1) in the basement membrane of epithelia, endothelia and smooth muscle, laminin-523 (α5β2γ3) in the retina and the central nervous system, and laminin-521 (α5β2γ1) in epithelia, endothelia, smooth muscle, neuromuscular junctions and glomeruli [94]. Laminin trimerization occurs in the endoplasmic reticulum and involves association of the three chains along their α-helical laminin coiled-coil domains to form the long arm [89]. Once trimers are secreted into the extracellular space, they polymerize to form a supramolecular network via interaction among the α, β and γ short arm end [89].

Unlike most of the other basement membranes of the body, the GBM changes its composition as the kidney develops [100]. During murine embryonic development, the renal vesicles of the metanephric nephron form at E12.5 [101] and during this stage there is a burst of laminin α1 chain expression [102]. As development proceeds and the renal vesicle starts to proliferate, laminin α5 becomes detectable in the basement membrane, and at the S-shape stage, both laminin α1 and laminin α5 are found in the developing GBM adjacent to the differentiating podocytes [100]. Eventually, as the capillaries begin to form, laminin α1 is eliminated by an unknown mechanism and laminin α5 remains

the only α chain of the GBM [100]. Likewise, laminin β1 and the collagen type IV α1α2α1 network are replaced by the mature forms laminin β2 and collagen α3α4α5 network [102] (Figure 1.4).

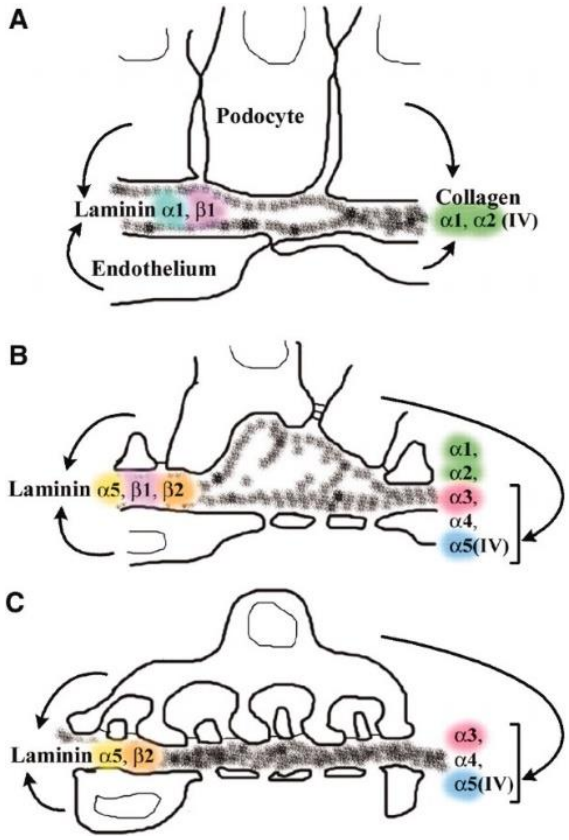

Figure 1.4. Diagram showing the stages and changes of the GBM assembly and the origin of the collagen type IV and laminin isoforms. At the beginning of renal vesicles development, both podocytes and endothelial cells produce laminin-111 and collagen IV α1α2α1 (**A**). As the renal fascicles proliferate and develop, laminin-511 and laminin-521, as well as collagen IV α1α2α1 and α3α4α5, are present in the glomerulus (**B**). Finally, in fully mature glomeruli, podocytes and endothelium cells produce exclusively laminin-521, while collagen IV α3α4α5 is produced by podocytes only (**C**). Image adapted from Abrahamson *et al.* [102].

Of all the mature components of the GBM, laminin α5 chain is the only one that is essential for a normal embryonic development as shown by the lethality of the mouse *Lama5* knockout. Mice lacking laminin α5 die at 14 -17 days of gestation of placental

insufficiency and incomplete neural tube closure; also present is digit septation, placentation and a small percentage of mice (20%) lacked one or both kidneys [103]. In the kidneys with normal nephrogenesis, the effect of the lack of laminin α5 resulted in aborted glomerulogenesis. As the glomerular constriction progresses, the cells are forced out the interior, leaving a cluster of podocytes adjacent to a group of endothelial and mesangial cells [103]. The result is a complete lack of vascularised glomeruli. Since the substitution of laminin α1 with laminin α5 could not occure in *Lama5*$^{-/-}$ embryos, none of these proteins were present in the GBM resulting in its breakdown. Consequently, endothelial cells and mesangial cells could not maintain their position in the glomerulus while podocytes failed to maintain a normal single layer arrangement and lacked foot processes and slit diaphragm [103].

Other murine models include a hypomorphic *Lama5* mutation, created by inserting a PGK*neo* cassette inserted into a *KpnI* site in intron 21, which results in proteinuria, haematuria and polycystic kidney disease (PKD). This is the first evidence that a primary defect in an extracellular matrix component can cause PKD [104]. A podocyte-specific deletion *Lama5* resulted in nephrotic syndrome with a variable rate of diseases progression (from few weeks to 8 months) possibly due to the mixed genetic background (C57BL/6J-CBA/J-129) [105].

Like in kidneys, laminin α5 is essential for the development and function of several tissues. Given the lethality of the *Lama5* null mice, studying the role in different organs has been proven to be challenging and has led to the production of conditional or transgenic murine models. In the lung, LAMA5 is required for complete lobar septation and visceral pleural basement membrane production, but not for morphogenesis [106]. Moreover, mice lacking *Lama5* in lung epithelial cells survived birth but presented

dilated airspaces, reduction or absence of alveolar cells and decrease proliferation [107]. Interestingly, mice showed increased mRNA levels of integrin α3, one of LAMA5's main binding partner, suggesting that the cells were trying to compensate the lack of interaction with laminin α5 producing more ligand [107]. In the intestine, a lack of *Lama5* leads to morphological defects of the smooth muscle layer. Conditional deletion of *Lama5* in the intestine after embryogenesis, resulted in villi fusion and increased goblet cell numbers, altering the morphology of mature cryptic-villus architecture [108, 109]. Laminin α5 also promotes cell proliferation in the developing tooth and regulates keratinocyte proliferation and migration [110-112], suggesting a role of LAMA5 in general epithelial replacement and possibly in wound healing.

In humans, two mutations have been described as causing syndromes [113, 114]. The mutations are localised in one of the C-terminal LG domains (V3140M [113]) and in the coiled-coil (R2659W [114]) and lead to a plethora of symptoms such as myopia, muscle weakness, skin anomalies and failure of neuromuscular transmission. None of the patients, however, had any signs of kidney impairment. The two mutations described seem to have a different mechanism in disease. In the study by Maselli *et al*, *in vitro* expression and adhesion assay showed reduced cell adhesion power and reduced binding with SV2A. In the study described by Sampaolo *et al*, cell binding is conserved but most of the genes shown to be deregulated in patients are involved in tissue inflammatory response, repair and ECM remodelling, hence the authors hypothesise a master regulatory role of LAMA5.

In respect to kidney disease, the mutation G3685R has been reported in two independent studies in patients affected by FSGS [115, 116], however, a mouse model carrying the same mutation and created by CRISPR/Cas9 gene editing, did not show any

phenotype (personal correspondence [117]). More recently, three different genetic variants have been identified in three families with nephrotic syndrome [118]. The variants are positioned in different domains of the protein: R747W in the LEa EGF-like domain, E1001G in the L4a domain and G2948 in the second LG domain. The patients, all homozygous for one of the mutations, exhibit early onset nephrotic syndrome between 18 months and 4 years of age. Only the children carrying the mutation E1001G underwent renal biopsy and were diagnosed with FSGS.

1.4.1 Laminin α5 Structure

As previously stated, the structure of the laminin α5 chain can be described as having a short and a long arm. As in most laminins, the short arm of laminin α5 begins with an N-terminal globular LN domain, followed by repeated rod-like region consisting of multiple EGF-like domains (LEa, LEb and LEc domains) in combination with two additional globular domains (L4a and L4b domains). The long arm starts with a long coiled-coil domain that joins the α5 chain to the β and γ chains and ends with LG domain which includes five similar but not identical modules with a hinge-like region between LG3 and LG4 [119] (Figure 1.5).

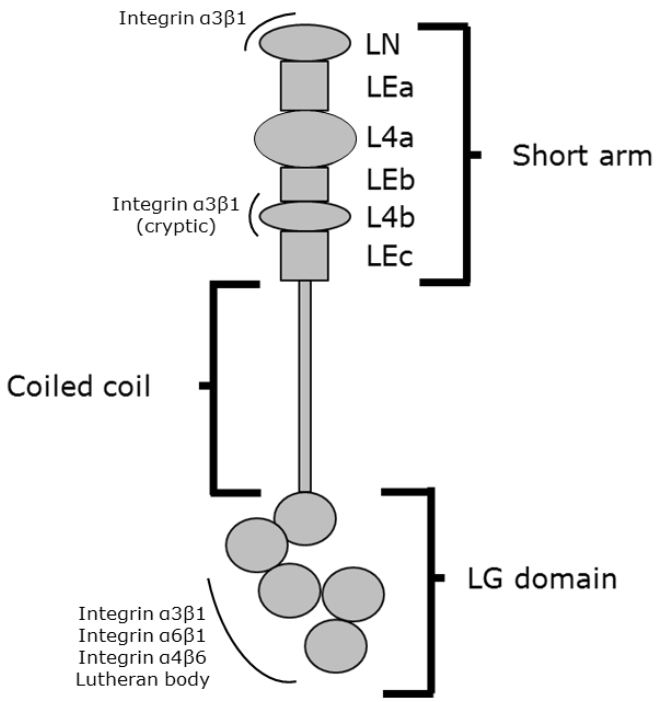

Figure 1.5. A schematic representation of laminin α5 chain structure with its main domains and binding sites for its major receptors.

Described as having a crystal structure that resembles a flower, the LN domain (previously known as VI domain) is a Swiss roll fold composed of eight beta strands, β1-β8, with β5-β6 being the loop involved in the network interaction and spontaneous heterotrimers polymerization with other laminins [120]. The LN domain is a minor binding site of LAMA5 [121, 122]. Experiments using integrin-blocking antibodies indicated integrin α3β1 as a potential major receptor. Other potential receptors were found in HSPG as suggested by the fact that heparin could inhibit cellular binding to the LN domain by 90% [123]. Additionally, the first 40 residues of the domain represent the signal peptide cleavage site for normal laminin secretion [99].

The L4a and L4b domains are probably the least well characterized LAMA5 domains. *In vitro* studies did not show any cell-binding proprieties of L4a domain, but active sequences within this region have been proved to promote neurite elongation [124]. The

L4b domain (previously known as domain IVa) contains two Arg-Gly-Asp (or RGD) sequences in both the human and murine protein. RGD sequences are often found in extracellular proteins and are known to be able to bind various integrins. Studies *in vitro* showed the capacity of the RGD sequences to bind β1 and αVβ3 indicating that they work as cryptic sites, but it is not clear if this function is maintained *in vivo* [125].

The C-terminal LG domain appears to be the major binding site of LAMA5 as demonstrated in both *in vivo* and *in vitro*. Yu *et al* used antibody-inhibition assays performed on LG1-LG2-LG3 and LG4-LG5 modules to understand which subdomains is specific for which receptor: the study showed how binding of integrins α3β1 and α6β1 was localised to the LG1-3 modules, while α-dystroglycan, binding was localised to the LG4-5 modules [126]. A follow up study by Ido *et al* showed how LG3 module is indispensable for integrin binding. However, when the modules were expressed individually, only LG4 was able of binding to α-dystroglycan, whereas neither LG3 nor any of the other LG modules retained the ability to bind to the integrins [127].

The same binding site for integrin on LG1-3 modules appear also to bind Lu/BCAM, but just in presence of the laminin coiled coil [128]. Lutheran (Lu) adhesion glycoprotein/basal cell adhesion molecule (BCAM) is expressed in different tissues and it is localised on the basal surface of many epithelial cells, adjacent to basement membranes containing laminin α5 [129]. To support the hypothesis that Lu/BCAM is strictly associated with LAMA5, it was shown that Lu/BCAM expression is drastically reduced in tissues from *Lama5* knockout mice and increased in transgenic mice that overexpress *Lama5* [130]. Mice with a genetic inactivation of Lu/BCAM showed irregular thickening of the GBM, reduction of the glomerular capillary lumens and enlargement of the smooth muscle layers of the intestine. However, they were still viable, fertile and did not show any

defect in development or into the function of organs [131]. It is still not clear though if the different integrins compete for the binding sites and therefore Lu/BCAM could inhibit integrin-mediated cell adhesion to LAMA5.

In the kidney, from different studies, it emerged that the LG1-LG2 domains are the most involved during development, while LG3-LG4-LG5 domains are more involved in maintaining the integrity of the GFB [132, 133].

1.4.2 Integrins as Laminin α5 Receptors

Integrins are transmembrane heterodimeric receptors containing non-covalently associated α and β subunits and play an important role in cell adhesion to ECM proteins, certain cell-cell interactions, and also the transduction of intracellular signals to the ECM [134]. The eighteen α subunit and the eight β subunits can form 24 different dimers [135] and although some subunits appear only in a single heterodimer, twelve integrins contain the β1 subunit, and five contain αV [136].

Each integrin can bind several different ligands, with ligand-binding specificity being dictated by both subunits. Laminins can potentially bind with a number of integrins: α1β1, α2β1, α3β1, α6β1, α7β1, α10β1, αVβ3 and α6β4 [136] and, in most cases, they have a preference for the laminin α5 chain as their ligand [20]. Integrin α1β1, α2β1, α10β1, α11β1 and αXβ2 can bind collagen, with α1β1 having a higher affinity for type IV collagen and α2β1 having a higher affinity for type I collagen [136-138].

Integrin activity is regulated by conformational changes [139]. They can adopt three different conformational states; inactive (low affinity) active or primed (with high affinity) and ligand occupied state [140]. The passage between inactive and active state depends on the signals transduced from the integrin cytoplasmic tail to the extracellular

ligand-binding pocket ("inside-out signalling"). The conformational change leads to ligand binding and transducing the signal from the ECM to the interior of the cell ("outside-in signalling") so that it can sense the extracellular environment and respond accordingly [141, 142].

In the kidney, podocytes express high levels integrin α3β1 that plays a crucial role in the link between these cells and the GBM [143]. Mouse models have been generated to study the role of β1 in development and disease. The lack of *Itgb1* leads to peri-implantation lethality and embryonic death at E6.5 [144, 145]. Its role in the GFB has been studied using a podocyte *Itgb1* specific deletion, where glomerular morphogenesis was conserved despite the defective GFB present at birth. The resulting proteinuria and progressive podocyte loss lead to renal failure by 3 weeks of age [146, 147]. In the same way, the α3 subunit has been shown to play a crucial role in development, with knock-out mice dying within the first day of birth from abnormal morphogenesis of lungs and kidneys, including a disorganised and thickened GBM [148]. A similar phenotype was observed in a murine model with a podocyte-specific deletion of *Itgα3*, where mice showed severe proteinuria from the first week of age, complete foot process effacement, with widespread lamination and protrusions of the GBM [149]. Patients with homozygous mutations in integrin α3 gene (*ITGA3*) showed a multi-organ disorder that included congenital nephrotic syndrome, interstitial lung disease, and epidermolysis bullosa [150]. Moreover, a mutation causing a gain of glycosylation in ITGA3 caused severe nephrotic syndrome and lethal lung disease [151].

Integrin α3β1 binds tightly to Cluster of Differentiation 151 (CD151, also known as Raph blood group), a tetraspanin member of the transmembrane four superfamilies (TM4SF) which is largely expressed in different cell types. It contributes fundamentally towards

integrin-dependent adhesion/signalling and functions as a signalling switch to balance Ras-related C3 botulinum toxin substrate 1 (Rac1) and Ras homolog gene family member A (RhoA) activities, leading to cell stability regulating the forces of cell adhesion and cytoskeletal tension [33, 152, 153]. In the kidneys, *CD151* is expressed at the base of the podocytes and colocalises with integrin α3 [149, 154]. *In vitro* experiments show that *Cd151*-deficient podocytes resulted in lower shear stress tolerance when cultured in laminin [149]. CD151 is needed for the correct assembly of of skin and kidneys. A human mutation resulting in the lack of CD151 integrin binding domain leads to haematuria, proteinuria and end-stage kidney disease (ESKD) associated with sensorineural deafness, pretibial epidermolysis bullosa, and β-thalassemia minor [155]. *Cd151*-null mice recapitulate the progressive kidney disease observed in humans but did not show any extra-renal phenotype [149]. Interestingly, the renal phenotype is strictly dependent on the genetic background of the mice, with FVB/N *Cd151*$^{-/-}$ mice displaying a similar pathology to humans, but C57BL/6J *Cd151*$^{-/-}$ mice retain normal kidney function but have defective keratinocyte migration and T lymphocyte hyperproliferation [156, 157].
This strongly suggests that integrin α3β1 is a crucial component of the GFB and that its interaction with CD151 increases the strength of podocyte integrin-laminin interaction necessary to resist the mechanical forces in the glomerulus.

1.4.2 Focal Adhesion Complexes

The binding of integrin and laminin triggers integrin clustering and the formation of multiprotein complexes called focal adhesions, located at the end of actin stress fibres. Depending on the protein they make contact with, cells form thick actin stress fibres,

with prominent focal adhesions on collagen or fibronectin, and thin stress fibres and smaller and fewer focal adhesions on laminin [158].

Focal adhesion complexes evoke both mechanical and chemical signals to regulate the cytoskeleton. In podocytes, mechanical signals are mediated by proteins such as talin, kindlin, α-actinin4 and vinculin that physically bind the cytoskeleton to the ECM, while chemical signals like paxillin, integrin-linked kinase (ILK) and focal adhesion kinase (FAK) regulate the activities of enzymes like GTPases (Figure 1.6).

Regulation of the podocyte actin network is essential to GFB integrity, as actin reorganisation is possibly the cause of foot process effacement, a common feature of glomerular diseases.

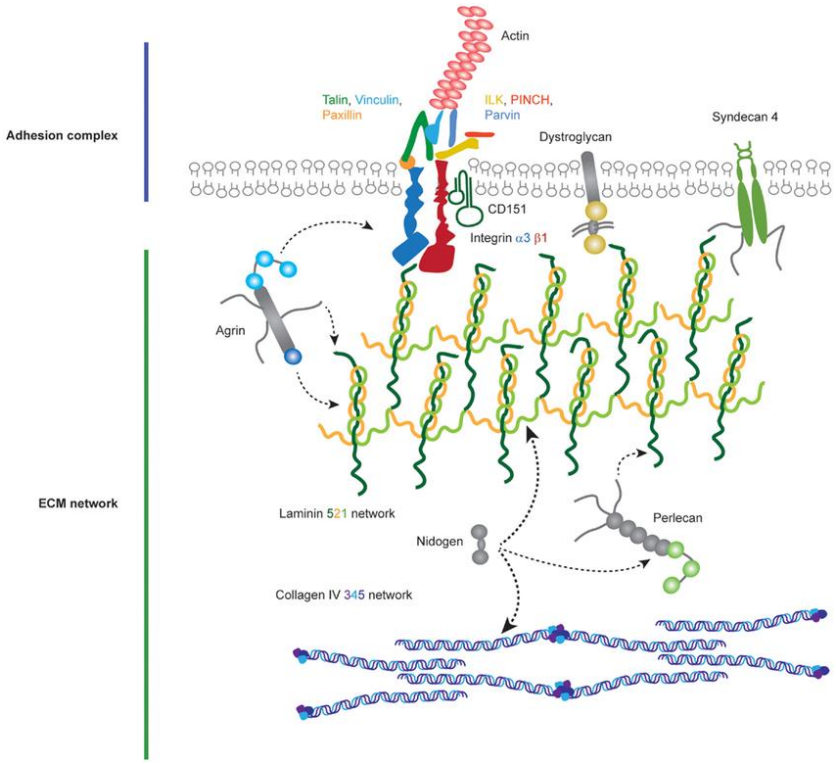

Figure 1.6. Molecular components of the focal adhesion complexes that form the podocyte-ECM interface and the interaction between components forming the ECM network. Laminin-521 and collagen IV α3α4α5 interact thanks the presence of nidogen and HSPGs (percalan). Podocyte foot processes highly express integrin α3β1, and its associated tetraspannin CD151, that binds laminin α5 chain of the GBM. Activated integrins recruit talin-vinculin-paxillin and ILK-PINCH-parvin to link to the actin cytoskeleton. Image adapted from Lennon *et al.* [64].

1.4.2.1 *Talin* 1

Talin 1, encoded by the gene *TLN1*, is a large protein, which is critical for integrin function in focal adhesion. It comprises a globular N-terminal domain (talin head) which contains the binding sites for β integrin tails [159], and a flexible rod domain, which contains additional binding sites for integrins, actin and vinculin [160, 161].

Talin 1 is involved in the first step of integrin activation "inside-out": when talin 1 head binds the cytoplasmatic domain of β integrins, it triggers a conformational change in the extracellular domain of integrins which activates the ligand binding function of integrins to the ECM [142]. Cells lacking talin 1 have reduced cell adhesion, spreading and migration [162].

In podocytes, talin 1 is required is required to keep the actin cytoskeleton morphology of the foot processes stable. Conditional podocyte-specific *Tln1*$^{-/-}$ mice developed proteinuria, podocyte effacement and reached ESRD around 8 weeks of age due to a dramatic disorganization of the actin network [163].

1.4.2.2 *Kindlin-2*

Proteins of the kindlin (or fermintin) family are indispensable to enable integrin activation through binding of β-integrin tails, and necessary for the integrin inside-out signalling in cooperation with talin-1 [164]. The kindlin family includes three proteins, kindlin-1 (*FERMT1*), kindlin-2 (*FERMT2*) and kindlin-3 (*FERMT3*), all with a FERM domain on the C-terminal end that mediates the integrin bindings. Kindlin-1 is mainly expressed in epithelial cells and mutations in *FERMT1* lead to Kindler syndrome (an autosomal recessive disease characterized by blistering, poikiloderma and photosensitivity in

childhood). Kindlin-3 is found in hematopoietic cells and mutations in *FERMT3* cause leukocyte adhesion deficiency. Kindlin-2 is ubiquitously expressed. No mutations in *FERMT2* have been reported and global deletion of *Fermt2* in mice results in peri-implantation lethality due to extensive detachment of the endoderm [165].

In the kidney, kindlin-2 is expressed in podocytes. In an *in vitro* study, Qu *et al.* showed its expression in cultured human podocytes and how its depletion impacted cell-matrix adhesion and reduced the deposition of fibronectin matrix [166]. Further *in vitro* studies proved that kindlin-2 stabilises podocyte morphology functionally linking cortical actin structures, plasma membrane tension and interactions with the ECM [167]. Podocyte-specific knockout of *Fermt2* results in alteration of the actin cytoskeleton organization leading to very severe proteinuria and kidney failure [168]: this phenotype is likely due to the activation of Rac1 in response of the reduction of Rho GDP-Dissociation Inhibitor α (RhoGDIα) that seems to be a kindlin-2 associated protein [168].

1.4.2.3 *α-Actinin 4*

The members of the α-actinin family are rod-shaped proteins with an N-terminal domain that binds actin, four spectrin-like repeats and C-terminal EF hands. The proteins form head-to-tail homodimers [169]. Of the four proteins that are part of the α-actinin family (ACTN1-4), α-actinin 4 is highly expressed in podocytes where it is involved in cell adhesion binding directly to β1-integrin and vinculin thus linking the actin network to the ECM. It also plays a role in creating cell junctions by serving as a linker between actin and proteins of the SD. α-Actinin 4 also contributes to cell signalling, interacting with proteins of the p13kinase pathway, and acts as a nuclear transcription activator [170].

Gain of function mutations in *ACTN4* have been reported to be the cause of a dominant form of FSGS, a common form of nephrotic syndrome affecting adults. All the mutations affect the N-terminal actin-binding domain and are associated with an increased binding of actin to F-actin forming abnormal cellular cytoskeletal protein aggregates within the cells that are rapidly degraded [171-173].

Although affected families show autosomal dominant inheritance disease, knockout mice recapitulate the human phenotype developing albuminuria and foot process effacement. Podocytes isolated from *Actn4*$^{-/-}$ mice showed reduced phosphorylation of β-integrin and weaker integrin-cytoskeleton linkages [174]. Homozygous mice for the knock-in mutation K228E developed a similar phenotype to the *Actn4*$^{-/-}$ mice, but *Actn4*$^{K228E/-}$ mice, that are closer genetically to the affected human patients, did not show any phenotype [172].

1.4.2.4 *Vinculin*

Vinculin is an adapter protein recruited by talin 1 that localises at the focal adhesions, binding the actin cytoskeleton, and at cell-cell junction [175]. It comprises an N-terminal head domain that binds talin 1, a proline-rich neck and a C-terminal tail that binds paxillin and F-actin bundles [176]. Vinculin assumes an inactive conformation before talin binds to its adhesion sites. This recruitment triggers a conformational change and vinculin is extended revealing an open active state [177] and allows the interaction of vinculin with several proteins like actin, paxillin and α-actinins [178].

In the kidney, vinculin is required to maintain glomerular barrier integrity. Patients affected by nephrotic syndrome showed differences in vinculin expression and

distribution [179]. Additionally, mice with a podocyte-specific vinculin knock out develop proteinuria and foot process effacement following injury *in vivo* [179].

1.4.2.5 *Paxillin*

Paxillin is a scaffolding protein that recruits enzymes and proteins involved in the intracellular signalling that ultimately results in the reorganization of the actin cytoskeleton and the assembly/disassembly of focal adhesions through the presence of docking sites for focal adhesion kinase (FAK), Src and vinculin on the N-terminal domains [180]. It localises to focal adhesions when phosphorylated on specific tyrosine and/or serine residues [181]. Moreover, paxillin also coordinates the spatiotemporal activation of signalling molecules, including Cdc42, Rac1, and RhoA GTPases, by recruiting guanine nucleotide exchange factors (GEFs), GTPase-accelerating proteins (GAPs) and G protein-coupled receptor kinase- interacting proteins (GITs) to focal adhesions [181].

Although its presence is crucial for the assembly and signalling of the focal adhesions and its phosphorylation is increased during glomerular immune injury [182], paxillin's role in the glomerulus has not been studied yet.

1.4.2.6 *Integrin-Linked Kinase*

Integrin-linked kinase (ILK) is a scaffold protein able to interact with the cytoplasmatic tail domain of β integrins [183]. It has three main domains with five ankyrin repeats towards the N-terminus that mediate the interaction with particularly interesting new cysteine-histidine-rich protein (PINCH) proteins forming a complex called PINCH-ILK-parvin, followed by a pleckstrin homology-like domain, and a C-terminal kinase domain

that mediates protein-protein interaction at focal adhesions, including with parvin proteins [184, 185].

ILK is necessary for normal embryonic development: *Ilk*$^{-/-}$ mice die during peri-implantation stage due to failure to organise the actin network in epiblast cells [186]. Specific *Ilk* deletion in podocytes resulted in an increased GBM thickness that preceded foot process effacement and proteinuria with re-localization of integrin α3 into a granular pattern along the GBM [187]. In humans, *ILKI* mRNA is overexpressed in children affected by nephrotic syndrome and patients affected by diabetic nephropathy [188, 189].

1.4.2.7 *Focal Adhesion Kinase*

FAK is a scaffold and a non-receptor tyrosine kinase involved in cellular adhesion and cell spreading. It binds to itself and cellular partners through four-point-one, ezrin, radixin, moesin (FERM) domain with integrin inducing its auto-phosphorylation at tyrosine 397 resulting in activation of signalling pathways required for focal adhesion turnover [190-192].

FAK is necessary for normal development: global deletion in mice is embryonic lethal due to profound migration defects [193]. In mice with induced glomerular injury, FAK is robustly activated at Tyr 397, and, vice versa, inhibition of FAK protects from podocyte experimental injury [192]. Interestingly, podocyte-specific deletion of FAK in mice did not affect renal function and did not produce proteinuria [192].

FAK inhibition also ameliorated the proteinuric phenotype in a model of Alport syndrome, where the abnormal accumulation of laminin α2 chain caused the upregulation of FAK at Tyr 397 [194].

1.4.2.8 *Rho GTPases Family*

The Ras homologue (Rho) GTPases family is a group of small G coupled proteins (guanine nucleotide-binding proteins) which belongs to the Ras superfamily, consisting of over 150 members in mammals. Proteins of this family play important roles in the regulation of cell polarity, gene expression and cell survival, but their main involvement in eukaryotic cells is to regulate actin cytoskeleton and all the actin-dependent processes such as migration, adhesion and morphogenesis [195]. Rho GTPases have two states, an inactive form bound to GDP, and an active GTP bound form. The passage between states is strictly regulated. The exchange of GDP for GTP, and therefore activation of Rho GTPase proteins, is catalysed by guanine nucleotide exchange factors (GEFs), while the passage to their inactive form is mediated by GTPase activating protein (GAPs) [195]. Additionally, guanine nucleotide dissociation inhibitors (GDIs) act as inhibitors preventing the GDP dissociation from the inactive state [195].

The Rho GTPases family consists of 20 members that are divided into eight subfamilies, Rho, Rnd, RhoD/F, RhoH, Rac, Cdc42, RhoU/V and RhoBTB [196], however most research focuses on the three most common members; Rac1 (Rac subfamily), RhoA (Rho subfamily) and Cdc42. These three proteins act in complex activation cascades with the antagonistic regulatory mechanism. Rac1 can be activated by Cdc42, and Rac1 and RhoA operate antagonistically [197]. Laminins activate Rac1 and Cdc42 promoting the formation of lamellipodia and filopodia, respectively. Their activation of RhoA is less pronounced and results in thinner actin stress fibres and smaller focal adhesions [158]. *In vivo* and *in vitro* studies have revealed that all three proteins are involved in kidney disease in various degrees. Mice lacking Cdc42 in the podocytes developed collapsing glomerulopathy and extensive foot process effacement leading to renal failure by 2

weeks of age which was associated with *in vivo* impaired actin polymerization by nephrin clustering [198]. Rac1 podocyte-knock out mice did not show any phenotype during the three months of study, but misregulation of their expression or their balance can influence the renal podocytes. Increased Rac1 activity is associated with proteinuric kidney disease and has been demonstrated to be harmful to podocytes in many studies [199-203]. Interestingly, treatment with a Rac1 inhibitor or glucocorticoid reduced proteinuria and the severity of the kidney damage [202, 204, 205]. Likewise, the overexpression of RhoA in podocytes induces kidney injury: *in vitro* enhanced RhoA activity stimulated actin polymerization as well as reduced glomerular nephrin expression and caused apoptosis of cultured podocytes [206]. *In vivo*, the impact of RhoA activation on podocyte health has been tested in two studies using doxycycline-inducible and podocyte-specific expression in mice. Both studies resulted in glomerular sclerosis and foot process effacement associated with albuminuria [206, 207]. The study of Wang *et al*, the expression of dominant negative RhoA in podocytes also induced foot process effacement and proteinuria. This result strongly suggests that, in addition to the lack of expression, is the basal activity of RhoA is also important for the integrity of podocytes.

1.5 ENU Mutagenesis

Since Russell's lab discovered in the late 1970s that N-Ethyl-N-nitrosourea (ENU) was a potent mutagen [208], it has been shown to be an effective tool to identify novel genes, pathways or functions of the gene in disease pathogenesis and progression. ENU is an alkylating agent that acts transferring a methyl or ethyl group to the oxygen or nitrogen sites on the nucleotide bases. The resulting DNA adduct creates a mismatch in the sequence that, if not corrected, during cell proliferation and DNA replication will convert in most cases in a hereditable point mutation (or more rarely, in a small deletion) [209]. ENU is usually administrated by a sequence of injections to an adult male mouse: it is estimated that an optimal dosage would result in one mutation every 1-1.5 Mb with a mutation rate that varies according to the gene size (larger genes have a higher chance of being mutated) [210]. The most common ENU induced mutations are A-T to T-A transversions or A-T to G-C transitions, while G-C to C-G transversions are rarely seen [210]. The preference for specific substitutions is a limiting factor of ENU mutagenesis because some amino acid changes will be underrepresented while genes or specific domains containing easily targeted amino acid will be more frequently mutated [210]. In spite of this limitation, ENU has been widely used to create mouse models of human disease.

1.5.1 Phenotype Driven Approach

Large-scale mutagenesis programs were launched back in 1997 in the UK (MRC Harwell) [211] and Germany (GBMH)[212, 213] and they are now performed all around the world [214].

ENU-based phenotype-driven screening (forward genetics) has been proved to be an effective methodology to study gene involvement in disease pathogenesis.

Forward genetics makes no assumption about the genetic basis and the models are identified just based on the expression of particular phenotypes, which is more likely to uncover a novel gene function. Another advantage is given by the production of mutations that can modify gene function in various ways in addition to the production of null alleles resulting in a total loss of gene function. The ENU-induced mutations could result in hypomorphs (partial loss of function), hypermorphs (increased of normal function), neomorphs (new gene function) and splice variants that better represent what happens in human patients.

Breeding schemes have been implemented to propagate the mutation and permit gene mapping (Figure 1.7). The ENU-treated males (G0), after an initial period of sterility, are crossed to wild-type females. The offspring resulting from this mating (G1) can be used to screen for dominant mutations. If a recessive screen is needed, the G1 males are mated to wild-type females and their offspring (G2) can then be intercrossed or the G2 females can be backcrossed to their G1 father. In both cases, the resulting G3 offspring will carry both recessive and dominant mutations and can, therefore, be screened (G3 screen). To assist in the mapping, wild-type females are usually from a different inbred strain [210].

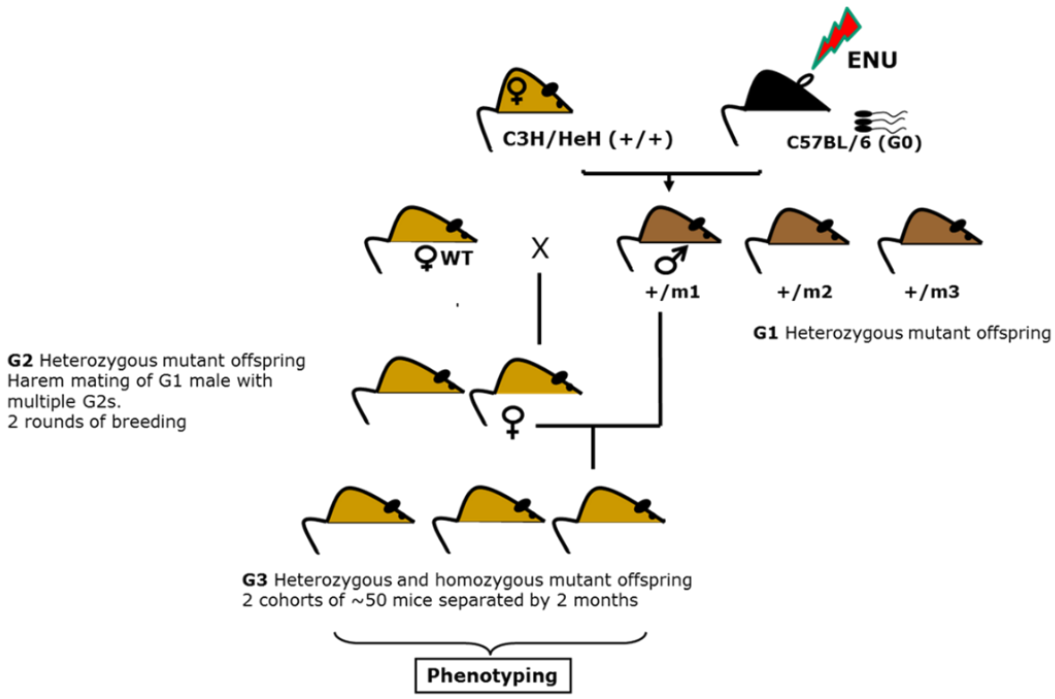

Figure 1.7. Breeding plan used for the recessive ENU mutagenesis screen, the Harwell ageing screen. Figure adapted from Goldsworthy *et al.* [215].

ENU-mutagenesis has been a useful tool also to identify novel models of kidney disease. As part of the Munich ENU mouse mutagenesis project [216], C3Heb/FeJ inbred mice were screened specifically for increased plasma urea levels. The project involved the screening of both G1 offspring (15,000 mice in total) and G3 (500 mice in total) collecting plasma and urine at three months of age [217]. The screen led to the identification of five mutant lines and causative mutations in genes such as *Pou3f3* (POU Class 3 Homeobox 3)[218] and *Kctd1* (potassium channel tetramerization domain containing 1)[219].

Other mutant lines derived from ENU-mutagenesis screens and used as models of glomerular basement membrane disease and/or nephrotic syndrome are *Col4a4*^{Aoba}, model of Alport syndrome (from the Scripps Research Institute), *Lamb2*^{nephertiti} (from the Australian Phenomics Facility) and *Ampd2*^{A341S} models of nephrotic syndrome (from the McLaughlin Research Institute)[91, 220, 221].

1.5.2 Gene Driven Approach

Genome-wide association studies in the human population have become a common approach to study the effect of genes on common and rare diseases. In the UK, the 100,000 Genome Project (https://www.genomicsengland.co.uk/the-100000-genomes-project/) aims to sequence more than 70,000 patients affected by cancer and rare disease, including renal pathologies. ENU can be a useful tool also in gene-drive screens (reverse genetics) using libraries of DNA and sperm derived from ENU-treated G1 males. After the identification of the gene of interests, the DNA library can be screened for mutations the same specific gene. Once a mutation is identified, the line can be recovered by *in vitro* fertilization (IVF) [210, 214]. Alternatively, embryonic stem (ES) cells can be treated and, therefore, mutated using ENU. The ES cells are then screened for mutations in a gene of interest. If the mutation is found, a parallel frozen cell archive can be microinjected into a murine blastocyst to create a chimeric mouse that carried the ENU-induced mutation [210].

1.6 Project Aims and Objectives

The aim of this project is to characterise a novel model of nephrotic syndrome resulting from an ENU-induced point mutation in the gene *Lama5*, encoding laminin α5 chain, a crucial component of the GBM recently associated with nephrotic syndrome in humans. The study will involve the following:

- Phenotypic analysis:
    - Urinalysis and clinical chemistry analysis to assess renal function
    - Histological study to examine the renal morphology.
    - Ultrastructural study using transmission electron microscopy (TEM) and scanning electron microscopy (SEM) to study the structure of the GFB.
- Gene identification using:
    - Whole genome mapping
    - Whole genome sequencing
- Functional characterisation studies using:
    - *In silico* analysis to predict the effect of the ENU-induced missense variant on the protein structure and/or function.
    - *In vitro* study of the impact of the ENU-induced missense variant on laminin α5 chain expression and secretion.
    - Gene expression, protein expression, immunofluorescence and proteomics analysis to investigate possible mechanisms involved in the pathogenesis of *Lama5*-dependent nephrotic syndrome.

CHAPTER 2

Experimental Methods

2. Experimental Methods

2.1 Mice

C57BL/6J and C3H-C3pde6b+ inbred mice were maintained in the Mary Lyon Centre in Harwell UK, in specific pathogen-free conditions. All animal procedures were carried out under the guidance issued by the Medical Research Council in "Responsibility in the Use of Animals for Medical Research" (July 1993) and in accordance with Home Office regulations (Home Office Project Licence No. 30/3070, "'New mouse models of human disease").

The MUTA-PED-C3pde-205 mouse line was derived from a G_3 pedigree produced in the MRC Harwell ENU mutagenesis screen as described previously [222]. Briefly, male C57BL/6J mice were mutagenized with ENU with three injections with one at 120mgkg^{-1} and two at 100mgkg^{-1} with 7 days between each dose. They were then mated to female C3H.Pde6b+ mice to generate G_1 founder males, heterozygous for ENU induced mutations. G_1 males were subsequently bred to female C3H.Pde6b+ mice to generate G_2 offspring. Lastly, G_2 females were mated back to the original G_1 founder to generate two G_3 cohorts of approximately 50 animals 3 months apart, with homozygous or heterozygous offspring. G3 animals entered a high-throughput phenotyping pipeline screened throughout their lifetimes (18 months).

To generate one backcross C3H-C3pde6b+ *Lama5*^{E884G} mutant mice (C3pde-*Lama5*^{E884G}), MUTA-PED-C3pde-205$^{+/E884G}$ mice were crossed with inbred C3H-C3pde6b+ for one generation and then intercrossed to create phenotyping cohorts.

To generate congenic C57BL/6J *Lama5*^{E884G} mutant mice (B6-*Lama5*^{E884G}), MUTA-PED-C3pde-205$^{+/E884G}$ mice were crossed with inbred C57BL/6J mice for a total of ten generations and then intercrossed to create phenotyping cohorts.

For gene validation, *Lama5*-tm1b mice were obtained from the international mouse phenotyping consortium (IMPC - http://www.mousephenotype.org/). This mouse line was created deleting the critical exons four, five and six. *Lama5*-tm1b$^{-/-}$ mice showed complete penetrant preweaning lethality. To generate the compound MUTA-PED-C3pde-205$^{+/E884G}$ mice were crossed to *Lama5*-tm1b$^{+/-}$ mice.

2.2 Initial Identification

2.2.1 Mapping and Next Generation Sequencing

DNA from affected mice and littermate controls were extracted using a GE Healthcare Illustra BACC2 kit according to the manufacturer's protocol and sent to GenProbe Life Sciences Ltd. to be tested in on the Illumina Golden Gate "Mouse MD Linkage Panel" (Oxford Genomics Centre, Wellcome Trust Centre for Human Genetics).

After identifying the candidate region that could contain the causative mutation, the DNA from the G_1 founder of the pedigree was sent for whole genome sequencing (WGS) employing the Illumina HiSeq platform (Oxford Genomics Centre, Wellcome Trust Centre for Human Genetics). The sequence was then analysed by the Bioinformatics group based at the MRC-Harwell, highlighting the possible coding and non-coding mutations and the confidence in each mutation based on reading depth of the WGS.

2.2.2 Mutation Validation

To confirm the mutation in *Lama5*, DNA samples from the tails of affected G3 animals and C57BL/6J control were extracted using GE Healthcare Illustra BACC2 kit according to the manufacturer's protocol. The DNA was then amplified by polymerase chain reaction (PCR) using the following designed primers to amplify the relevant locus:

Forward 5'-AAACTCCAGGGGGTTGAAGC-3'

Reverse 5'-AGCGAAGGACCACTACTTGC-3'

Phusion High-Fidelity PCR Kit (New England BioLabs) was used as the polymerase. The reaction conditions for a 50 µl reaction were 10 µl 5X HF Reaction Buffer, 1 µl (10 nM) dNTPs, 2.5 µl 10 µM Forward Primer, 2.5 µl 10 µM Reverse Primer, 2 µl DNA, 0.5 µl (0.8 U) Phusion HiFi Polymerase, 31.5 µl of double-distilled water. Standard PCR settings were as follows: starting temperature 98°C for 30 seconds, then 40 cycles alternating at 98°C for 10 seconds, 63°C for 30 seconds, 72°C for 20 seconds and final elongation at 72°C for 10 minutes. Store at 8°C.

PCR products were purified using QIAquick PCR Purification Kit (QIAGEN) according to the manufacturer's instructions and sequenced with amplification primers using overnight Sanger sequencing by Source BioScience (UK). Results were analysed using Seqman pro (DNASTAR, USA).

2.2.3 Genotyping

The mice of the pedigree are routinely genotyped by performing LightScanner (Idaho Technology, USA) high-resolution DNA melting analysis with LCGreen and a LunaProbe

developed by the GEMS core facility using DNA extracted from ear biopsies. To distinguish between animals with different genotypes for the single point mutation, a 3' blocked oligonucleotide (LunaProbe) was designed so that sits directly over the single nucleotide polymorphisms (SNP) and exhaustive asymmetric PCR was performed. This creates two products, one is the full PCR product between the normal primers, and the other is a hybridised product with the probe bound to the opposite strand. Hybridised products were then heated on a LightScanner and the and the fluorescence emitted by bound LCGreen was monitored using a high-resolution melting curve analysis performed with the manufacturer's software. Because the probe matches the mutant sequence, it melts at a higher temperature than the wild-type (Figure 1.1). The result is a different shaped curve depending on the genotype.

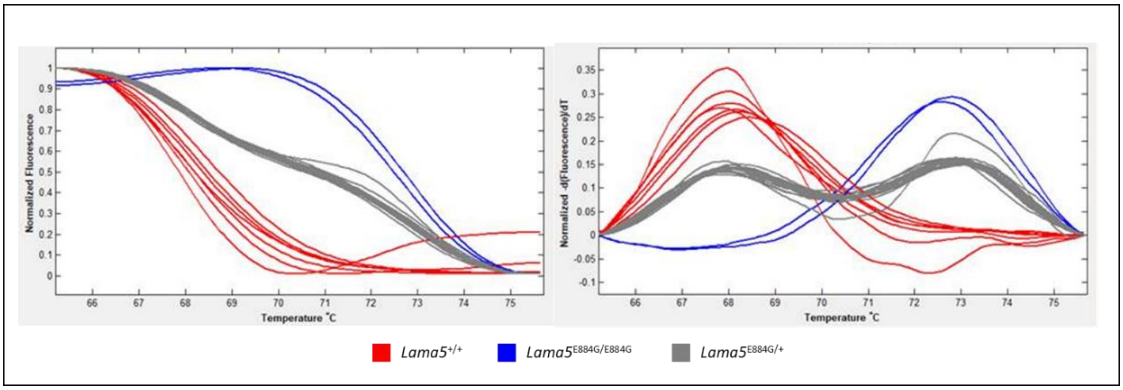

Figure 2.1. Example of a LightScanner output for the genotyping of the *Lama5*^{E884G} lines. Depending on the genotype, the melting curve has a different shape (in red wild-type, in blue homozygote for the E884G mutation, and in grey homozygote for the E884G mutation).

Primer pairs and probe are as follows:

Forward 5'- GGGTTGAAGCCAAAGCGTA -3' (highlighted in light blue)

Reverse 5'- ATGCCTGTCCCACTCAGATA -3' (highlighted in light red)

Probe-FWD 5'- CTCCCCTAGTTCCAGCCGCATGTG -3' (highlighted in light yellow)

Lama5 genomic sequence with primers and probe highlighted:

AGCAGCTCCCATCTCTGCACCAAGCCCAGGGAGGGGGCAGCATGGTTCACCTGGATAGCCATCA
TGTGTGCGTAGCCTCTCCAGCTAAAGTTCTCAAACTCCAGGGGGTTGAAGCCAAAGCGTACAGC
GTGGCCCTCGGGAGTGGCCGCCTCC(T/C)CTAGTTCCAGCCGCATGTGGTGCAGGTCTGGCAA
GTAGTGGTCCTTCGCTGGCCTGCCATGAAACAGGTATCTGAGTGGGACAGGCATGGCCCTACAT
GGCC

The reaction conditions for a 10 µl reaction were 5 µl of Hot Shot PCR master mix (Diamond, Clent Life Science, UK), 1 µl LCGreen, 0.5 µl reverse primer (20 ng/µl), 0.1 µl forward primer (20 ng/µl), 0.5 µl probe (20 ng/µl), and 0.9 µl double-distilled water. Standard PCR settings were as follows: starting temperature at 95oC for 2 min, then 55 cycles alternating at 95°C for 30 seconds, 60°C for 30 seconds, 72°C for 30 seconds. The hybridisation step was at 95°C for 30 seconds, 25°C for 30 seconds and 15°C for 30 seconds.

2.3 C3pde-*Lama5*^{E884G} Phenotyping and Characterization

2.3.1 Metabolic Caging and Urinalysis

A time course analysis using metabolic caging and terminal bleeds were performed on cohorts of homozygous and wild-type C3pde-Lama5^{E884G} mice at 7, 12, 15, 20 and 22 weeks of age. Mice were singly housed for overnight in metabolic cages (Techniplast) to collect urine for further analysis.

Urine was diluted 1:10 with double-distilled water, 10 µl of the diluted urine are combined with 2.5 µl of sample buffer (NuPAGE, Invitrogen), 1 NuPAGE Antioxidant reducing agent. Samples of 5 µl from three male wild-types, three male homozygous

and three female homozygous, were loaded onto sodium dodecyl sulfate-polyacrylamide gel electrophoresis (SDS-PAGE) precast gel (NuPAGE 4-12% Bis-Tris). As controls, 1 μg/μl and 2 μg/μl bovine serum albumin (BSA) was prepared in the same way and loaded, as well as 5 μl of SeeBlue Plus2 Pre-stained Protein Standard (Invitrogen) as size ladder. The SDS-PAGE was run for 1 hour at 200 V with MOPS running buffer (NuPAGE MOPS SDS Running Buffer 20X).

The gel was then stained with 25 ml of Quick Blue (Triple Red) on the shaker for 30 minutes.

2.3.2 Clinical Biochemistry Analysis of Plasma and Urine

Blood samples were obtained through retro-orbital sinus with a prior intraperitoneal injection of euthatal. Plasma was collected by centrifuging at 8000g, for 10 minutes at 4°C. Plasma was kept at °C and processed within a week.

Plasma concentrations of albumin, urea, creatinine, total cholesterol, HDL and LDL were measured on an AU400 Olympus analyser by the clinical chemistry core team at MRC Harwell.

2.3.3 Gene Expression Analysis

RNA was extracted from ~30 mg of kidney cortex using RNeasy Mini Kit (QIAGEN) following the manufacturer's protocol then the concentration was measured by using the NanoDrop (Thermo Fisher Scientific).

cDNA was synthesised using high capacity cDNA reverse transcription kit (Thermo Fisher Scientific). The RNA was diluted to a concentration of 200 ng/μL to form a total volume

of 10 µL and mixed with 2 µL of 10X RT Buffer, 0.8 µL of 25x dNTP mix (100mM), 2 µL 10x of RT random primers, 1 µL Multiscribe reverse transcriptase and 4.2 µL of Nuclease-free water. The reagents so combined were run on a PCR block using the following program: 25°C for 10 minutes, 37°C for 120 minutes and 85°C for 5 minutes. Store at 4°C.

The cDNA synthesised was diluted 1:50 with double-distilled water to obtain 2ng/µL cDNA for TaqMan assay (Thermofisher). The reaction conditions for a 15 µL reaction were 10 µL of 2X TaqMan fast universal PCR master mixes, 1 µL of the target genes and reference genes 20x TaqMan Assay (Table 2.1), 4 µL of double-distilled water. The mix was dispensed in MicroAmp Fast Optical 96-Well Reaction Plate (Thermofisher) and 5 µL of 2 ng/µL cDNA were added, three technical replicates for each sample to isolate sources of variation in measurements, and three biological replicates for each genotype were used. The plate was sealed with an optically clear adhesive lid and run on a 7500 fast real-time PCR System (Applied Biosystems™). Results were analysed using Taqman 7500 software. Alongside the gene of interested, three different housekeeping genes (*Hprt1*, *Tbp* and *Gapdh*) were assessed and the one with a more even expression across all the samples (*Hprt1*) was chosen to normalise the expression of the target genes.

Gene	Role	Taqman Probe
Nphs1	Slit diaphragm	Mm00497828_m1
Nphs2	Slit diaphragm	Mm01292252_m1
Podx1	Apical domain	Mm00449829_m1
Pdpn	Apical domain	Mm01348912_g1
Lama5	Extracellular matrix	Mm01222029_m1
Lama2	Extracellular matrix	Mm00550083_m1
Lama1	Extracellular matrix	Mm01226102_m1
Agrn	Extracellular matrix	Mm01264855_m1
Itga3	Laminin receptor	Mm00442910_m1
Itgb1	Laminin receptor	Mm01253230_m1
Lu	Laminin receptor	Mm00522338_m1
Actn4	Integrin signall mediators	Mm00502489_m1
Tln1	Integrin signall mediators	Mm00456997_m1
Fermt2	Integrin signall mediators	Mm00600590_m1
Pxn	Integrin signall mediators	Mm00448533_m1
Ilk	Integrin signall mediators	Mm01274281_g1
Fak	Integrin signall mediators	Mm00433209_m1
Src	Integrin signall mediators	Mm00436785_m1
Hprt1	Endogenous control	Mm00446968_m1
Gapdh	Endogenous control	Mm99999915_g1
Tbp	Endogenous control	Mm00446973_m1

Table 2.1. List of genes and associated Taqman probes used in the gene expression study.

2.3.4 Immunoblotting

Kidneys were obtained from terminal wild-type and *Lama5*$^{E884G/E884G}$ animals, snap frozen at the time of dissection and stored at -80°C until required.

Proteins from a whole kidney were extracted by homogenising the tissue in RIPA buffer (150mM NaCl, 1% NP-40, 0.5% DOC, 0.1% SDS, 50mM Tris, pH 7.5) containing phosphatase (Roche) and protease (Roche) inhibitors in Precellys CK28 homogenisation tubes. Protein concentration was measured by Bradford assay and measured on a 96 wells Nunc plate (Thermo Fisher). Bovine serum albumin (BSA) at a concentration of 1.4 mg/mL, 1 mg/mL, 0.5 mg/mL, 0.25 mg/mL, 0.125 mg/mL and 0.06 mg/mL were used as standards.

LDS sample buffer (Invitrogen) and reducing agent (Invitrogen) were mixed to 20 µg of proteins and loaded in an SDS-PAGE 4-12% Bis-Tris gel (Invitrogen). Electrophoresis was performed for 200 V for 60 minutes at room temperature.

The proteins were transferred to hybond polyvinylidene difluoride (PVDF) membrane (GE Healthcare) using an X-Cell Blot Module (Invitrogen). After the transfer, PVDF membranes were blocked in 5% w/v milk powder in phosphate buffered saline (PBS) with 0.1% Tween-20 (PBS-T) for 60 minutes with gentle shaking. Primary antibodies (Appendix 8.1.1), anti-integrin β1 (1:1000), anti-ILK (1:1000), anti-paxillin (1:5000), anti-CDC42 (1:1000) and anti-RhoA (1:10000) were in 5% w/v milk powder in PBS-T for 60 minutes with gentle shaking. The membranes were washed for 3 times in 0.1% PBS-T. Secondary antibodies (Appendix 8.1.2) diluted in 5% w/v milk powder in 0.1% PBS-T for 60 minutes at room temperature, and then washed again in 0.1% PBS-T protected from light. The membranes were then dried in the dark.

Fluorescent blots were scanned using a LI-COR Odyssey Cl-x or SA scanner (LI-COR Biosciences) to visualise bound antibodies. Image Studio Lite software (LI-COR Biosciences) is used for quantification and analysis (Median, 3-pixel border background). Protein expression target proteins has been normalised to the expression of wither α-tubulin (1:2000) or β-actin (1:3000).

2.4 *In Vitro* Analysis of Laminin Assembly

2.4.1 Laminin α5 Clone Propagation and Site-Directed Mutagenesis

Full-length *Lama5* clone in pSK+II vector, kindly gifted by Professor Jeff Miner, was transformed in XL-10 gold E.coli (Agilent) for 30 minutes and heat shocking at 42°C for 30 seconds, plated on 100µg/mL ampicillin Luria-Bertani (LB) agar plates and incubated at 37°C overnight. Colonies were picked and grown overnight at 37°C with shaking in 100µg/mL liquid LB broth. Colonies are picked and grown for a further 24 hours in LB broth.

DNA was extracted using QIAprep Spin Miniprep Kit (Qiagen) according to manufacturer's protocol. Briefly, bacteria were pelleted, lysed and centrifuged to pellet cell membranes and organelles. The supernatant was applied to a spin column and DNA bound by centrifugation. Bound DNA was briefly washed before being eluted in 10mM Tris buffer.

pSK+II-*Lama5* has then used as a template for site-directed mutagenesis of the E884G mutation using Q5 site-directed mutagenesis kit (NEB) and the following primers to introduce the point mutation:

Forward 5'-CTGGAACTAGgGGAGGCGGCC-3'

Reverse 5'-CCGCATGTGGTGCAGGTC -3'

PCR was performed according to manufacturer's protocol with an initial denaturation of 98°C followed by 25 cycles of 98°C for 10 seconds, 70°C for 30 seconds and 72°C for 2 minutes.

Kinase, Ligase and DpnI (KLD) reaction were performed according to the kit instructions for 5 minutes at room temperature. Mutagenised vector was transformed into 50µL of NEB-5α competent cells. 950 µL of super optimal broth (SOC) was added to the bacteria and then incubated for 1 hour at 37°C with shaking. 100 µl were plated on 100µg/mL ampicillin LB agar plates overnight. DNA is again extracted using plasmid midi kit (Qiagen). Sanger sequencing using the following primers confirmed the presence of the mutation:

Forward 5'-AAACTCCAGGGGGTTGAAGC-3'

Reverse 5'-AGCGAAGGACCACTACTTGC-3'

2.4.2 Cloning of the Laminin α5 Chain Short Arm

2.4.2.1 *Amplification, Insertion and Transformation*

Different fragments of the laminin α5 chain were cloned following the protocols of the OPPF (https://www.oppf.rc-harwell.ac.uk/OPPF/protocols/): LN-LEa, LN-L4a-LEb, LN-L4a-L4b-LEc and L4a.

pSK+II-*Lama5* and pSK+II-*Lama5*-E884G vectors were used as template to amplify the targeted ORFs. Three different expression vectors were used: pOPINTTGneo, with a C-terminus His tag and internal signal sequence, pOPINTTGneo-Fc, with a C-terminus His and FC tags and internal signal sequence, and pOPINEneo, with a C-terminus His tag. The sequence of the vectors can be found at https://www.oppf.rc-harwell.ac.uk/OPPF/protocols/cloning.jsp.

ORFs were amplified using Phusion Flash (Thermoscientific) or KOD Xtreme™ Hot Start DNA Polymerase (Novagen). For Phusion Flash, a reaction of 50 µl was set up as follows:

25 µl of Phusion Flash Master Mix, 3 µl of 10 µM of forward primer (Table 2.2), 3 µl of 10 µM of reverse primer (Table 2.2), 2 µl of ~10-20 ng/ µl template plasmid, and 17 µl of sterile water. Standard PCR settings were as follows: starting temperature at 98°C for 10 seconds, then 29 cycles alternating at 98°C for one second, 60°C for 5 seconds, 68°C for 15 seconds per kb, and then 68°C for 2 minutes.

For KOD Xtreme™ Hot Start DNA Polymerase, a reaction of 50 µl was set up as follows: 25 µl of 2X KOD Hot Start Buffer, 10 µl of dNTP mix, 1 µl of KOD Hot Start, 3 µl of 10 µM of forward primer (Table 2.2), 3 µl of 10 µM of reverse primer (Table 2.2), 2 µl of ~10-20 ng/ µl template plasmid, and 6 µl of sterile water. Standard PCR settings were as follows: starting temperature at 94°C for 2 min, then 29 cycles alternating at 98°C for 10 seconds, 60°C for 30 seconds, 68°C for 1 minute per kb, and then 68°C for 2 minutes.

Ligation in the destination vectors was carried out using the In-Fusion® HD EcoDry™ Cloning Plus (Takara). Briefly, 1µl (100ng) of the appropriate linearised pOPIN vector (provided by the OPPF) was added to a 10-250 ng of PCR product. The mix was incubated for 30 minutes at 42°C and the reaction stopped diluting the reaction with 40 µl of Tris EDTA (TE) buffer. The In-Fusion reaction was transformed into OmniMaxII competent cells (Thermofisher) heat shocking the cells for 30 seconds at 42°C. After being incubated for one hour in 1.2 mL of SOC medium, 20 µl of cells were plated on 50 mg/mL of carbenicillin LB agar plates and then incubated overnight at 37°C. The day after, colonies were picked and grown overnight at 37°C. The plasmid mini-preps were performed on the Bio-Robot 8000 (Qiagen).

All experiments were performed in triplicates.

Fragment	Vector	Primers
LN-LEa	pOPINTTGneo	Forward: gcgtagctgaaaccggcCGCACTCCCGGGGGCGATGG Reverse: gtgatggtgatgtttCTTTGGTTCACAGCCTTGACCCAGGG
LN-LEa	pOPINTTGneo-Fc	Forward: gcgtagctgaaaccggcCGCACTCCCGGGGGCGATGG Reverse: cagaacttccagtttCTTTGGTTCACAGCCTTGACCCAGGG
LN-LEa	pOPINEneo	Forward: aggagatataccatgGCGAAGCGCGGAGGGCAGCT Reverse: gtgatggtgatgtttCTTTGGTTCACAGCCTTGACCCAGGG
LN-L4a-LEb	pOPINTTGneo	Forward: gcgtagctgaaaccggcCGCACTCCCGGGGGCGATGG Reverse: gtgatggtgatgtttGCGCTCTGTGGCCCCGAAAC
LN-L4a-LEb	pOPINTTGneo-Fc	Forward: gcgtagctgaaaccggcCGCACTCCCGGGGGCGATGG Reverse: cagaacttccagtttGCGCTCTGTGGCCCCGAAAC
LN-L4a-LEb	pOPINEneo	Forward: aggagatataccatgGCGAAGCGCGGAGGGCAGC Reverse: gtgatggtgatgtttGCGCTCTGTGGCCCCGAAACAGA
LN-L4a-L4b-LEc	pOPINTTGneo	Forward: gcgtagctgaaaccggcCGCACTCCCGGGGGCGATGG Reverse: gtgatggtgatgtttTTCACAGTGTATGCCATGGCCCCC
LN-L4a-L4b-LEc	pOPINTTGneo-Fc	Forward: gcgtagctgaaaccggcCGCACTCCCGGGGGCGATGG Reverse: cagaacttccagtttTTCACAGTGTATGCCATGGCCCCC
LN-L4a-L4b-LEc	pOPINEneo	Forward: aggagatataccatgAGCGCACCGGGCGCTCTTGG Reverse: gtgatggtgatgtttTTCACAGTGTATGCCATGGCCCCC
L4a	pOPINTTGneo	Forward: gcgtagctgaaaccggcTGCCGCCCTAACACCCAAGGACCC Reverse: gtgatggtgatgtttCGTGGGGCTTACGGCACCCACCT
L4a	pOPINTTGneo-Fc	Forward: gcgtagctgaaaccggcTGCCGCCCTAACACCCAAGGACCC Reverse: cagaacttccagtttCGTGGGGCTTACGGCACCCACCT

Table 2.2. List of primers used to amplify the different fragments of the LAMA5 short arm.

2.4.2.2 *Expression in Mammalian Cells for Immunoblotting*

HEK-293T (ECACC 12022001) cells were maintained in Dulbecco's modified Eagle's medium (DMEM), supplemented with 10% foetal bovine serum (FBS) and 1x penicillin/streptomycin, and kept in a 5% CO_2, 37°C environment. When required, cells are split 1:20-1:40 by first washing with pre-warmed PBS, and detached using 0.05% trypsin.

OPPF transfection and immunoblotting protocol. HEK-293T cells were plated in 24-well plates at a concentration of 1.5-2*10^5 cells/ml, 16-24 hours prior transfection. DNA vectors were transfected using 2 µl of GeneJuice (EMD Millipore) per 1 µg of plasmid DNA, mixed with 60 µl serum-free DMEM. After 10 minutes incubation at room temperature, the DNA/GeneJuice cocktail was added to the cells and incubated at 37°C in a 5% CO_2 environment.

After 72 hours, the conditioned medium was harvested and centrifuged for 15 minutes at 6000 g at 4°C, and then 20 µl were used for immunoblotting as previously described. In the meantime, cells were lysed with lysis buffer (NPI-10, DNase and protease inhibitors), and 20 µl used for immunoblotting as previously described.

MRC Harwell transfection and immunoblotting. HEK-293T cells were plated in 6-well plates at a concentration of $2.5x10^5$ cells/well, 16-24 hours prior transfection. DNA vectors were transfected using per ~1 µg of plasmid DNA, or in 6-well plates using 4 µl of jetPRIME (Polyplus) reagent per 2 µg of plasmid DNA, mixed with 200 µl of jetPRIME buffer. The mixture was incubated at room temperature for 10 minutes, then added dropwise to the cell medium and incubated at 37°C with 5% CO_2 for 72 hours. Conditioned medium was harvested and clarified for 15 minutes at 6000 g at 4°C. A 20 µl sample was mixed to LDS buffer and reducing agent and used for immunoblotting as previously described. The cells were lysed using x1 LDS buffer with added proteinase inhibitors, then 20 µl were loaded onto an SDS-PAGE gel and run as with immunoblotting.

2.4.3 Cloning of the Full-Length Laminin α5 Chain

2.4.3.1 *Amplification, Insertion and Transformation*

Using pSK+II-*Lama5* and pSK+II-*Lama5*-E884G vectors as templates, full-length laminin α5 chain was cloned into a pCMV6-AC-His vector. PCR was performed using Phusion polymerase with the following primers:

Forward: 5'-AGATCTGCCGCCGCGATCGCATGGCGAAGCGCGGA-3'

Reverse 5'-GTTTCTGCTCGAGCGGCCGCTCAATGCCAAAGTAGCGGG -3'

PCR is performed using a touchdown protocol with an initial denaturation of 95°C for 10 minutes followed by cycles of 95°C for 10 seconds, 62°C (2x), 60°C (2x), 58°C (2x), 56°C (15x) for 20 seconds and 72°C for 8 minutes with a final elongation step of 10 minutes. PCR products were run of a 2% agar gel and the band of the right size (~11.3 kb) was purified using QIAquick gel extraction purification kit (Qiagen) according to manufacturer's protocol of binding DNA to a spin column, washing briefly and finally eluting in 10mM Tris buffer. pCMV6-AC-His was linearised with a double digestion using SgfI (Promega) and MluI (Promega) restriction enzymes for four hours at 37°C.

Purified PCR products were ligated onto linearised pCMV6-AC-His using Quick-Fusion cloning kit (Biotool). Briefly, a reaction of 10 µl with 20-100 linearised vector, 10-100 ng of the insert, 1 µl of fusion enzyme and 2 µl of 5X fusion buffer was set up and incubated for 30 minutes at 37°C. The resulting mix was transformed into NEB-5α competent cells as previously described.

2.4.3.3 *Expression in Mammalian Cells*

HEK-293 cells stably expressing human *LAMB1* (HA-tagged) and human *LAMC1* (FLAG-tagged) were a kind gift of Prof Peter Yurchenco and Dr Karen McKee[223] and were maintained in DMEM, supplemented with 10% FBS, 500 µg/ml G418 (Sigma) and 100 µg/ml zeocin (Invitrogen), and kept in a 5% CO_2, 37°C environment. When required, cells are split 1:5-1:10 by first washing with pre-warmed PBS, and detached using 0.05% trypsin for a minute.

Stable laminin β1γ1 HEK-293 cells were plated in 6-well plates at a concentration of $5x10^5$ cells/well, 16-24 hours prior transfection. pCMV6-AC-His-*Lama5* and pCMV6-AC-

His-*Lama5*-E884G were transfected using jetPRIME. After 72 hours, conditioned medium was harvested and cells lysed. Samples of medium and cell lysate were used for immunoblotting experiments.

2.5 B6-*Lama5*^{E884G} Phenotyping and Characterization

2.5.1 Metabolic Caging and Urinalysis

A time course analysis using metabolic caging and terminal bleeds were performed on cohorts of homozygous and wild-type LAMA5-E884G-B6-IC mice at 5, 15 and 25 weeks. Mice were singly housed for 24 hours in metabolic cages (Techniplast) to collect urine for analysis and to measure water intake and urine output.

Urine creatinine was quantified using an AU400 Olympus analyser. Urinary protein concentration was quantified using Bradford protein assay (Biorad) using BSA at a concentration of 1.4 mg/mL, 1 mg/mL, 0.5 mg/mL, 0.25 mg/mL, 0.125 mg/mL and 0.06 mg/mL as standards, and then normalised to urine creatinine.

2.5.2 Clinical Biochemistry Analysis of Plasma

Blood samples and plasma analysis were performed as described in 6.3.2

2.5.3 Light and Electron Microscopy

Kidneys were collected from male wild-type and male *Lama5*$^{E884G/E884G}$ mice at 5, 15 and 25 weeks of age to investigate the progression of the glomerulopathy phenotype.

For light microscopy, kidneys fixed in 10% neutral buffered formaldehyde were embedded in paraffin wax and sectioned at 5 µm using a Finesse ME microtome (Thermo Electron). Kidney sections were stained with haematoxylin and eosin (H&E), periodic acid-Schiff (PAS) and Masson's trichrome (MT) stain.

For TEM, $1mm^3$ cubes of kidney cortex were fixed in 3% glutaraldehyde and 4% formaldehyde in 0.1 M PIPES and post-fixed with 1% osmium tetroxide in 0.1 PIPES. After serial dehydration in increasing concentration of ethanol, the blocks were stained with 2% uranyl acetate for 20 minutes. The tissue was then embedded in epoxy resin (TAAB) and polymerised overnight at 60˚C. Semithin sections of 500 nm were cut and stained with toluidine blue staining to make sure of the presence of glomeruli in the tissue block (Figure 2.2). Golden ultrathin sections (70-80 nm) were cut with a diamond knife and collected them on copper/palladium grids. For better contrast, grids were stained with lead citrate. The ultrathin sections were visualised on a Hitachi HT7700 transmission electron microscope.

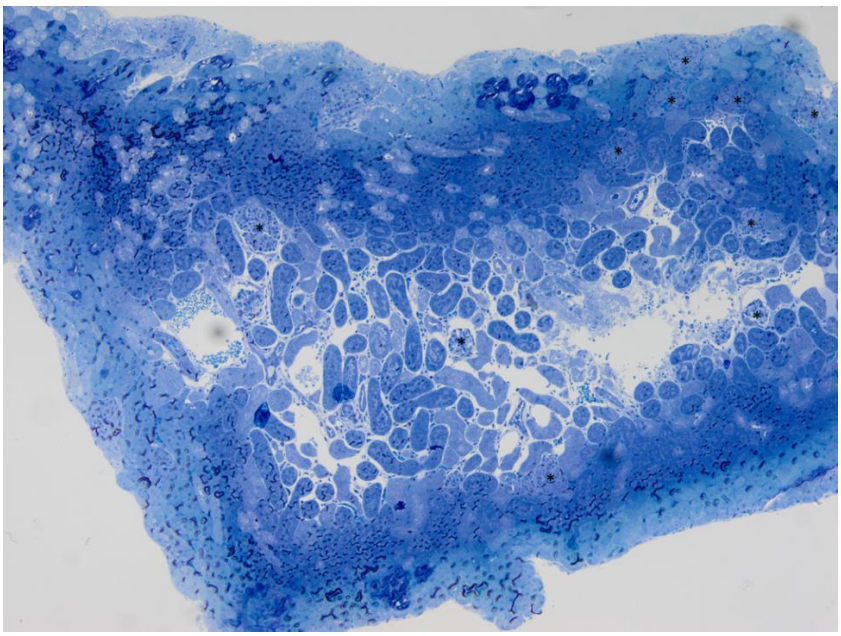

Figure 2.2. Representative histology of a semithin section. Sections were cut and stained to make sure that at least four glomeruli (asterisk) were present in the block.

For SEM, 1mm^3 cubes of kidney cortex were fixed in 3% glutaraldehyde and 4% formaldehyde in 0.1 M PIPES and post-fixed with 1% osmium tetroxide in 0.1 PIPES. Samples were then dehydrated through increasing strength of ethanol solutions and critical point dried using an Emitech K850 (EM Technologies LTD). Three specimens per animals were then mounted on stubs using silver paint (Agar Scientific) and sputter coated with platinum using a Quorum Q150T sputter coater (Quorum Technologies). The specimens were untimely visualised with a JEOL LSM-6010 (Jeol Ltd.).

2.5.4 Immunofluorescence

Primary antibodies (Appendix 8.1.1) rabbit anti-mouse laminin α5 (clone 1586) [224], rabbit anti-mouse laminin β1 (clone 1065) and rabbit anti-mouse laminin β2 (clone 1117) [225] were generously provided by Prof Jeff Miner (Washington University, USA). Mouse anti-human active integrin β3 (clone WOW-1) [226] mouse anti-human active integrin β3 (clone AP5) [227] were a kind gift from Prof Sanford Shattil (UC San Diego, USA) and Dr Peter Newman (Blood Center of Wisconsin, USA) respectively.

For immunofluorescence analysis, kidneys were fixed in Tissue-Tek® (Sakura) using isopentane on dry ice. Cryosections of 10 µm of different genotype were placed on the same slide kept at -20°C until needed. Sections were fixed with ice-cold acetone for 10 minutes at 20˚C, then blocked using 5% goat serum (normal serum) in PBS for 30 minutes at room temperature. The sections were then stained with different primary antibodies at 4˚C overnight and Alexa-conjugated secondary antibody (Appendix 8.1.1) for 30 minutes at room temperature. Images were taken using a Zeiss LSM 700 inverted

confocal microscope on the same day using the same pinhole, gain, offset and laser intensity using the 63x NA 1.4 plan-apochromat oil-immersion objective.

2.5.5 Murine Glomeruli Isolation and Protein Extraction

The glomeruli from 15 weeks (wild-type n= 5 and homozygotes n=5) and 25 weeks (wild-type n= 5 and homozygotes n=4) old male mice were isolated following a modified Dynabeads-based protocol previously described [228]. The mice were perfused with Dynabeads® M-450 Tosylactivated (Thermofisher) diluted in PBS, the kidneys collected were then minced and the glomeruli were gathered by a Magnetic Particle Concentrator DynaMag™-2 (Thermofisher). For the glomeruli used for fractionated protein extraction, the incubation with collagenase I at 37˚C was skipped to avoid digestion of the ECM component of the glomerulus.

The isolated glomeruli were incubated for one hour in ice-cold TB buffer (10 mM Tris, 150 mM NaCl, 25 mM EDTA, 1%Triton X-100) then centrifuged at 14000x g for 10 minutes to obtain cellular fraction 1. The remaining pellet was incubated for one hour in ice-cold EB buffer (20 mM ammonium hydroxide, 0.5% Triton X-100) then centrifuged at 14000x g for 10 minutes to obtain cellular fraction 2. The remaining pellet was incubated for 30 minutes in deoxyribonuclease-ribonuclease buffer (25 µg/mL DNase, 25 µg/mL RNase) to degrade DNA and RNA, then centrifuged at 14000x g for 10 minutes to obtain nuclear fraction. The final ECM enriched pellet was resuspended in sample buffer (7% SDS, 30% glycerol, 0.2 M Tris-HCl pH 6.8, 0.01% bromophenol blue, 10% β-mercaptoethanol) to obtain the ECM fraction [229]. All the steps were carried on ice or at 4˚C.

2.5.6 Mass Spectrometry Analysis

The samples obtained by protein extractions were prepared for liquid chromatography-tandem MS analysis. The two cellular component fractions were combined and run, along with the ECM fraction, on a Bis-Tris 4-12% SDS-PAGE for 3 minutes at 200 V. The gels were then stained with Coomassie staining to visualise the protein samples. After washing with double-distilled water, the "gel top" proteins were cut into slices and then in 1 mm^3 pieces, and then given to the MS facility core at the University of Manchester for in-gel proteolytic digestion, offline peptide desalting and actual MS run. All the samples were run blindly, in a random sequence of genotype and age.

Quantitative analysis was carried out using the software using Progenesis LCMS (Non Linear Dynamics Ltd) in association with the use of Mascot (Matrix science) used to identify the proteins. Statistical analysis was performed on proteins identified by at least three unique peptides.

2.5.7 Immunoblotting

Immunoblotting was performed as described in 6.3.4.

For rat anti-mouse integrin β1 clone 9EG7 (1:100, BD Pharmingen) proteins were run on SDS-PAGE under non-reducing conditions.

CHAPTER 3

Identification of Chronic Renal Disease Resulting from a Mutation in *Lama5*

3. Identification of Chronic Renal Disease Resulting from a Mutation in *Lama5*

3.1 Initial Identification

3.1.1 The Harwell Ageing Screen

MRC Harwell has been a pioneer of ENU-based phenotype-driven screens since the 1990s [211]. To study recessive mutations causing age-related or late-onset diseases, a large-scale mouse screen, the Harwell ageing screen, was established at MRC Harwell Institute. A total of 157 pedigrees, each comprising around 100 mice, entered the phenotyping pipeline and a total of 105 distinct mutant lines were identified in 72 of the pedigrees [222]. The G3 mice were periodically put through a variety of phenotyping procedures to assess vision, hearing, behaviour, body composition, musculoskeletal abnormalities, defects in heart conduction and different organ profiles by clinical chemistry analysis (Figure 3.1). The pipeline ran from 12 weeks to 18 months of age. After being euthanized and terminally bled, selected mice were sent for a complete pathological examination of tissues to assist in the confirmation or determination of a phenotype [222].

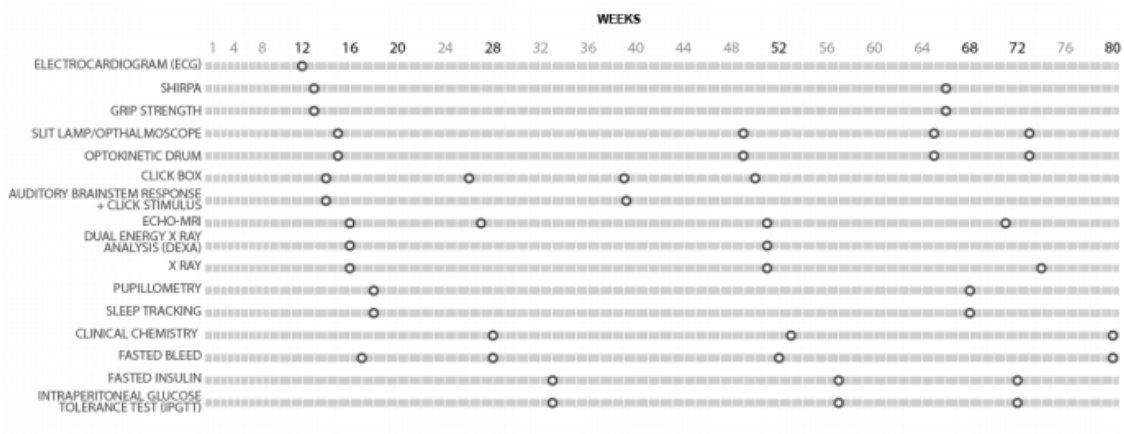

Figure 3.1. Graphic display of the Ageing Screen pipeline: the mice were phenotyped at the time points outlined in the figure (circles). In addition to the tests of the phenotype pipeline, mice are weighed every 3 months up until 12 months of age and then monthly from 12 months onwards. Image adapted from Potter *et al.* [222].

3.1.2 Pedigree MUTA-PED-C3pde-205

During the analysis of the clinical chemistry data from the pedigree MUTA-PED-C3pde-205 (MPC-205) at 6 months of age, six mice out of 70 were identified with higher levels of urea, creatinine and amylase and lower levels of albumin than their littermates (Figure 3.2 A and D). Based on the breeding scheme used to generate the G3 screening pedigrees (described in chapter 2, section 2.1), the expected ratio of homozygous mice for the causative mutation is 1:8 mice. Chi-square test was used to establish whether a normal Mendelian inheritance was conserved. Chi-squared equals 0.988 with one degrees of freedom and a two-tailed P value of 0.03203, indicating a normal ratio between observed (6 putative homozygotes and 64 heterozygotes/wild types) and expected mice (8.75 homozygotes and 61.25 heterozygotes/wild types). The clinical chemistry results indicated kidney impairment but the mice did not show any other signs of poor health or any other abnormal readings on the parameters analysed during the routine panel. Total lactate dehydrogenase (LDH) plasma levels, a marker of tissue

damage, appeared to be normal. Parameters such as alkaline phosphatase (ALP), alanine transaminase (ALT) and aspartate aminotransferase (AST) were within the normal range, suggesting that liver function is maintained at normal levels. As liver function appears to be normal, decreased plasma albumin was attributed to kidney impairment.

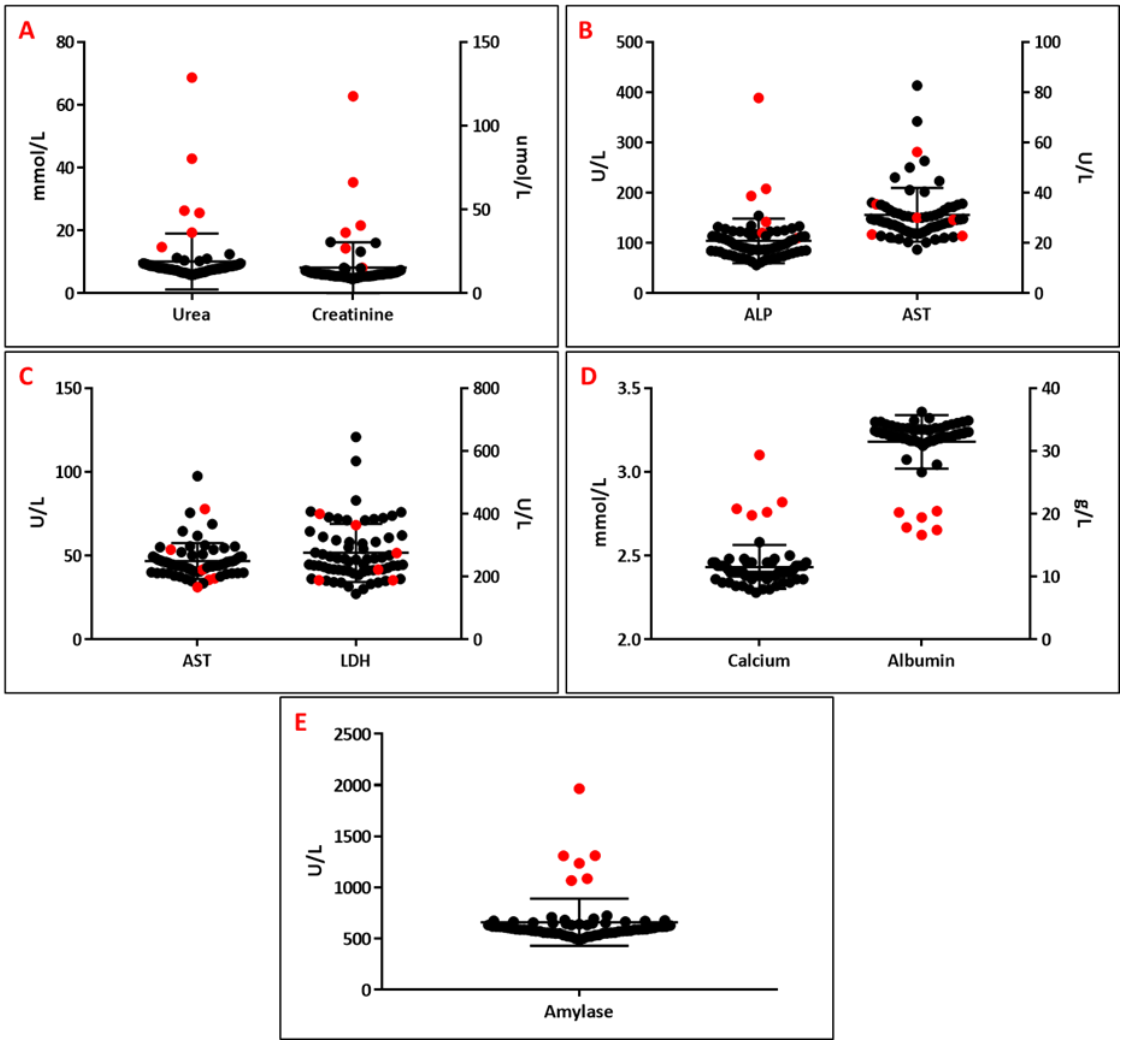

Figure 3.2. Clinical chemistry analysis of the pedigree MUTA-PED-C3pde-205 at 6 months of age. Outliers (in red) exhibit higher levels of urea, creatinine (**A**) and amylase (**E**), and lower levels of albumin (**D**) when compared to the other mice of the pedigree. The same mice also exhibit hypercalcemia (**D**), the common secondary effect of kidney impairment due to an abnormal phosphorus/calcium metabolism. The mice did not show altered liver function or tissue damage (**B** and **C**).

The affected mice did gradually deteriorate and were eventually culled at 9 months of age for welfare concerns, including loss of weight and piloerection, or died suddenly.

The bodies were potted in 10% formalin and sent for a default post-mortem analysis. The resident pathologist could not see any histopathological lesion in any organs but the kidneys, which exhibited signs of CKD (Figure 3.3).

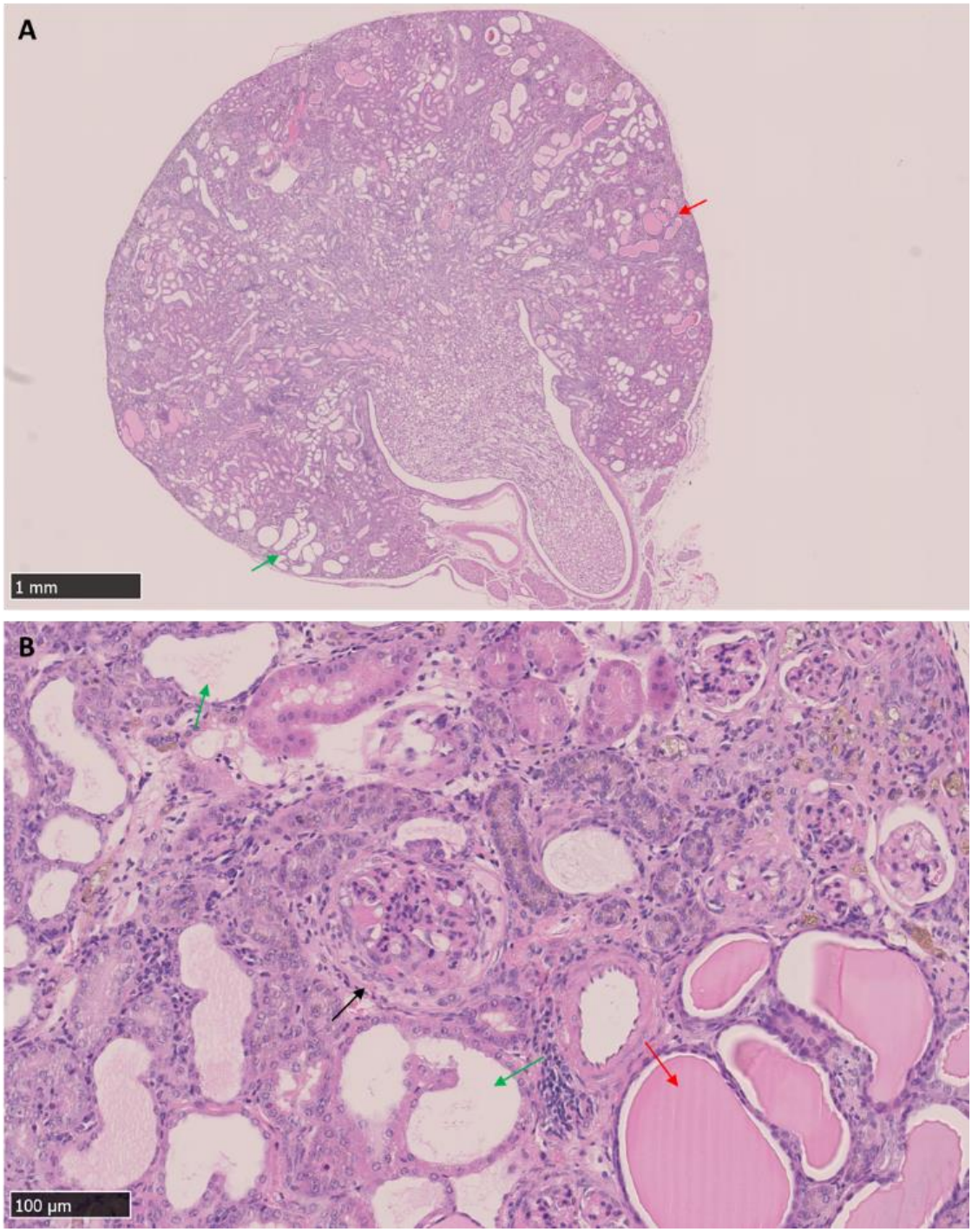

Figure 3.3. H&E stained sections of kidneys of one of the outliers identified in the pedigree MPC-205. The affected mice showed typical lesion of CKD: fibrosis of the Bowman's capsule (black arrow), dilated tubules (green arrows) with protein casts (red arrows). Scale bar represents 1 mm (**A**) and 100 µm (**B**).

Using the elevated kidney markers and the CKD histological lesions as the affected traits, samples of five affected mice and a control littermate were sent for mapping using the Illumina Golden Gate "Mouse Medium Density (MD) Linkage Panel" [230]. This panel includes 1,449 SNPs to have a uniform distribution across the mouse genome with a density of around three SNPs per five megabases, of which at least one is informative for crosses involving C57Bl/6J mice [230]. Since the ENU treatment is firstly carried out on the C57BL/6J G0, the region(s) carrying the causative mutation should be either homozygous (for recessive alleles) or heterozygous (for dominant alleles) for C57BL/6J when compared with C3H-C3pde SNPs in the same region. The chromosomal region containing the possible causative mutation was mapped to chromosome 2, in a region between 171 Mb and the end of the chromosome (Figure 3.4), as this was the only region where all the affected were homozygous for C57BL/6J. This region, of approximately 10 Mb, contains 242 genes (Appendix 8.2). The best candidate was identified in the gene coding for laminin α5 chain, *Lama5*, a major component of the GBM involved in both glomerular development and preservation of the GFB.

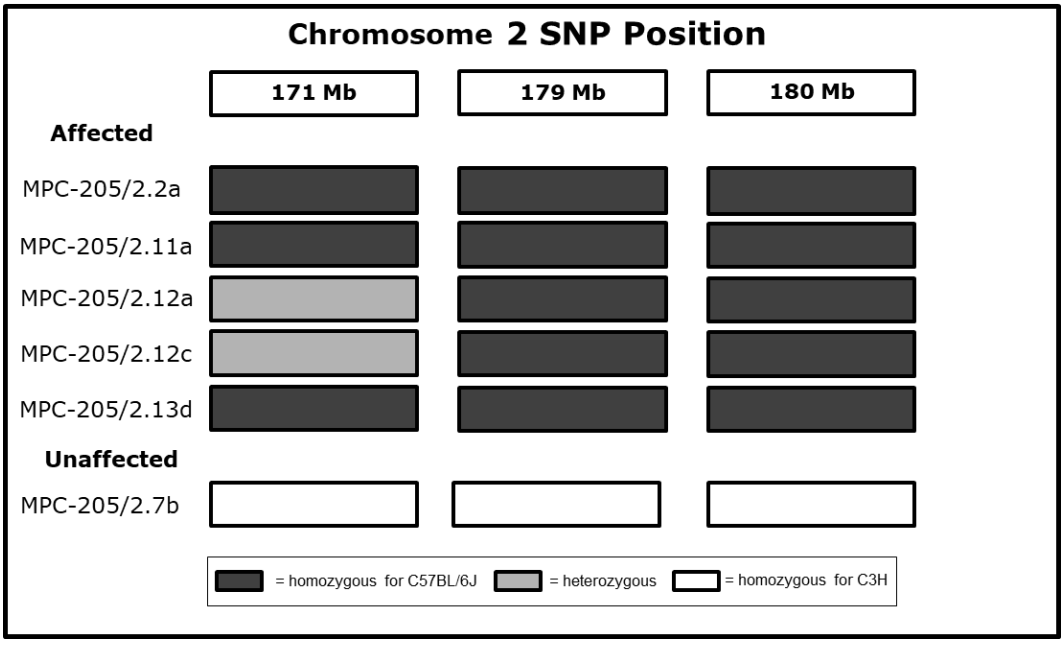

Figure 3.4. Graphic display of the candidate region on chromosome 2. DNA from five affected mice and one unaffected control was sent for mapping: ENU treatment is carried out on the male G0 C57BL/6J hence the region carrying the causative mutation is homozygous for C57BL/6J when compared with C3H-C3pde6b+ (C3H) SNPs.

To identify the mutation underlying the observed phenotype, WGS analysis performed by Wellcome Trust Centre for Human Genomics sequencing facility and analysed by the MRC Harwell bioinformatics team on the DNA from the G_1 pedigree founder. Using a scoring system based the read depth, a high confidence score was given to variants observed in a number of reads, on the contrary variants that were only found in a one or low numbers of reads was assigned a low confidence score (meaning that the variant is more likely to represent an error rather than a real mutation). This analysis identified 23 mutations in the candidate region, five of which were high confidence. Four of the high confidence mutations were intragenic variants, the fifth mutation was a coding mutation in *Lama5* mutation (Table 3.1).

The candidate mutation, in exon 22, resulted in a missense variant consisting of an A to G transition at nucleotide 2651. The nucleotide change results in a glutamic acid (E) to a

glycine (G) substitution at amino acid 884 in the LAMA5 protein. Sanger sequencing of DNA from an affected mouse and C57BL/6J wild-type control confirmed the A to G transition (Figure 3.5 A).

Chromosome	Position	Reference	Alteration	Functional Class	Gene Description	Gene Name
chr2	174640611	A	G	upstream_gene_variant	zinc finger protein 831	Zfp831
chr2	180630538	T	C	intron_variant	transcription factor-like 5 (basic helix-loop-helix)	Tcfl5
chr2	178110353	C	T	intergenic_variant	.	.
chr2	180827429	C	T	upstream_gene_variant	predicted gene 14340	.
chr2	178110363	T	C	intergenic_variant	.	.
chr2	179906554	T	A	intergenic_variant	.	.
chr2	181242002	T	C	5_prime_UTR_variant	cDNA sequence BC006779	BC006779
chr2	179379742	T	A	intergenic_variant	.	.
chr2	173488306	T	C	intergenic_variant	.	.
chr2	179187050	A	G	intergenic_variant	.	.
chr2	174153756	T	A	intron_variant	predicted gene 10714	.
chr2	178641261	T	C	intergenic_variant	.	.
chr2	180023388	T	C	upstream_gene_variant	LSM14 homolog B (SCD6, S. cerevisiae)	Lsm14b
chr2	173944795	C	T	intergenic_variant	.	.
chr2	179906558	T	A	intergenic_variant	.	.
chr2	181246554	C	T	upstream_gene_variant	cDNA sequence BC006779	BC006779
chr2	173944800	C	T	intergenic_variant	.	.
chr2	179252099	T	C	intergenic_variant	.	.
chr2	179381932	T	A	intergenic_variant	.	.
chr2	178818573	T	A	intergenic_variant	.	.
chr2	180196271	A	G	missense_variant	laminin, alpha 5	Lama5
chr2	174505629	T	C	intergenic_variant	.	.
chr2	178797493	G	T	intergenic_variant	.	.

Table 3.1. List of the mutations included in the candidate region on chromosome 2. In light grey are shown the mutations with a low confidence score, in dark grey the mutations with a medium confidence score, in yellow the mutation with a high confidence score. *Lama5*^{E884G} missense variant is the only coding high confidence mutation resulting from the WGS analysis.

The glutamic acid residue is well conserved back to Drosophila (Figure 3.5 B) and is part of the L4a domain on the short arm of the laminin α5.

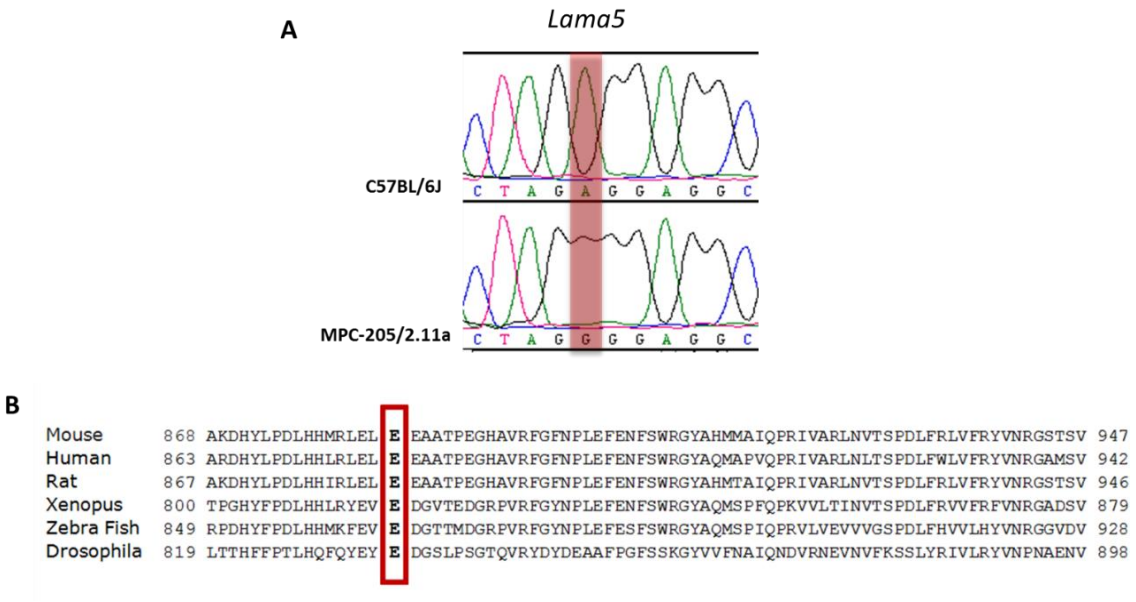

Figure 3.5. Result of the Sanger sequencing of C57BL/6J control and an affected mouse from the MPC-205 mouse line used to validate the mutation in *Lama5* (**A**). Comparison between the amino acid sequence of different species shows how the E884 residue is conserved down to Drosophila (**B**).

In order to assess the effect of this amino acid substitution, different web-based protein prediction algorithms were consulted through their online interfaces for *in silico* analysis. The software predicted the mutation to be deleterious for the function or structure of the protein (Table 3.2).

Variant	PROVEAN	SIFT	SNAP	Meta-SNP	PhD-SNP
	-6.613	0.000	0.725	0.691	0.587
E884G	Deleterious	Deleterious	Deleterious	Deleterious	Deleterious
	cutoff= < -2.5	cutoff= <0.5	cutoff= >0.5	cutoff= >0.5	cutoff= >0.5

Table 3.2. Protein prediction software PROVEAN, SIFT, SNAP, Meta-SNP and PhD-SNP described the *Lama5*^{E884G} mutation as deleterious.

Given the close association of *Lama5* with renal development and function, I worked on the hypothesis that the missense variant was the causative mutation for the renal phenotype observed in the MPC-205 pedigree.

A LightScanner assay [231] was set up to genotype retrospectively the whole pedigree analysing the DNA extracted from the tails of the MPC-205 mice. Genotyping results demonstrated only mice homozygous for the *Lama5*^{E884G} mutation exhibited a phenotype (Figure 3.6). Furthermore, there was no detectable phenotype in the heterozygous mice.

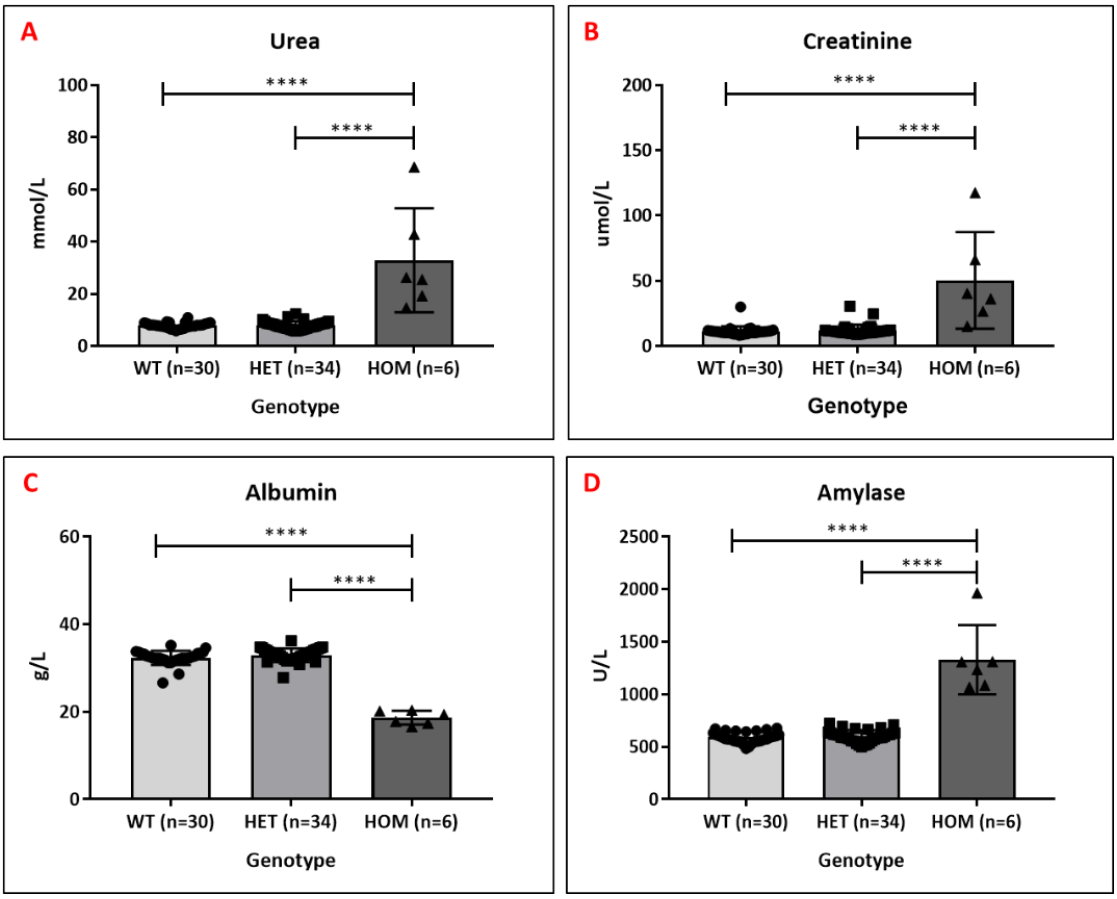

Figure 3.6. Results of the clinical chemistry analysis of the pedigree MUTA-PED-C3pde-205 at 6 months of age, with the animals grouped according to their genotype. The homozygous mice are the only ones showing alteration in the concentration of kidney markers (urea, **A** and creatinine, **B**), albumin(**C**) and amylase (**D**). The values shown are means ± SEM. One-way ANOVA **** $p<0.0001$.

3.2 Gene Validation

To confirm the causative mutation, we ordered a *Lama5* global knock-out, the *Lama5*-tm1b line, from the IMPC. Tm1b alleles are produced by the deletion of a critical exon and the neomycin cassette using a Cre recombinase that recognises loxP sites flanking the critical exons, resulting in a null allele. In the case of *Lama5,* the deleted critical exons are exons 4, 5 and 6 (Figure 3.7 A). As in the previously described *Lama5* knockout line [103], *Lama5*-tm1b$^{-/-}$ died between E14.5 and E18.5 (Figure 3.7 B and C) with complete penetrance. No phenotype was observed in heterozygous mice.

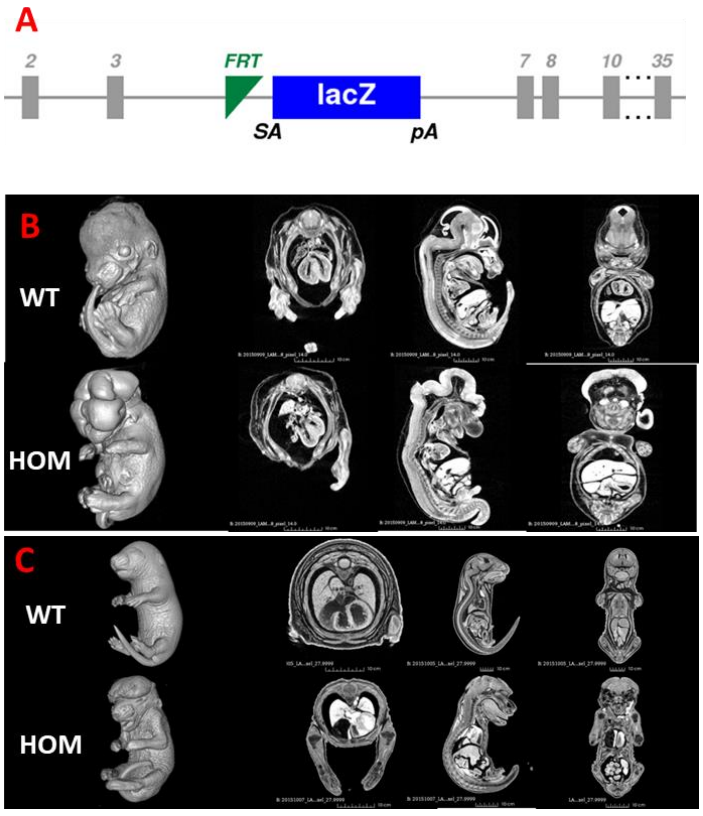

Figure 3.7. **A**: Graphic representation of the *Lama5*-tm1b allele. Critical exons 4, 5 and 6 are deleted and result in a null allele. The LacZ cassette expresses LacZ in tissues where *Lama5* is knocked out. Image adapted from http://www.mousephenotype.org/. **B-C**: Microtomography (µCT – far left) images of *Lama5*-tm1b$^{-/-}$ embryos and wild-type controls. *Lama5*-tm1b$^{-/-}$ showed preweaning lethality due to a strong phenotype of exencephaly, dying between E14.5 and E18.5. The image was taken by Zsombor Szoke-Kovacs (team LacZ, MRC Harwell Institute).

To validate the link between the phenotype and the mutation in *Lama5*, a cross between *Lama5* knockout mice line (*Lama5*-tm1b) and the line carrying the E884G mutation was set up to generate compound heterozygotes (*Lama5*$^{E884G/-}$). Since heterozygous *Lama5*$^{E844G/+}$ mice and *Lama5*$^{+/-}$ mice did not show any kidney impairment, the phenotype should be present only in mice carrying the E884G mutation inherited from the MPC-205 line and the *Lama5*-tm1b allele.

As expected, compound heterozygous mice (*Lama5*$^{E884G/-}$) developed the same phenotype as the original phenotype, but with a more rapid progression. At 22 weeks of age, the mice had to be culled due to welfare concerns and analysis of plasma confirmed ESRD (Figure 3.8). The littermates used as controls (*Lama5*$^{+/+}$, *Lama5*$^{+/-}$, *Lama5*$^{E844G/+}$) did not show any sign of proteinuria or variation in renal function markers in the plasma analysis, confirming the *Lama5*^{E884G} as the causative mutation underlying the observed nephrotic syndrome phenotype.

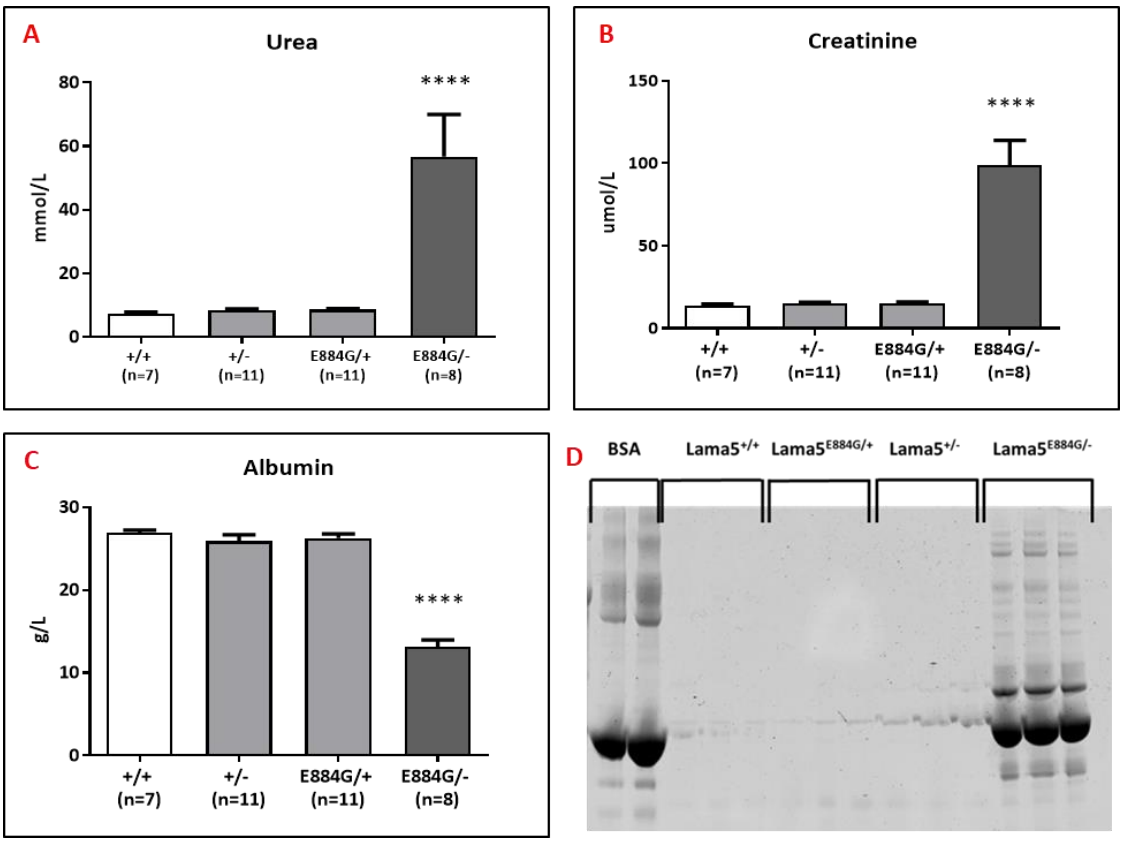

Figure 3.8. The clinical chemistry analysis of plasma confirmed kidney insufficiency (**A** and **B**) and hypoalbuminaemia (**C**) in *Lama5*$^{E884G/-}$ mice. The values shown are means ± SEM. One-way ANOVA **** p<0.0001. Coomassie blue stained gel shows the presence of albumin in the urine of *Lama5*$^{E884G/-}$ mice at 21 weeks of age (**D**).

3.3 C3pde-Lama5^{E884G} Phenotyping and Characterization

3.3.2 Phenotyping

To establish the experimental cohorts, the line was rederived by *in vitro* fertilization (IVF) using the sperm from the G1 male founder of the MPC-205 pedigree, and backcrossed for one generation onto C3H-C3pde6b+ and then intercrossed. Since the heterozygous mice of the original MPC-205 pedigree did not show any phenotype, the time course analysis was performed on cohorts of wild-type (C3pde-*Lama5*$^{+/+}$) and homozygous (C3pde-*Lama5*$^{E884G/E884G}$) mice to identify the earliest time point where kidneys start to

lose their normal function and also to study disease progression. At 7, 12, 15, 20 and 22 weeks of age, mice of both sexes were put through metabolic cages to collect urine, were terminally bled to collect plasma, and tissue was harvested for further analysis. Interestingly, after the first backcross, the disease became more severe and aggressive, with the mice reaching the humane endpoint around 26 weeks of age instead 9 months as in the original pedigree.

3.3.2.1 *Inheritance*

Given the pre-weaning lethality found in *Lama5* null mice, it could be possible that the mutation E884G had some effect on embryonic development. To exclude the possibility of embryonic lethality, the total number of genotyped mice of the C3pde-*Lama5* line (hence all the mice that made it to weaning) was compared with the expected Mendelian inheritance from a heterozygous intercross (1 wild type: 2 heterozygotes: 1 homozygote). Based on 291 genotyped mice with a ratio of 91:121:79, the chi-square value obtained was 0.0099 with an expected Mendelian ration of 72.75:145.5:72.75 (Figure 3.9). This value indicates that the E884G mutation does not result in a loss of mice before weaning (72.75 expected mice versus 79 observed) and that its inheritance follows the Mendelian ration. However, there was a reduction in the number of heterozygous mice (145 expected mice versus 121 observed) in favour of wild types (72.75 expected mice versus 91 observed). This could be due to the effect of additional mutations still present in the one generation C3H-C3pde6b+ backcross mice, such as the identified donor splice in the gene *Ptprq* (encoding protein tyrosine phosphatase, receptor type Q) [222] also identified in the pedigree MPC-205.

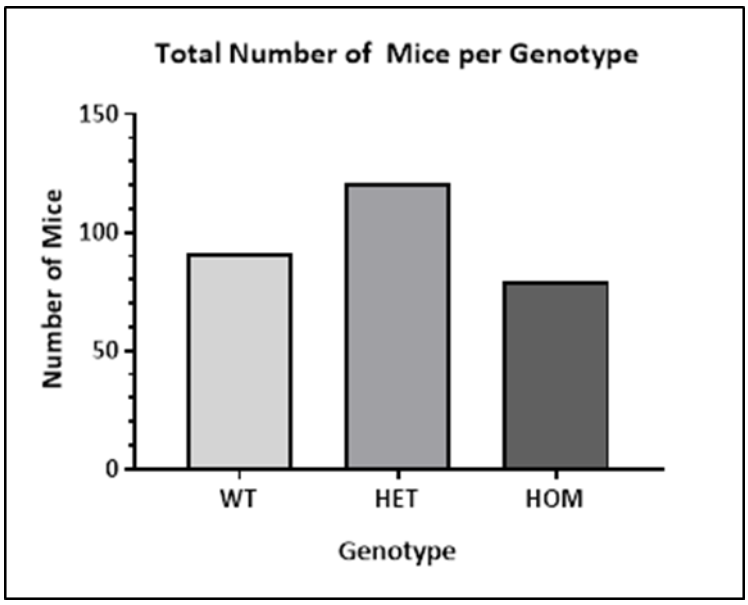

Figure 3.9. Total numbers of mice from each genotype from the C3pde-*Lama5* line.

3.3.2.2 *Clinical Chemistry and Urinalysis Time Course Analysis of the C3pde-Lama5$^{E884G/E884G}$ Phenotype*

Blood samples were collected from wild-type and homozygous mice at each time point by puncture of the retro-orbital sinus as a terminal procedure. The analysis of plasma from cohorts of control and homozygous C3pde-*Lama5*$^{E884G/E884G}$ showed a progressive deterioration of the renal function (Figure 3.10 A, B and C) with age-related increased levels of urea and creatinine. Albumin levels were decreased before signs of kidney impairment (at 12 weeks).

Before being culled, the mice were singly housed in metabolic cages overnight and urine was collected. To assess the presence of proteinuria, the same amount of urine sample was run on a SDS-PAGE gel and stain with Coomassie blue stain. After staining, a large band of the same size as BSA was apparent in all C3pde-*Lama5*$^{E884G/E884G}$ samples at all

ages but was absent in samples from *Lama5*$^{+/+}$ mice (Figure 3.10 D). Hence, the analysis of urine showed a severe proteinuria as early as 7 weeks.

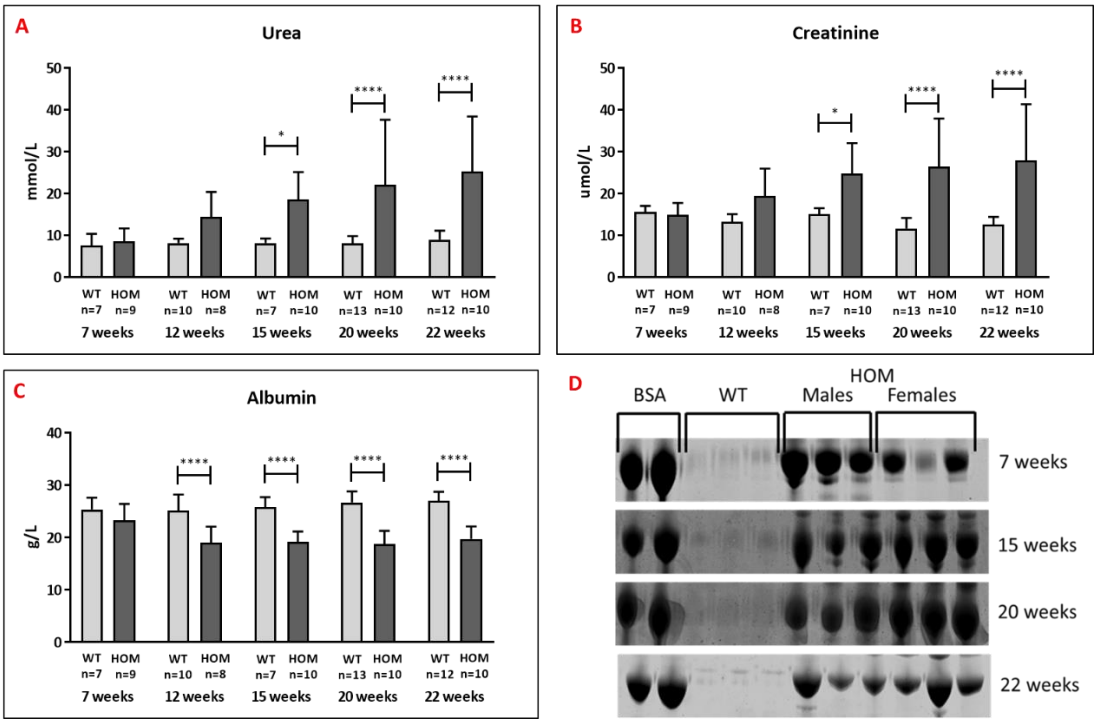

Figure 3.10. Clinical chemistry analysis of plasma shows worsening of renal function with high urea (**A**) and creatinine (**B**) levels and a low level of albumin (C). Hypoalbuminaemia seems to be one of the earliest changes. Coomassie blue-stained SDS-PAGE gels at different time points. A band of the same size of the BSA controls is present in all homozygous mice, both males and females, at all time points including at 7 weeks of age when the clinical chemical plasma did not show alteration in the renal markers (**D**). The values shown are means ± SEM. Two-way ANOVA with Bonferroni post-hoc test *p<0.05, **** p<0.0001.

Because the mice showed two of the fundamental symptoms of nephrotic syndrome, analysis of lipid metabolism was added to the clinical chemistry panel. Homozygous mice at 12, 20 and 22 weeks of age indeed showed significantly increased levels of total cholesterol, LDL and HDL indicating an abnormal lipoprotein homeostasis (Figure 3.11).

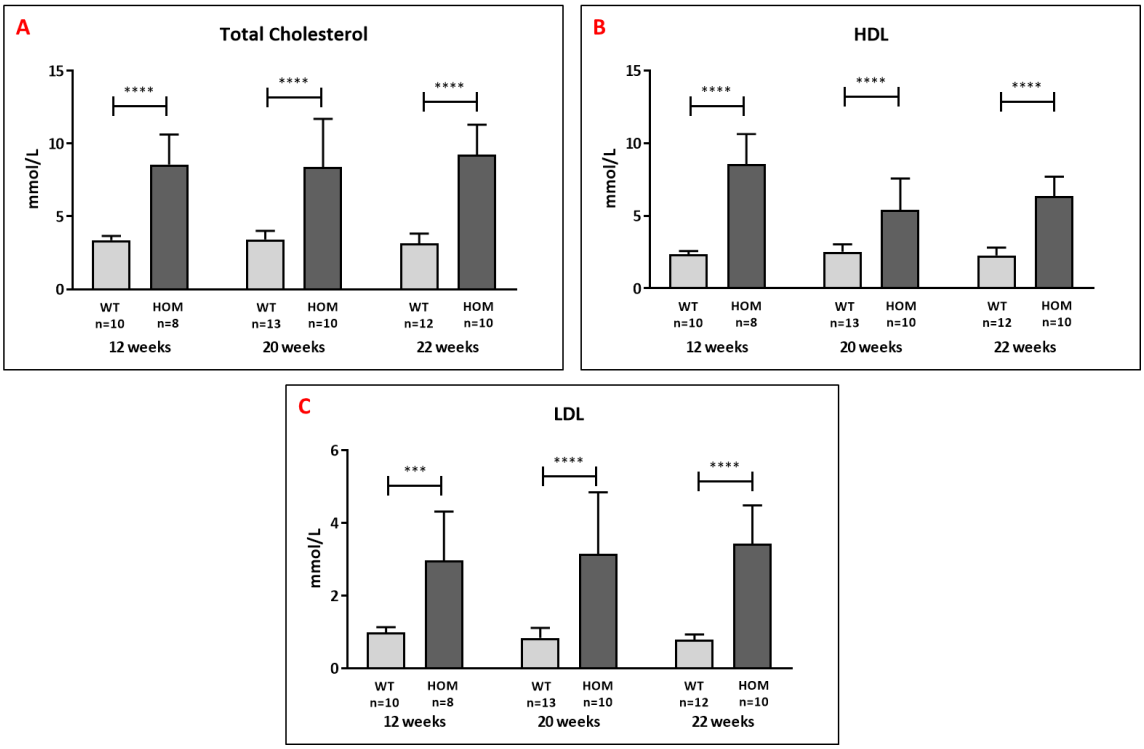

Figure 3.11. Abnormal lipid metabolism indicated by higher plasma concentration of total cholesterol (**A**), HDL (**B**) and LDL (**C**), which is a classic symptom of nephrotic syndrome. The values shown are means ± SEM. Two-way ANOVA with Bonferroni post-hoc test ***p<0.001, **** p<0.0001.

3.3.2.3 *Histological Analysis*

The clinical chemistry and urinalysis data suggested that *Lama5*$^{E884G/E884G}$ mice were affected by a progressive nephrotic syndrome, so histological analysis of the kidneys was carried out to further characterise the pathology development. The H&E stained kidney slides from mice of different ages showed the typical lesions of CKD from 12 weeks of age. The kidneys were globally compromised and the glomeruli presented with sclerotic Bowman's capsules and obliteration of the Bowman's space. The tubules were dilated and often contained protein casts (Figure 3.12).

Giving the vital role of the laminin α5 chain in murine development and formation of a functional vascularised glomerulus, histological analysis was also performed at

additional earlier time points. No lesions or signs of abnormal development were observed at 7 or 14 days suggesting a normal kidney growth.

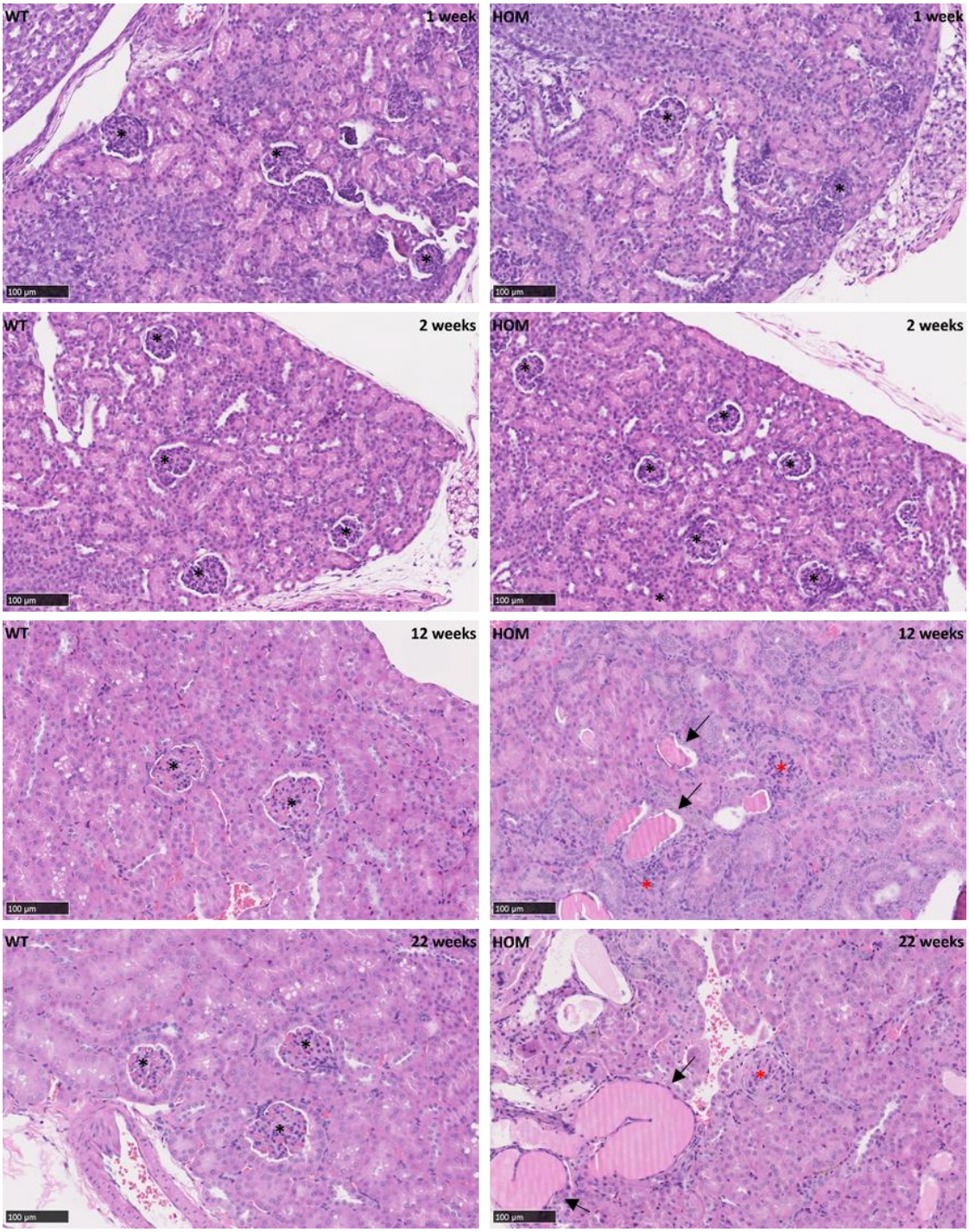

Figure 3.12. Time course of histology on wild-type and *Lama5*$^{E884G/E884G}$ kidneys. Kidneys from homozygotes did not differ from the wild-type controls at 1 and 2 weeks: the glomeruli (black stars) are surrounded by the Bowman space and the tubules do not appear enlarged, indicating normal kidney development. At 12 and 22 weeks of age, the kidneys from *Lama5*$^{E884G/E884G}$ mice showed abnormal glomeruli (red starts) with sclerosis of the Bowman capsule with obliteration of the Bowman space, and enlarged tubules with protein casts, in comparison with wild type controls. Scale bar represents 100 µm.

3.3.2 Possible Mechanisms Involved in the Development of Nephrotic Syndrome in *Lama5*$^{E884G/E884G}$ Mice

3.3.2.1 *Gene Expression Analysis*

As a first approach to study the possible mechanisms involved in the pathogenesis of the *Lama5*-releted nephrotic syndrome, the expression of a set of genes involved in the composition of different structures of the glomerular filtration barrier was assessed by quantitative reverse transcription PCR (RT-qPCR) on three biological replicates per time points. The genes chosen encode proteins expressed in the apical domain of the podocyte body (podocalyxin and podoplanin), in the slit diaphragm (nephrin and podocin), in the GBM (laminin α5, laminin α2, laminin α1 and agrin) and laminin α5 receptors (integrin α3, integrin β1 and Lutheran body).

In general, mRNA levels of genes coding for some proteins of the slit diaphragm (nephrin and podocin) and of the apical domain of the podocyte body (podocalyxin) in C3pde-*Lama5*$^{E884G/E884G}$ samples did not show any difference when compared with wild types of the same age after disease onset (at 15 and 22 weeks). However, both nephrin and podocin were upregulated at 7 weeks (Figure 3.13 A and B). The mRNA levels of the gene coding for podoplanin, another protein expressed in the apical domain and upregulated in the course of inflammation [232], were overexpressed in C3pde-*Lama5*$^{E884G/E884G}$ and the increase in expression was elevated further with the age of the mice (Figure 3.13 D).

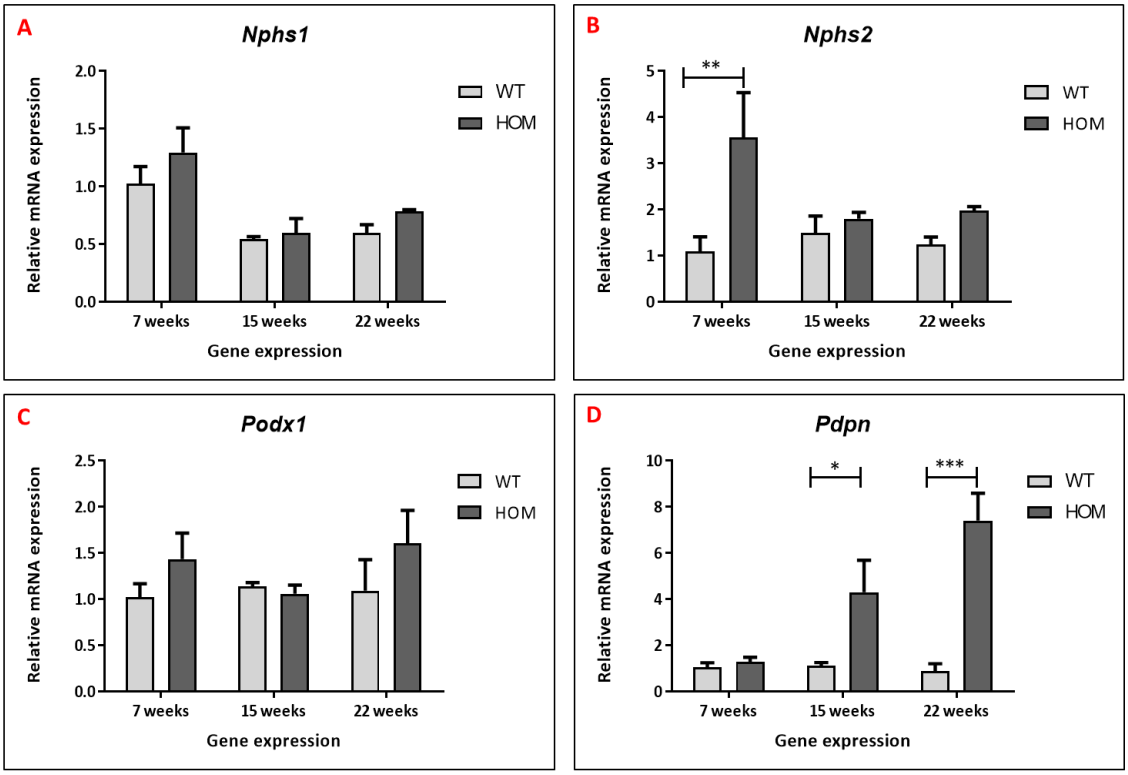

Figure 3.13. Results of the gene expression of some genes encoding proteins of the slit diaphragm (nephrin, *Nphs1* - **A**, and podocin, *Nphs2* - **B**) and the apical domain of the podocyte body (podocalyxin, *Podx1* - **C**, and podoplanin, *Pdpn* - **D**). The mRNA level of *Pdpn* is upregulated and increased as the mice aged (relative expression normalised to *Hprt1*). The values shown are means ± SEM. Two-way ANOVA with Bonferroni post-hoc test * $p<0.05$, ** $p<0.01$, *** $p<0.001$.

For the ECM component, the expression of all the laminin α chains (*Lama5*, *Lama2* and *Lama1*) was assessed, in addition to agrin (*Agrn*) since the agrin protein is associated with the laminin-521 trimer (Figure 3.14). In a normal fully developed glomerulus, the laminin α5 chain is the only α chain present in the GBM. *Lama2* and *Lama1* are only expressed in the mesangial matrix or, in the case of *Lama1*, as during embryonic renal development.

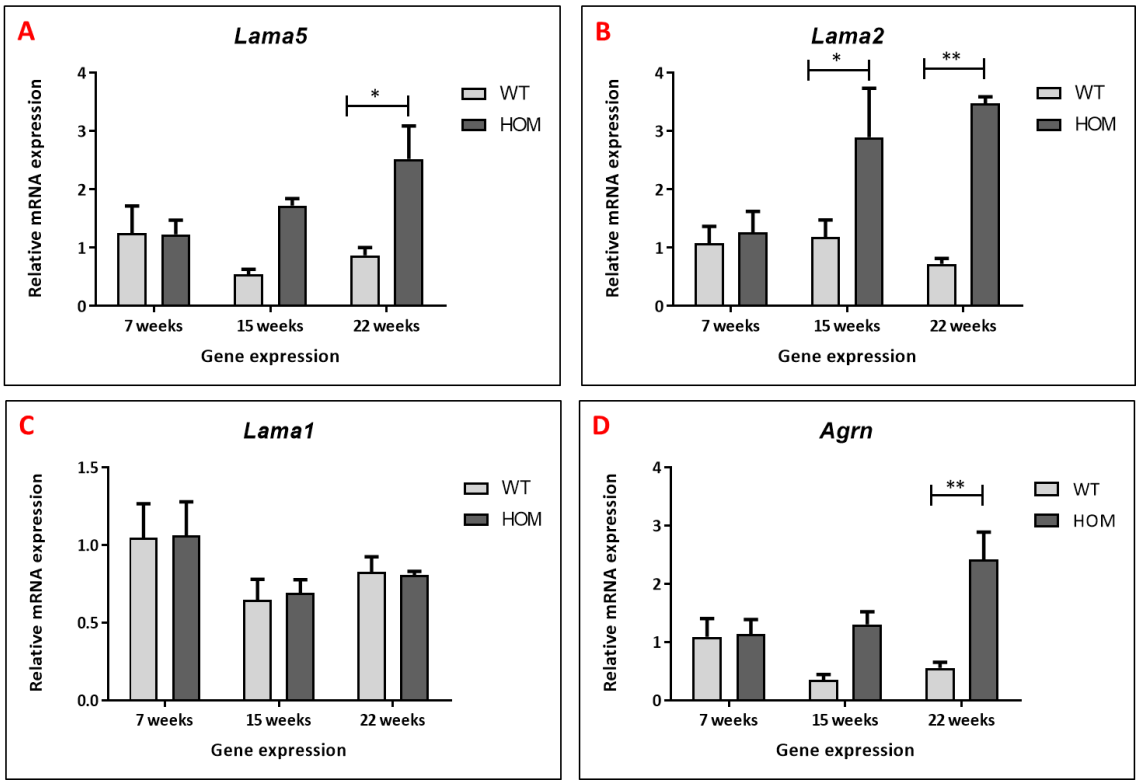

Figure 3.14. Results of the gene expression of some genes encoding proteins of the GBM. The mRNA levels of *Lama5* (**A**), *Lama2* (**B**) and *Agrn* (**D**) appear to be upregulated and increased as the mice aged (relative expression normalised to *Hprt1*). The values shown are means ± SEM. Two-way ANOVA with Bonferroni post-hoc test * p<0.05, ** p<0.01 * p<0.05, ** p<0.01, *** p<0.001.

The mRNA levels of the genes coding for the main LAMA5 receptors, integrin α3β1 and Lu/BCAM, were also elevated (Figure 3.15).

The upregulation of laminin α5 chain receptors, in particular, integrin α3β1, could suggest an abnormal signalling is being sent from the LAMA5-receptor interaction.

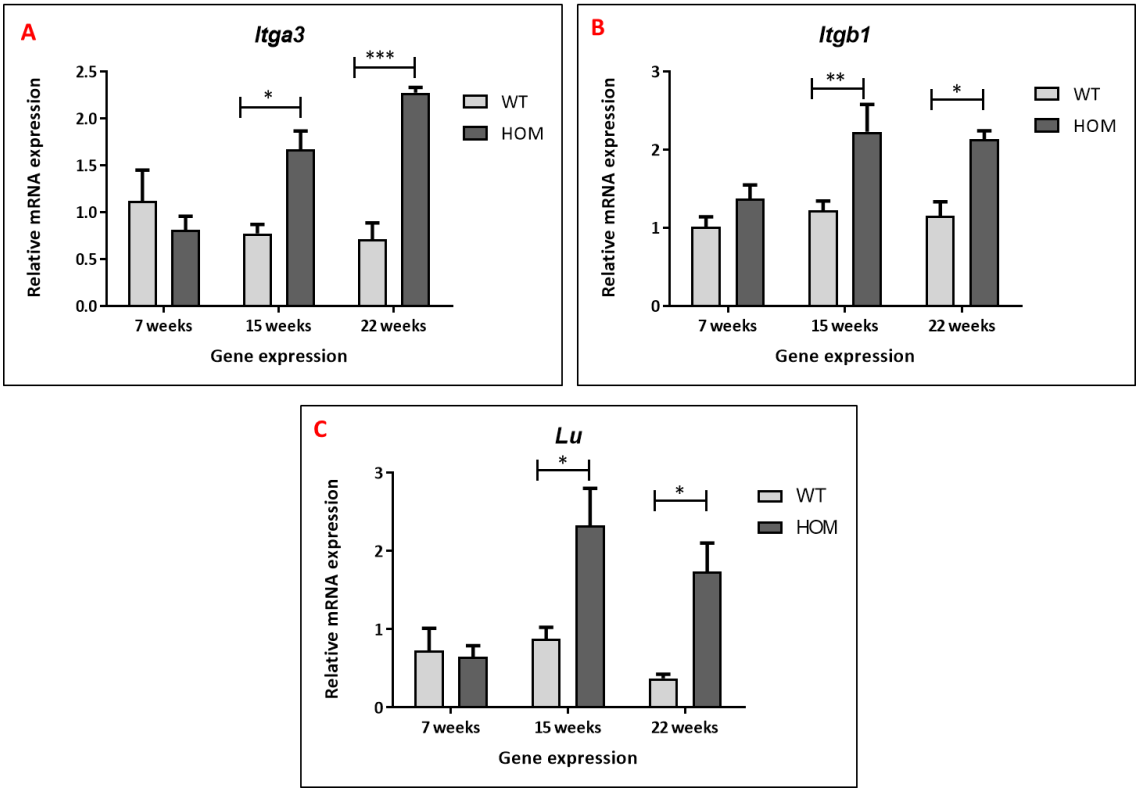

Figure 3.15. Results of the gene expression of some genes encoding proteins of the main LAMA5 receptors, integrin α3 (*Itga3*, **A**), integrin β1 (*Itgb1*, **B**) and Lutheran body (*Lu*, **C**). The mRNA levels of all the receptors appear to be upregulated after disease onset (relative expression normalised to *Hprt1*). The values shown are means ± SEM. Two-way ANOVA with Bonferroni post-hoc test * $p<0.05$, ** $p<0.01$, *** $p<0.001$.

Once LAMA5 and integrins are bound, the signals travel through mechanical mediators, such as α-actinin4 (*Actn4*), talin-1 (*Tln1*) and kindlin-2 (*Fermt2*), and chemical mediators like paxillin (*Pxn*), ILK (*Ilk*), FAK (*Fak*) and Src (*Src*) (Figure 3.16), forming focal adhesions and maintaining the actin cytoskeleton. In cells like podocytes, which present a large number of interdigitating processes, it is critical to their function maintain cell morphology. I, therefore, looked at the gene expression of some of these molecules to explore the possible effect on the integrin signalling. The mRNA levels of most of the genes encoding for the chemical signal mediators (paxillin, ILK, FAK and Src) were

increased in the C3pde-*Lama5*$^{E884G/E884G}$ samples, especially at 22 weeks. These results strengthened the hypothesis that the mutation in laminin α5 resulted in an abnormal signal though integrins.

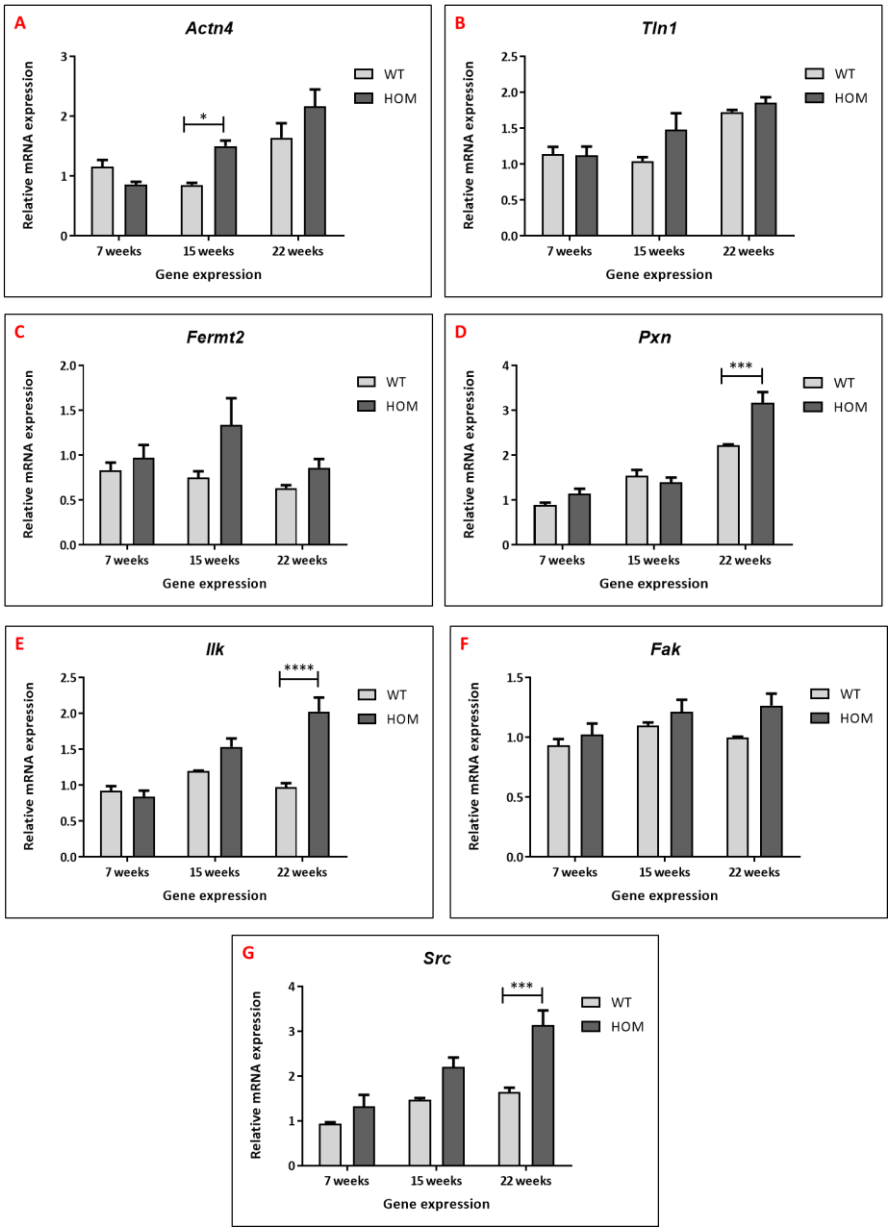

Figure 3.16. Results of the gene expression of some genes coding for proteins of the LAMA5-ITGB1 mediators in wild-type and mutant mice. Mechanical mediators (α-actinin 4 - **A**, talin-1 – **B**, and kindilin - **C**) are not different but all the genes, but genes involved in chemical signalling (paxillin –**D**, ILK – **E**, and Src -**G**) appeared to be upregulated at 22 weeks. Relative expression normalised to *Hprt1*. The values shown are means ± SEM. Two-way ANOVA with Bonferroni post-hoc test * p<0.05, *** p<0.001, **** p<0.0001.

3.3.2.2 *Protein Expression Study*

To investigate in more thoroughly the role of focal adhesion proteins in the pathogenesis of nephrotic syndrome in the C3pde-*Lama5*$^{E884G/E884G}$ mice, the protein expression of some of the integrin signalling mediators was assessed by immunoblotting on whole kidneys.

Proteins expression of the integrin β1 correlated with the mRNA levels being increased at 22 weeks of age in kidney samples from *Lama5*$^{E884G/E884G}$ animals (Figure 3.17).

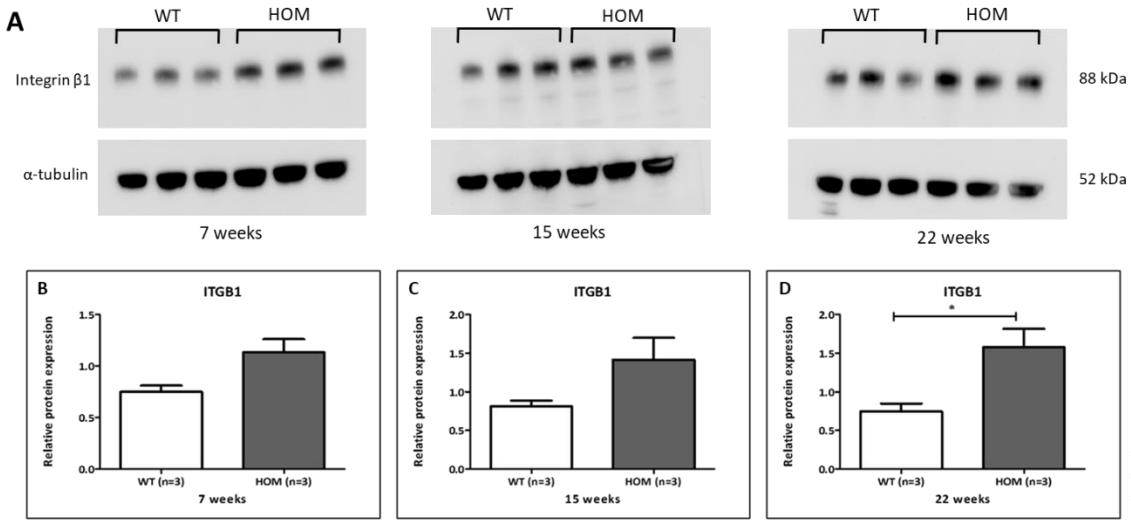

Figure 3.17. Results of the protein expression of integrin β1. At 22 weeks At 22 weeks, the ITGB1 protein levels resulted upregulated in homozygotes compared to wild-type controls. Relative expression normalised to β-tubulin. The values shown are means ± SEM. Unpaired parametric T-test * p<0.05.

Paxillin and ILK are major components of two different pathways of the ECM-integrin axis. Paxillin is activated by phosphorylation by the FAK-Src complex, while ILK is part of the ILK/PINCH/parvin complex. The mRNA levels of the genes encoding for these proteins, Pxn and *Ilk*, were both upregulated in homozygous mice at 22 weeks, but the

protein levels in C3pde-*Lama5*$^{E884G/E884G}$ were normal when compared with wild-type (Figure 3.18).

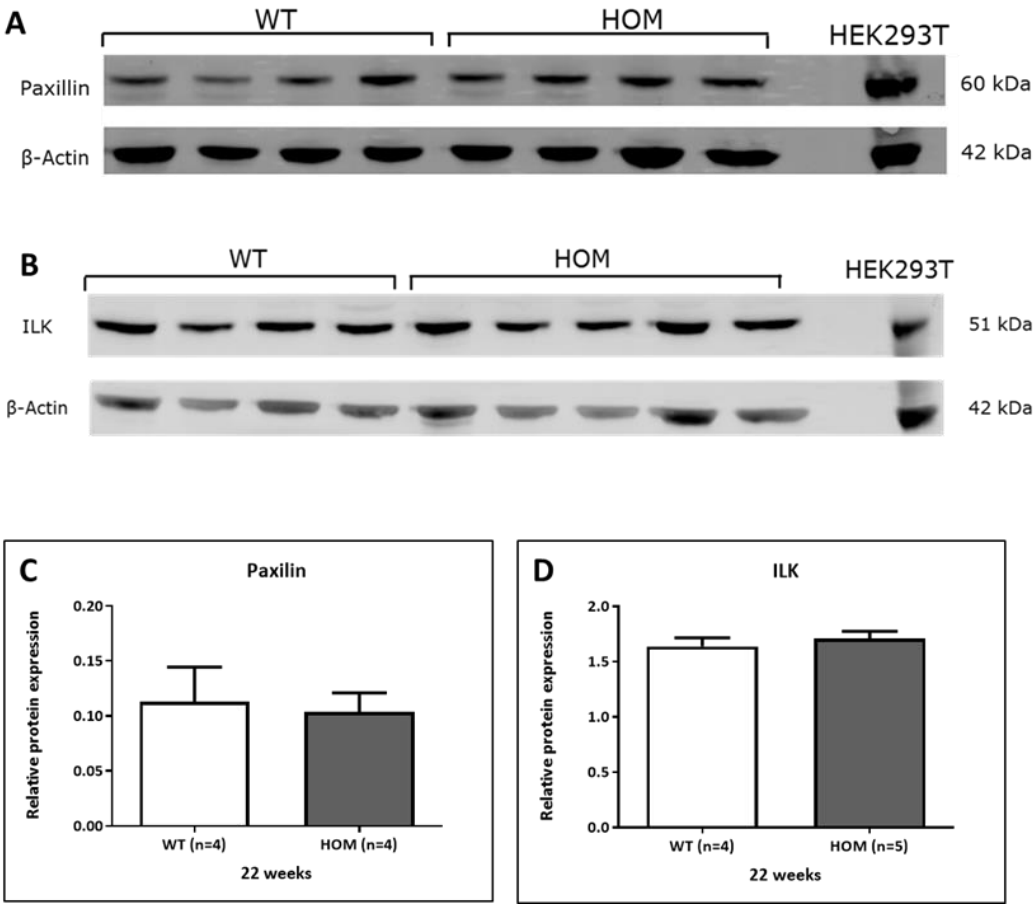

Figure 3.18. Results of the protein expression of paxillin (**A**-**C**) and ILK (**B**-**D**) in wild-type and mutant mice. Although the equivalent genes were upregulated in homozygous mice at 22 weeks, the protein levels at the same point were unchanged. HEK293T cell lysate was used as positive control to demonstrate antibody specificity. Relative expression normalised to β-actin. The values shown are means ± SEM.

Chemical signalling mediators like paxillin and ILK also regulate the activities of small GTPases, like CDC42 and RhoA. Immunoblotting analysis was therefore performed to study the downstream effect of chemical mediators (Figure 3.19). The total protein levels of CDC42 were unchanged, but there was an approximately three-fold increase in total RhoA in homozygous mice.

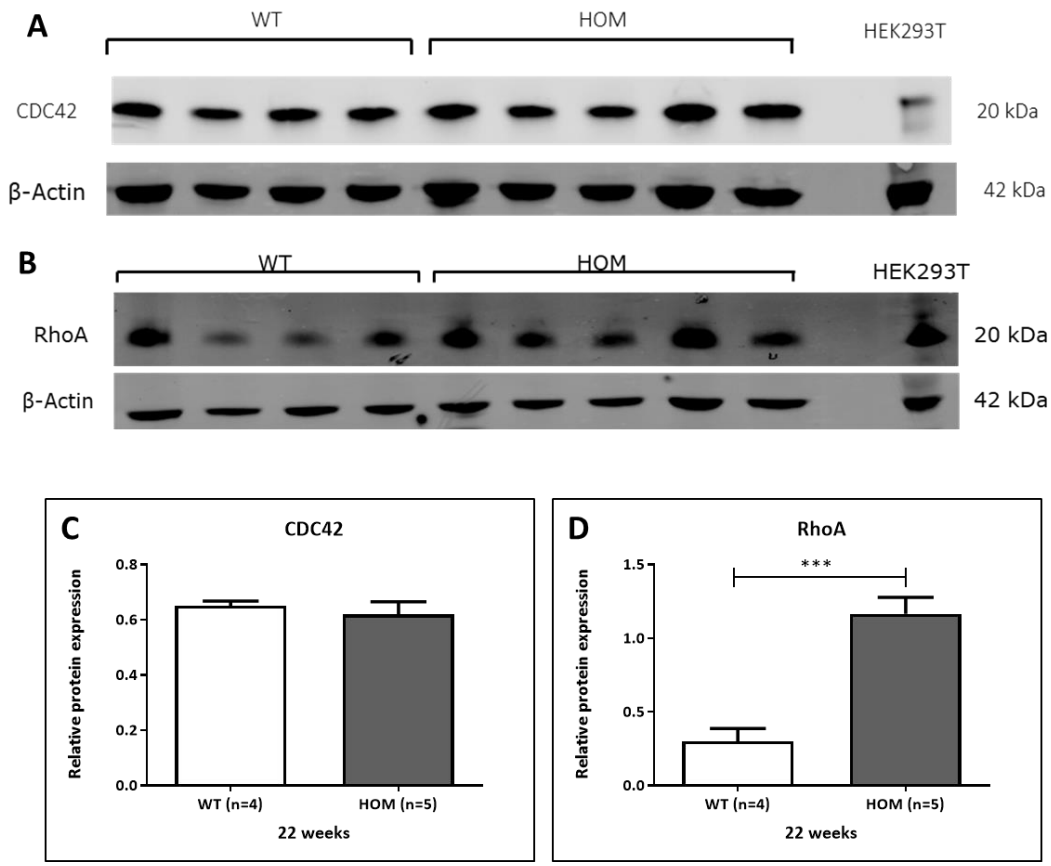

Figure 3.19. Results of the protein expression of CDC42 (**A**-**C**) and RhoA (**B**-**D**) in wild-type and mutant mice. CDC42 protein levels of C3pde-*Lama5*$^{E884G/E884G}$ do not differ from the wild-type controls, however, RhoA expression is significantly increased. HEK293T cell lysate was used as positive control to demonstrate antibody specificity. Relative expression normalised to β-actin. The values shown are means ± SEM. Unpaired parametric T-test *** $p<0.001$.

3.4 Chapter 3 Summary and Discussion

Employing a combination of SNP mapping and WGS analysis, a single coding mutation was identified in the gene encoding laminin α5 chain, a major component of the GBM and necessary for normal glomerular development, as responsible for a nephrotic phenotype in a pedigree of mice arising from the Harwell ageing screen.

The mutation, resulting in the substitution of a glutamic acid to a glycine at amino acid 884, lies in the L4a domain, one of the globular domains of the protein short arm the function of which is still unknown. However, the deleterious effect of the E884G mutation was been predicted by five different protein prediction software packages. After retrospectively genotyping all the mice of the MPC-205 pedigree, no phenotype could be observed in heterozygous animals indicating that *Lama5* is haplosufficient.

When rederived and backcrossed for one generation onto C3H.Pde6b, the homozygous animals exhibit an earlier onset of disease and progressed to ESRD much quicker than the homozygotes in the original MPC-205 pedigree. The *Lama5*$^{E884G/E884G}$ mice of the original pedigree were indistinguishable from their littermates and could only be identified at 6 months because of altered clinical chemical kidney markers. On the contrary, C3pde-*Lama5*$^{E884G/E884G}$ showed histological signs of CKD from 12 weeks of age, and hypercreatinemia and hyperazotemia from 15 weeks of age. This difference in onset and progression is probably due to the mixed background of the mice, with the mice being approximately 81.25% C3H.Pde6b versus 18.75% C57BL/6J after one backcross onto C3H.Pde6b while in MPC-205 the percentages are respectively 62.5% versus 37.5%. C57BL/6 is well known to be less susceptible to fibrosis in different organs including renal fibrosis [233], an important factor in the progression of kidney disease and ESRD. Several

studies have compared renal disease progression in C57BL/6J versus other strains such as 129/Sv and FVB [157, 234-236] and found that C57BL/6J develop a renal related phenotype either much slower or if challenged (for example with induced hypertension [236]).

Since one of the limitations of using ENU as mutagenesis is the presence of numerous random mutations, the pathogenicity of E884G had to be proven by a genetic complementation with a knock out allele. Indeed, only the animals carrying the E884G allele and the null allele developed the expected nephrotic phenotype.

Preliminary results on the possible pathways involved using gene expression analysis and suggested that there might be some specific response to the *Lama5* mutation resulting in the alteration of the constituency of the GBM and the interaction between LAMA5 and the podocytes. The change in mRNA levels of integrin α1β3 and protein levels of integrin β1, and mRNA levels of integrin signal mediators suggested a perturbation of focal adhesion pathway that maintains actin cytoskeleton stability, but at the protein level, the only significantly upregulated protein was RhoA. This result would not exclude a change of this pathway since most of the elements involved have to be phosphorylated to be activated. It is, therefore, possible that the total protein is normal but specific amino acid residues are more phosphorylated.

Although these preliminary results looked promising, the study presented has some weaknesses. Glomeruli represent a minimal part of the kidney mass. Podocytes, for example, make up less than 2% of the kidney mass [228]. Both gene expression and protein expression studies were carried using renal cortex or whole kidney, this means that other renal structure could mask upregulation or downregulation of mRNA and protein levels of target gene/proteins, resulting in false positive or false negative. Moreover, the mixed background could also have an effect on the pathways since the

C3H.Pde6b are more prone to develop kidney lesion and because of the possible effect of other mutations co-inherited. Therefore, the changes observed may be secondary to disease as they only occur at later time points.

To overcome the limitations in this preliminary characterization of the phenotype, all further experiments have been carried on a congenic C57BL/6J background so to avert the additional effect of possible concomitant ENU mutations and the susceptibility of C3H.Pde6 mice to accelerated renal disease.

CHAPTER 4

In Vitro Analysis of Laminin Assembly

4. *In Vitro* Analysis of Laminin Assembly

In order to be delivered into the extracellular space, proteins enter the secretory pathways, compromised of the rough ER, ER exit sites (ERESs), the ER-to-Golgi intermediate compartment (ERGIC), the Golgi complex and the post-Golgi, to carry the proteins to their final destination [237]. To be able to enter this pathway, the proteins contain an ER signal sequence (generally at the N-terminus) to translocate them into the ER and that is cleaved by a signal peptidase following co-translational processing [238]. Once the proteins are folded in the ER, they are incorporated into COPII (membrane-coating coat protein II) vesicles and exit the ER to be transported to the Golgi cisternae, and from there, the secretory vesicles take them to the cell surface.

Several studies have been carried out to characterise the function of the main binding domains (NH2-terminal LN domain and COOH-terminal LG domains) but not much is known about the function of the other domains, in particular L4a. To characterise the mutated L4a domain and its role in cell binding, I submitted a proposal to the Oxford Protein Production Facility (OPPF) for access to their facilities and expertise. The aim of the proposed study was to express different fragments of the LAMA5 short arm *in vitro* and purify the secreted proteins from conditioned medium, with the intent being to generate an adhesion assay to investigate the effect of the mutation on the primary role of laminin α5 chain on cell-adhesion.

4.1 Cloning and Expression Screening of the Laminin α5 Chain Short Arm

Each of three different short arm fragments (LN-LEa, LN-L4a-LEb, LN-L4a-L4b-LEc) were cloned at the OPPF using three different vectors, two with an internal signal and one that uses the native signal sequence. The fragment containing only the L4a domain was inserted only in the two vectors with the internal signal sequence since it lacks a native one (Table 4.1). Site directed mutagenesis was employed to introduce the E884G point mutation into each of the fragments. Because of the lack of a crystal structure of the L4a domain, the OPPF offered their help to obtain a crystallised form of the wild type and mutated fragments to look at the effect of the mutation on the three-dimensional structure of the LAMA5 short arm.

The experiment had to be carried out in two rounds of cloning and expression screening to be sure that all the fragments were correctly inserted into the vectors.

After two rounds, the wild-type fragments were secreted, whilst none of the mutated proteins were detected in the conditioned medium but could be detected in the cell lysate (Figure 4.1).

Well	Fragment	aa_N	aa_C	Vector	MW (Da)
A01	LN-LEa	41	849	pOPINTTGneo	88,555
B01	LN-LEa	41	849	pOPINTTGneo-Fc	115,145
C01	LN-LEa	2	849	pOPINEneo	88,830
D01	LN-L4a-LEb	41	1641	pOPINTTGneo	175,065
E01	LN-L4a-LEb	41	1641	pOPINTTGneo-Fc	201,655
F01	LN-L4a-LEb	2	1641	pOPINEneo	175,339
G01	LN-L4a-L4b-LEc	41	2167	pOPINTTGneo	231,687
H01	LN-L4a-L4b-LEc	41	2167	pOPINTTGneo-Fc	258,277
A02	LN-L4a-L4b-LEc	2	2167	pOPINEneo	231,961
B02	L4a	855	1454	pOPINTTGneo	66,988
C02	L4a	855	1454	pOPINTTGneo-Fc	93,579
D02	LN-LEa Mutant	41	849	pOPINTTGneo	88,483
E02	LN-LEa Mutant	41	849	pOPINTTGneo-Fc	115,073
F02	LN-LEa Mutant	2	849	pOPINEneo	88,757
G02	LN-L4a-LEb Mutant	41	1641	pOPINTTGneo	174,993
H02	LN-L4a-Leb Mutant	41	1641	pOPINTTGneo-Fc	201,583
A03	LN-L4a-LEb Mutant	2	1641	pOPINEneo	175,267
B03	LN-L4a-L4b-LEc Mutant	41	2167	pOPINTTGneo	231,615
C03	LN-L4a-L4b-LEc Mutant	41	2167	pOPINTTGneo-Fc	258,205
D03	LN-L4a-L4b-LEc Mutant	2	2167	pOPINEneo	231,889
E03	L4a Mutant	855	1454	pOPINTTGneo	66,916
F03	L4a Mutant	855	1454	pOPINTTGneo-Fc	93,507
G03	Secretion control				
H03	Secretion control				

Table 4.1. Cloning plan of the experiment carried out at the OPPF. Each row corresponds to the fragment cloned, the vector used, the amino acidic position of the N and C terminus of the open reading frame (ORF) and the expecting molecular weight of the fragment. The well position identified the fragment in the immunoblotting experiment (Figure 4.1).

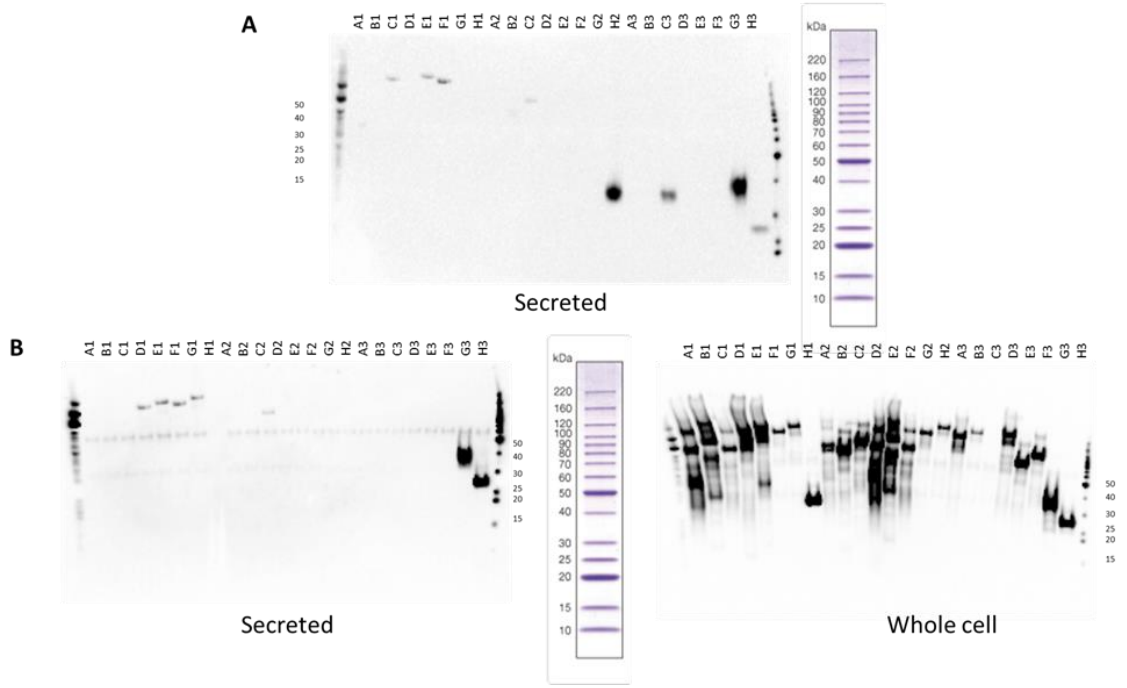

Figure 4.1. Images of the two rounds of cloning and screening of the LAMA5 short arm fragments. In both rounds (**A** and **B** "secreted") 293T did not secrete the E884G mutated proteins, but they appended to be expressed in the whole cell lysate (**B** "whole lysate).

Since the experiments at OPPF were carried out in a high throughput manner, I scaled up the reaction and re-screened the fragment that gave the most consistent results being secreted in both runs, LN-L4a-LEb. I, therefore, cloned the fragment in the pOPINGTTneo vector (N-terminal his tag and internal signal sequence), scaled up the volumes of cells and transfections and used wet protein transfer method to validate previous results. Again, the fragments containing the mutation were not secreted, although a band of the right size product was found in the cell lysate (Figure 4.2), suggesting that the mutant protein is misfolded and not secreted.

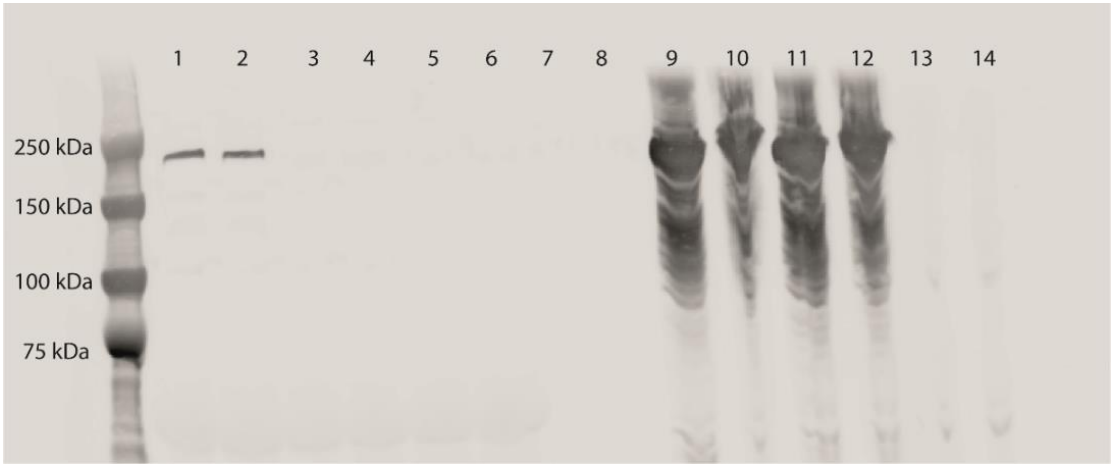

Figure 4.2. Confirmation of the impaired secretion of the mutated LN-L4a-LEb 6xHis-tagged fragment (expected band size: 175 kDa, primary antibody anti-6xHis tag). In the conditioned medium of 293T cells wildtype LN-L4a-LEb is normally expressed (lanes 1 and 2), but completely absent when the E884G mutation is present (lanes 3 and 4). However, the protein is present in the cell lysate of both conditions (lanes 9, 10, 11 and 12). Medium (lane 5 and 6) and cell lysate (lanes 13 and 14) from untransfected cells were used as negative controls. Lane 7 and 8 are empty.

4.2 Cloning and Expression Screening of the Full Length Laminin α5 Chain Full Length

The complete absence of laminin α5 protein results in embryonic lethality between 12.5 and 18.5 days due to incomplete neural tube closure and placental vascular defect [103]. All mice homozygous for the E884G mutation survived until adulthood, and hence the mutant laminin α5 must be incorporated into the ECM for the animals to develop normally and age, even though the short arm fragments were not secreted.

Working on this hypothesis, I examined the *in vitro* expression and secretion of the full-length protein. Laminin alpha 5 was amplified and inserted into a pCMV6 vector with a 6xHis tag at the C-terminal. The insertion of the ORF was confirmed by Sanger sequencing and revealed the presence of the stop codon (TGA) and an extra base (G).

Since the 6xHis tag is expressed at the C-terminal end, the stop codon had to be deleted for LAMA5 to be expressed with the tag. Moreover, the presence of the extra base resulted in the 6X His tag being out of frame. To correct the sequence, site directed mutagenesis primers were designed to delete the additional TGAG.

After confirming the TGAG deletion and the correct insertion of *Lama5*, site directed mutagenesis was used to introduce the E884G point mutation. The two pCMV6-LAMA5 constructs were transfected into HEK293T and after, 72 hours, the medium and the whole cell lysate were screened as previously described to assess secretion and cell expression. Results showed expression of the wild-type and mutated LAMA5 in the cell lysate, confirming correct transfection of the pCMV6-LAMA5 constructs, but the absence of secreted protein, even in the case of control constructs (Figure 4.3).

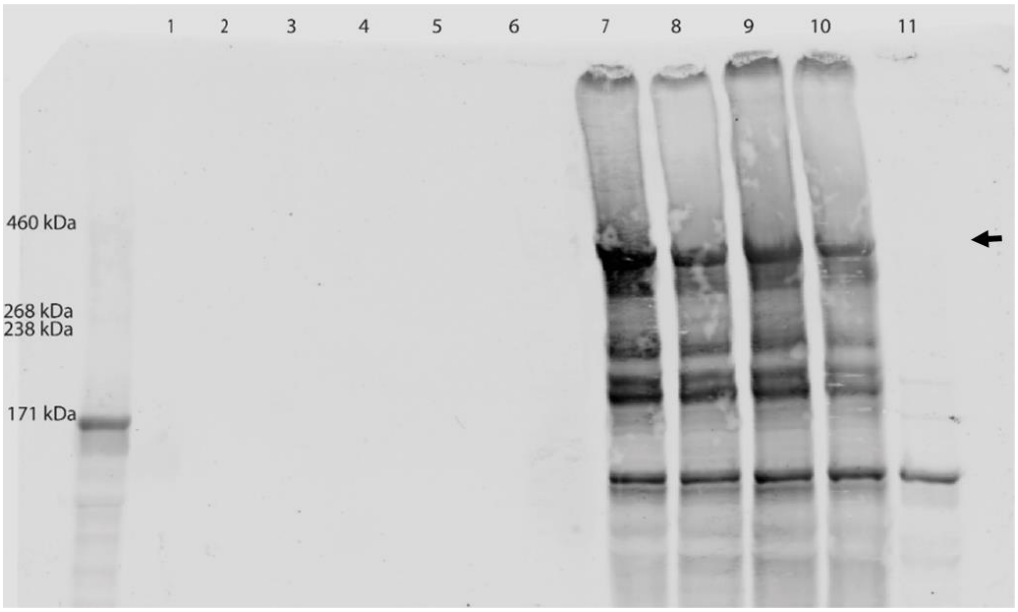

Figure 4.3. Screening of secreted and cell expressed full-length 6xHis-tagged laminin α5 transfected in HEK293T cells. The protein (arrow, expected size 404 kDa, primary antibody anti 6xHis tag) could be detected neither in the medium of the cells transfected with control protein (lane 1 and 2) nor in the one of the cells transfected with the mutated protein (lane 3 and 4). On the contrary, normal cell expression was found in wild-type (lane 7 and 8) and mutant (lane 9 and 10). Untransfected cells (lane 11) and their medium (lane 5) were used as negative control. Lane 6 is empty.

This negative result was probably due to the absence of a laminin β and γ chain since the laminin monomers are not secreted. Therefore, the experiment was repeated using a HEK293 cell line stably expressing human laminin β1 and human laminin γ1 (kind gift of Prof P. Yurchenco and Dr K. McKee[223]), which have more than 90% homology with the corresponding mouse proteins (Appendix 8.3).

The contemporary expression of the three-laminin chains allowed the secretion of both wild-type and mutant laminin α5, confirming that the mutant protein is excreted from the cell. Nonetheless, in the presence of the E884G mutation, laminin α5 protein secretion was greatly reduced (Figure 4.4 A). With the aim of quantifying the ability of HEK293 cells to secrete the transfected constructs, the amount of secreted laminin α5 protein detected in the medium was normalised to the amount of laminin α5 protein detected in the corresponding cell lysate. Considering the highest ratio found in the controls to be equal to 100%, the secretion of the other samples were expressed as a percentage of the control sample secretion. Indeed, the secretion of the mutant protein was reduced by 67.9% ±7.9 (Figure 4.4 B).

The findings support the hypothesis that the mutation E884G affects protein folding and results in a hypomorph.

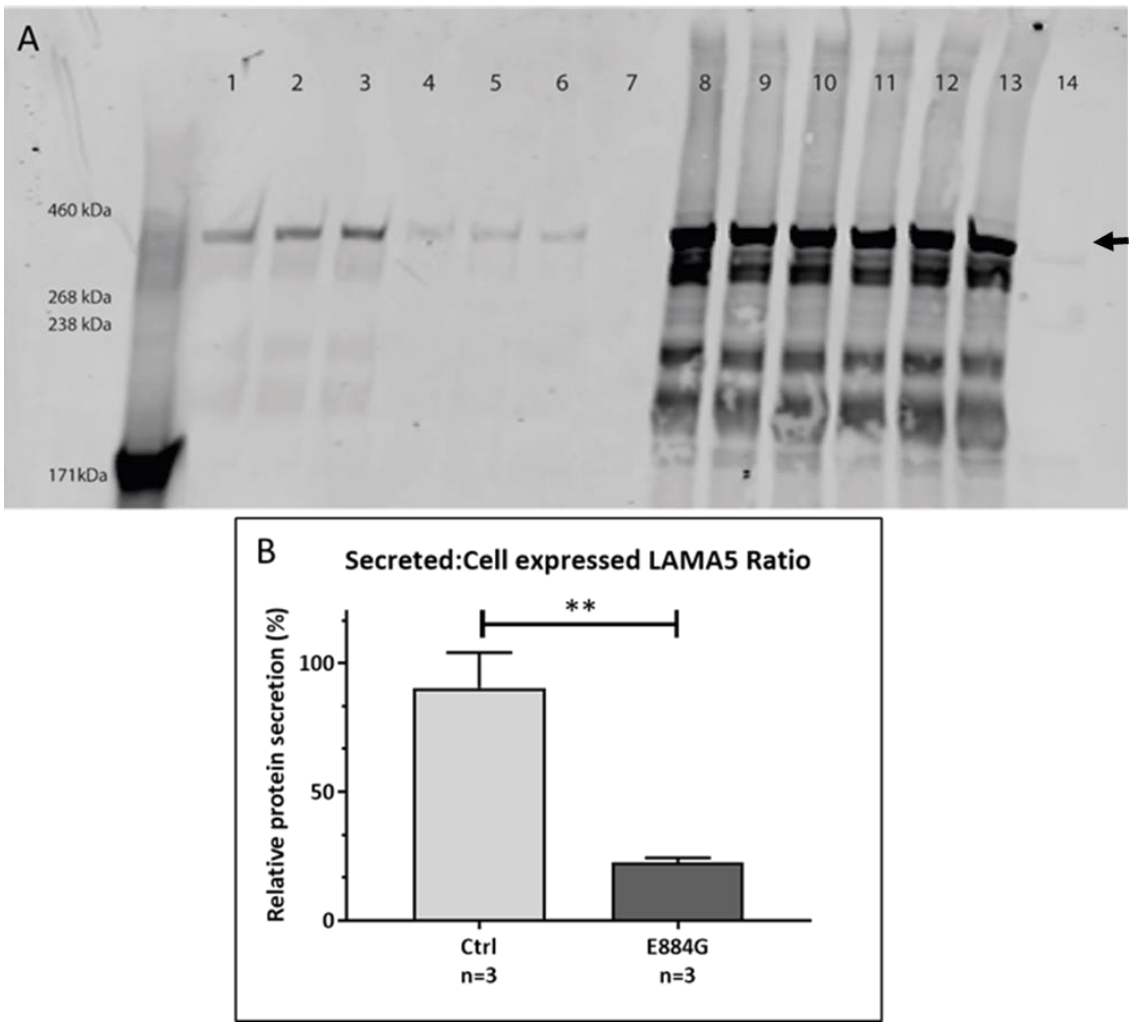

Figure 4.4. Screening of secreted and cell expressed full-length 6xHis-tagged laminin α5 transfected in HEK293 cells stably expressing human laminin β1 and human laminin γ1. **A**: Control pCMV6-LAMA5 construct (arrow, expected size 404 kDa, primary antibody anti-6xHis tag) could be detected as secreted protein in the medium (lane 1, 2 and 3) and expressed in the cell lysate (lane 8, 9 and 10). In presence of the E884G mutation, protein abundance in the medium was dramatically reduced (lane 4, 5 and 6), even though LAMA5 is expressed in cell lysate (lane 11, 12 and 13). Untransfected 293 cells (lane 14) and their medium (lane 7) were used as negative control. **B**: Graphical representation of the relative protein secretion. The values shown are means ± SEM. Unpaired parametric T-test ** $p<0.01$.

4.3 Chapter 4 Summary and Discussion

The production and purification of laminin fragments is a well described method to study the function and the crystal structure of the different laminin chains [120, 124, 125, 128]. With this approach, it was possible to perform adhesion assays to identify laminin α5 binding partners and peptides with amino acidic active sequences with specific functions such as promotion of neurite elongation. This methodology was not applicable because screening of laminin α5 short arm fragments showed that those carrying the E884G mutation were not secreted *in vitro*. This also limited the possibility of obtaining the crystal structure of the LAMA5 short arm and in particular, of the yet uncrystallised and characterised L4a domain.

Similar results were observed in *in vitro* studies of mutations in the laminin β2 found in nephrotic syndrome patients. The mutations *LAMB2*^{R246Q}, *LAMB2*^{R245W} and *LAMB2*^{C321R} all result in impaired secretion of the short arm fragment screened [89]. Moreover, HEK293 cells stably transfected with a construct carrying the C321R mutation and transgenic mice expressing full-length rat laminin β2 cDNA with an engineered C321R mutation, showed ER stress suggesting an accumulation of unfolded or unsecreted proteins in the ER [90].

Even though the screening of protein fragments give an indication of the effect of the mutation on the structure/function of the laminins under investigation, the complete absence of secreted protein it is not compatible with embryonic development, in the case of laminin α5, or leads to a short lifespan, in the case of laminin β2. This limitation is evident by studying *in vitro* the mutated full length laminin α5 chain. In fact, even though the secretion is dramatically reduced, the secreted mutant protein is detectable

in three days conditioned medium of HEK293 cells expressing three laminin chains (human laminin β1, human laminin γ1, and transfected murine laminin α5). This result provides insight into two aspects of the mechanism for disease in L*ama5*$^{E884G/E884G}$ animals. Firstly, *Lama5*^{E884G} is capable of interacting with other laminin chains, allowing for trimer formation and explaining why embryonic lethality was not seen in *Lama5*$^{E884G/E884G}$ mice. On the other hand, this suggests that *Lama5*^{E884G} secretion is significantly reduced in comparison to wild types and it is this reduction in protein and hence trimer levels that likely leads to disease.

Whether the rescue of the *in vitro* secretion depends on a higher stability of the full-length protein or it is due to a stabilising effect of the other laminin chains might have formed the mature heterotrimer.

CHAPTER 5

Analysis of the *Lama5*^{E884G} mutation congenic on a C57BL/6J background

5. Analysis of the *Lama5*^{E884G} mutation congenic on a C57BL/6J background

5.1 B6-Lama5^{E884G} Phenotyping

To study the effecte of the E884G mutation on disease progression on a C57L/6J congenic background, B6-*Lama5*$^{+/E884G}$ were intercrossed and I time course study was set up phenotyping wild-type (B6-*Lama5*$^{+/+}$) and homozygous mice (B6-*Lama5*$^{E884G/E884G}$) at 5, 15 and 25 weeks of age.

For each time point, samples have been collected to characterize the pathology and the molecular changes that occur at the very early time points of disease. Mice were individually housed for 24 hours in metabolic cages to measure water intake and urine production, and to collect urine for further analysis. Mice were then terminally bled and kidneys were harvested with different techniques depending on the experiments that followed. To keep the experiment as consistent as possible, kidneys harvested from male animals have been used for histology, electron microscopy, and immunofluorescence, whilst the females have been perfused with Dynabeads M450 tosylactivated and the kidneys harvested to isolate the glomeruli for immunoblotting. A second cohort of male mice aged 15 and 25 weeks was bred and perfused with Dynabeads to isolate the glomeruli for mass spectrometry analysis.

5.1.1 Metabolic Cages and Urinalysis

After 24 hours in singly housed in metabolic cages, the water intake and the urine production did not show any difference between homozygous mutant mice and wild-type controls (Figure 5.1 A and B) excluding polydipsia and polyuria at any of the time points. The urine was tested for the presence of erythrocytes and leukocyte with dipsticks. Although the presence of red blood cells was not detected in any of the samples, all the 25 weeks old B6-*Lama5*$^{E884G/E884G}$ mice and some of the 15 weeks old B6-*Lama5*$^{E884G/E884G}$ mice showed some degree of leukocyturia (Figure 5.1 C). To assess the levels of proteinuria, instead of using the SDS-PAGE method as with the C3pde-*Lama5* cohorts, a quantitative approach was taken calculating the urinary protein-urinary creatinine ratio. Results showed mild proteinuria at 15 weeks and severe proteinuria at 25 weeks in the homozygotes (Figure 5.1 D).

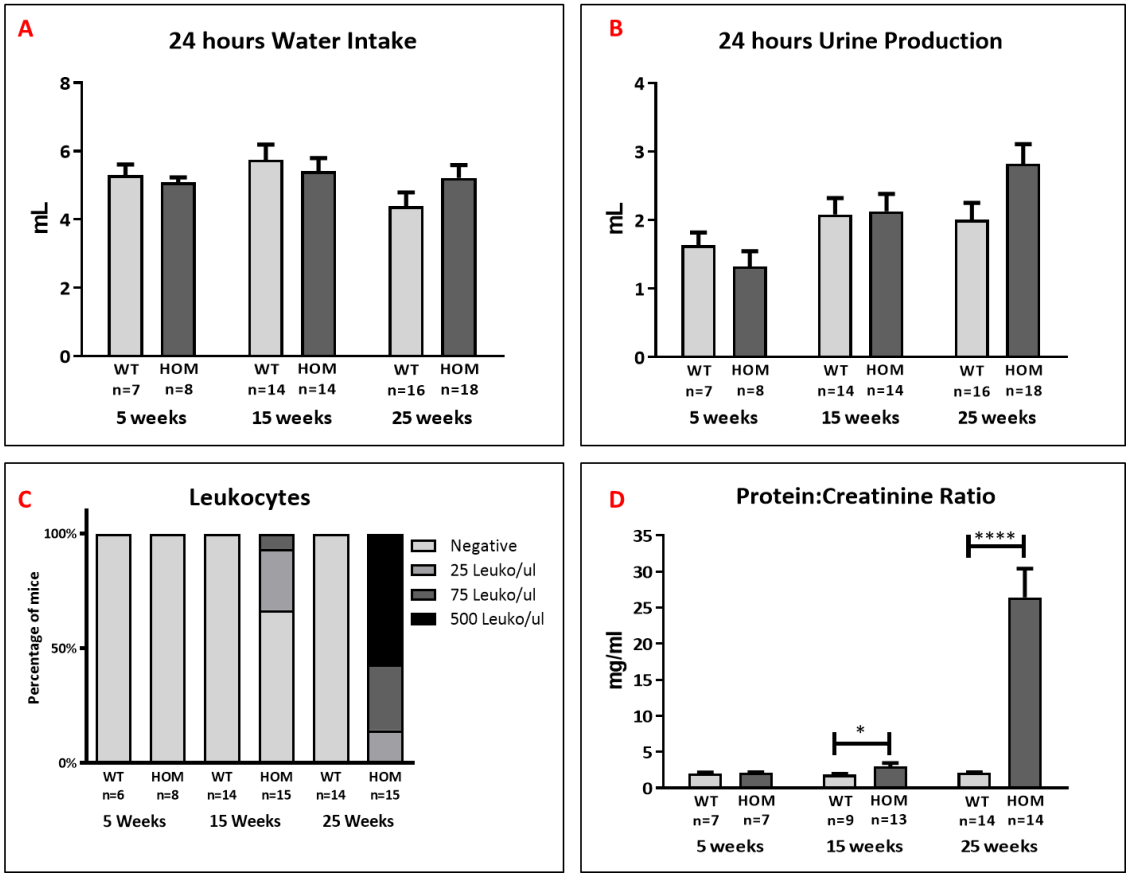

Figure 5.1. Results from metabolic caging studies showed that polydipsia (**A**) and polyuria (**B**) are absent in homozygous mice as indicated by the normal levels of water intake and urine production, however, urine dipstick and urinalysis showed leukocyturia (**C**) and proteinuria (**D**) at 15 and 25 weeks. The values shown are means ± SEM. Two-way ANOVA with Bonferroni post-hoc test * p<0.05, **** p<0.0001.

5.1.2 Clinical Chemistry Analysis

The plasma from blood collected by retro-orbital sinus puncture was analysed to measure urea and creatinine as the main markers for kidney function, with albumin, total cholesterol, LDL and HDL (Figure 5.2). The levels of plasma albumin mirrored the proteinuria results, with the B6-*Lama5*$^{E884G/E884G}$ mice showing mild hypoalbuminaemia at 15 weeks of age and more severe hypoalbuminaemia at 25 weeks (Figure 5.2 C). Homozygous mice also exhibited altered lipid metabolism with increased levels of total cholesterol, LDL and HDL (Figure 5.2 D, E and F). Markers of kidney functions were either

slightly elevated at 25 weeks (urea), or normal (creatinine) in comparison with wild-type controls (Figure 5.2 A and B).

Creatinine clearance is the volume of plasma that is cleared of creatinine per unit time and it is often used as an indicator of glomerular filtration rate (GFR), the flow rate of filtered fluids through the glomeruli, and hence of kidney function. It is calculated using the formula (UxV)/P with U= urinary creatinine in umol/L, V= urinary flow rate in ml/minute, P= plasma creatinine in umol/L. No difference between wild-types and homozygotes was detected at any age (Figure 5.2 C).

These results, in combination with the urinalysis data, suggest that even if the B6-*Lama5*$^{E884G/E884G}$ are nephrotic from 15 weeks of age, they conserve a normal renal function at all ages investigated, even in presence of severe proteinuria.

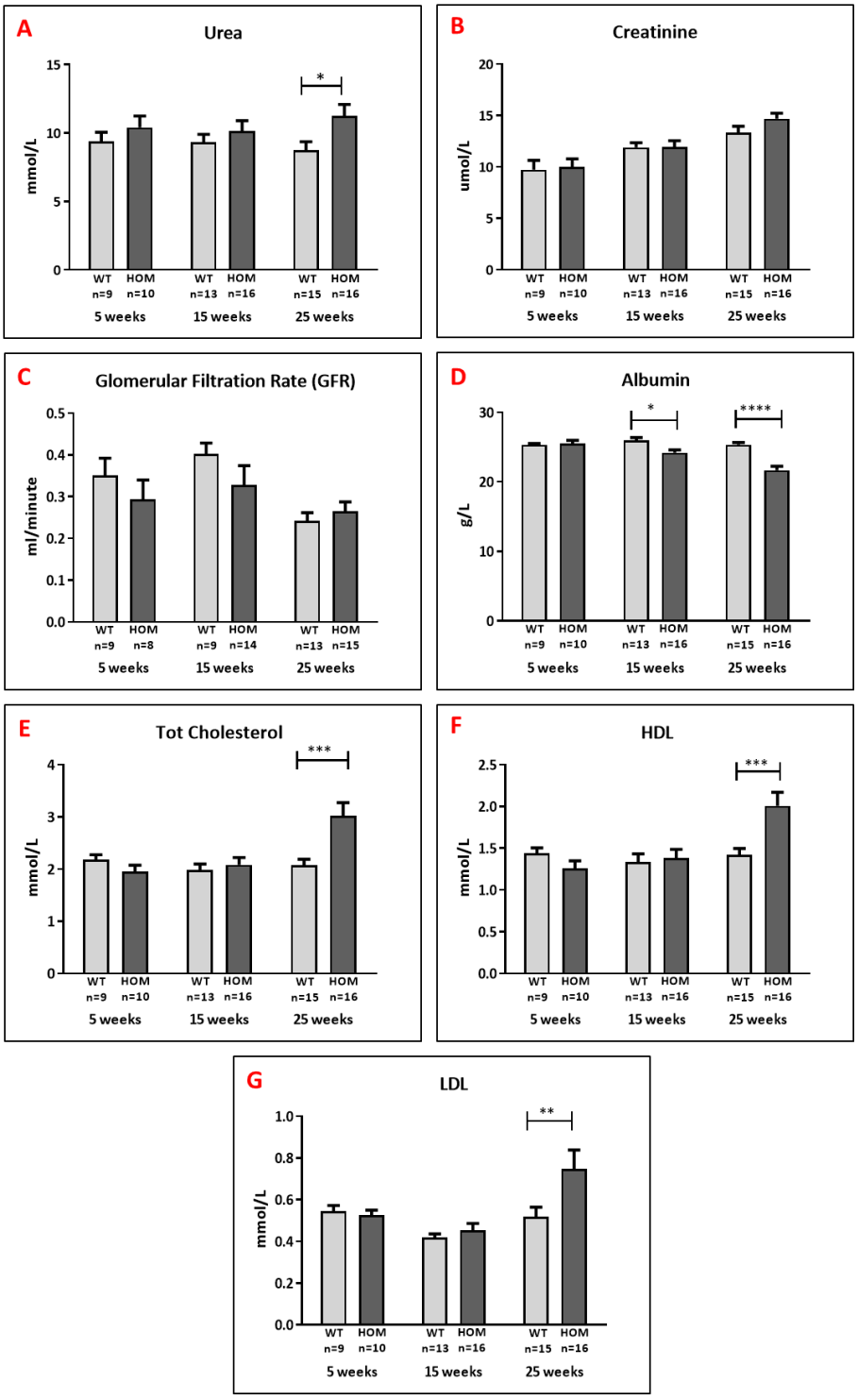

Figure 5.2. Results of the clinical chemistry analysis. B6-*Lama5*$^{E884G/E884G}$ exhibited a nephrotic phenotype with hypoalbuminaemia starting from 15 weeks (**C**) and hypercholesterolaemia at 25 weeks (**D**, **E** and **F**). Even though urea is slightly more elevated in homozygous plasma compared to wild-type samples (**A**), there is no difference in creatinine levels (**B**). Creatinine clearance, an indicator of GFR and its normal values confirm that the homozygous mice have a well-functioning kidney at all ages. The values shown are means ± SEM. Two-way ANOVA with Bonferroni post-hoc test * $p<0.05$, ** $p<0.01$, *** $p<0.001$, **** $p<0.0001$.

5.1.3 Histopathological Analysis and Glomerular Ultrastructure

Kidneys from mutant mice and wild-type controls were processed to look at possible histopathological features and ultrastructure of the glomerulus, and to determine the correlation of gross histopathology with the urine and plasma analysis.

For light microscopy analysis, kidney sections were stained with three different stains: H&E as routine stain, PAS to delineate glomerular cells, mesangial matrix changes of the GBM, and MT to highlight possible fibrosis. Kidneys of affected animals did not show any glomerular (Figure 5.3) or tubular (data not shown) lesions compared with unaffected controls, even at 25 weeks of age when the same B6-*Lama5*$^{E884G/E884G}$ exhibited severe proteinuria, leukocyturia, hypoalbuminaemia and hypercholesterolaemia.

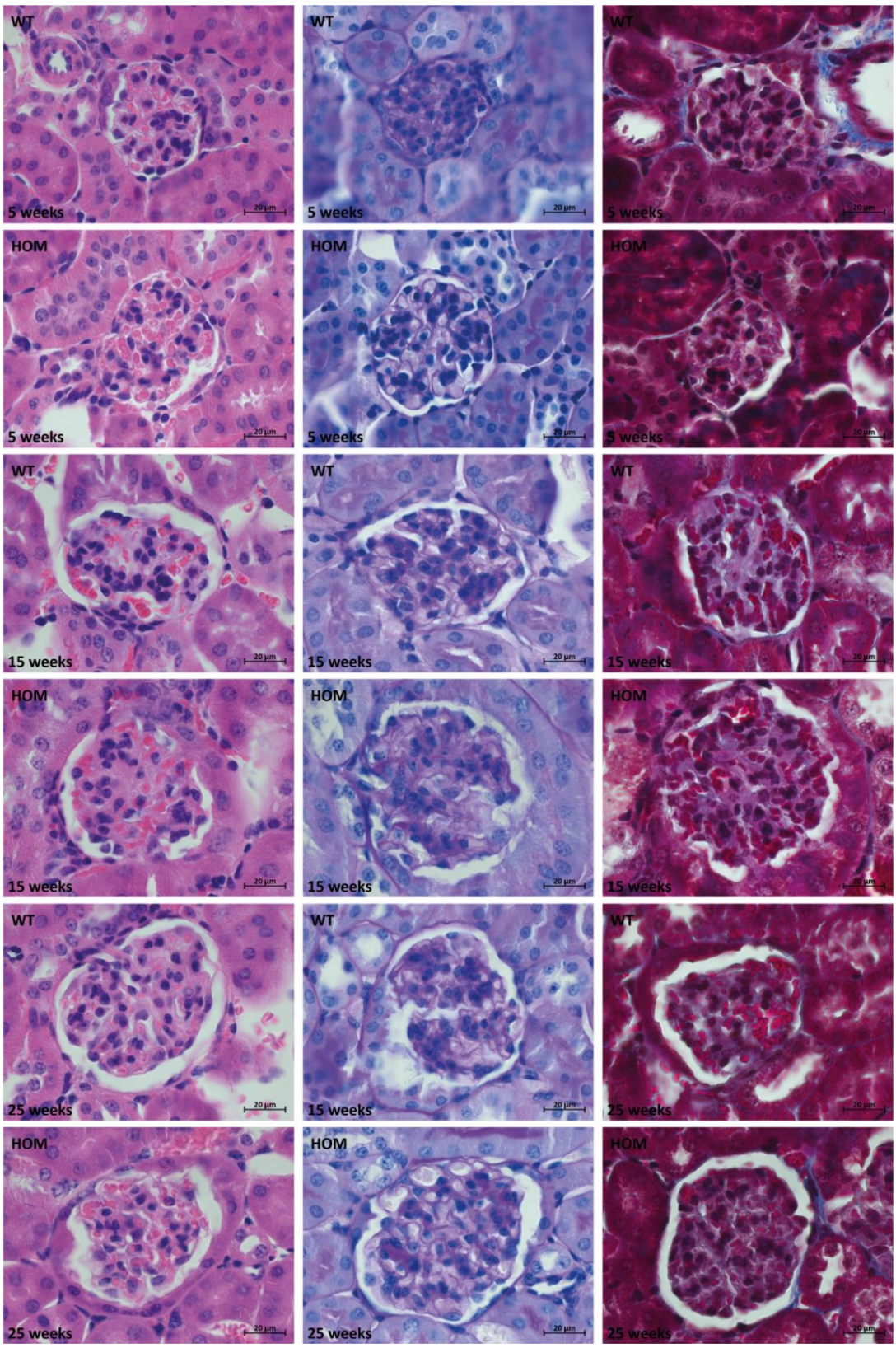

Figure 5.3. Results of the histological time course study. H&E (first column), PAS (middle column) and MT (right column) stains were used to study kidney architecture. No difference was identified between affected mice and wild-type controls. Scale bar represents 20 µm.

To look at the glomerular ultrastructure, samples from the same kidneys assessed by histology were processed for TEM at 5, 15 and 25 weeks, and for SEM at 15 and 25 weeks. TEM showed a normal renal ultrastructure at 5 and 15 weeks, but irregular subepithelial GBM and podocyte foot process effacement at 25 weeks. Podocyte invasion of the GBM also appears to be present, a feature identified by Randles *et al.* in a number of glomerular diseases, the implication of which remains unclear [239]. The subendothelial GBM and the glomerular endothelium remain normal (Figure 5.4).

The foot process effacement was confirmed by SEM (Figure 5.5). At 25 weeks, the foot processes from homozygotes appeared completely flattened. No difference was seen at 15 weeks with either TEM and SEM although B6-*Lama5*$^{E884G/E884G}$ mice of this age were mildly proteinuric.

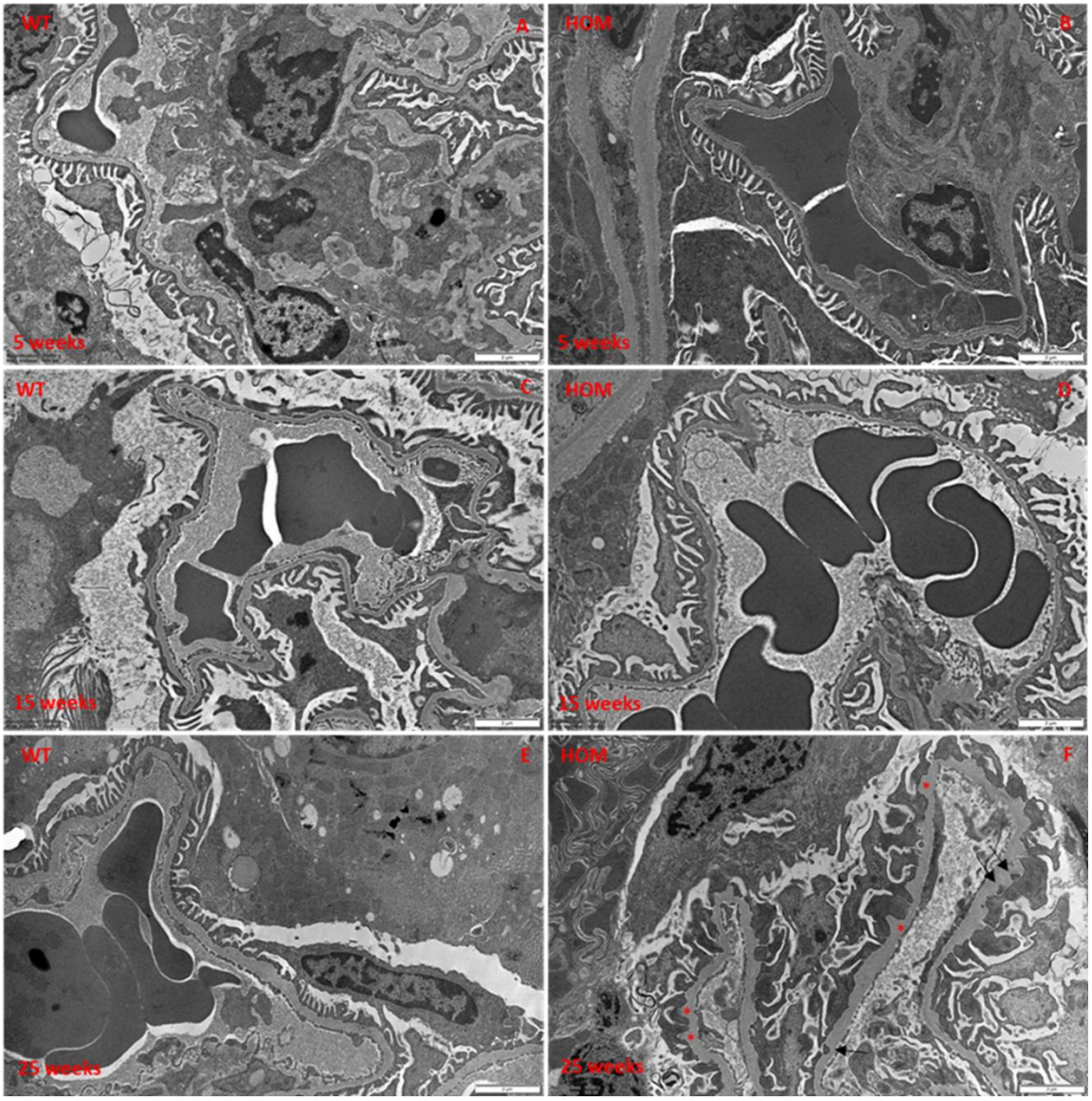

Figure 5.4. Results of TEM time course study on wild type and B6-*Lama5*$^{E884G/E884G}$ kidneys. The GBM maintains its ribbon-like appearance, and podocyte foot processes are clearly distinguishable in both wild type (**A** and **C**) and homozygous mice at 5 and 15 weeks (**B** and **D**). At 25 weeks of age mutant mice (**F**) developed irregular GBM (red stars), loss of foot process definition and partial fusion (foot process effacement) and what appears to be podocyte foot process invasion of the GBM (arrows), while aged matched wild type maintain a normal appearance of the GFB (**E**). Scale bar represents 2 µm.

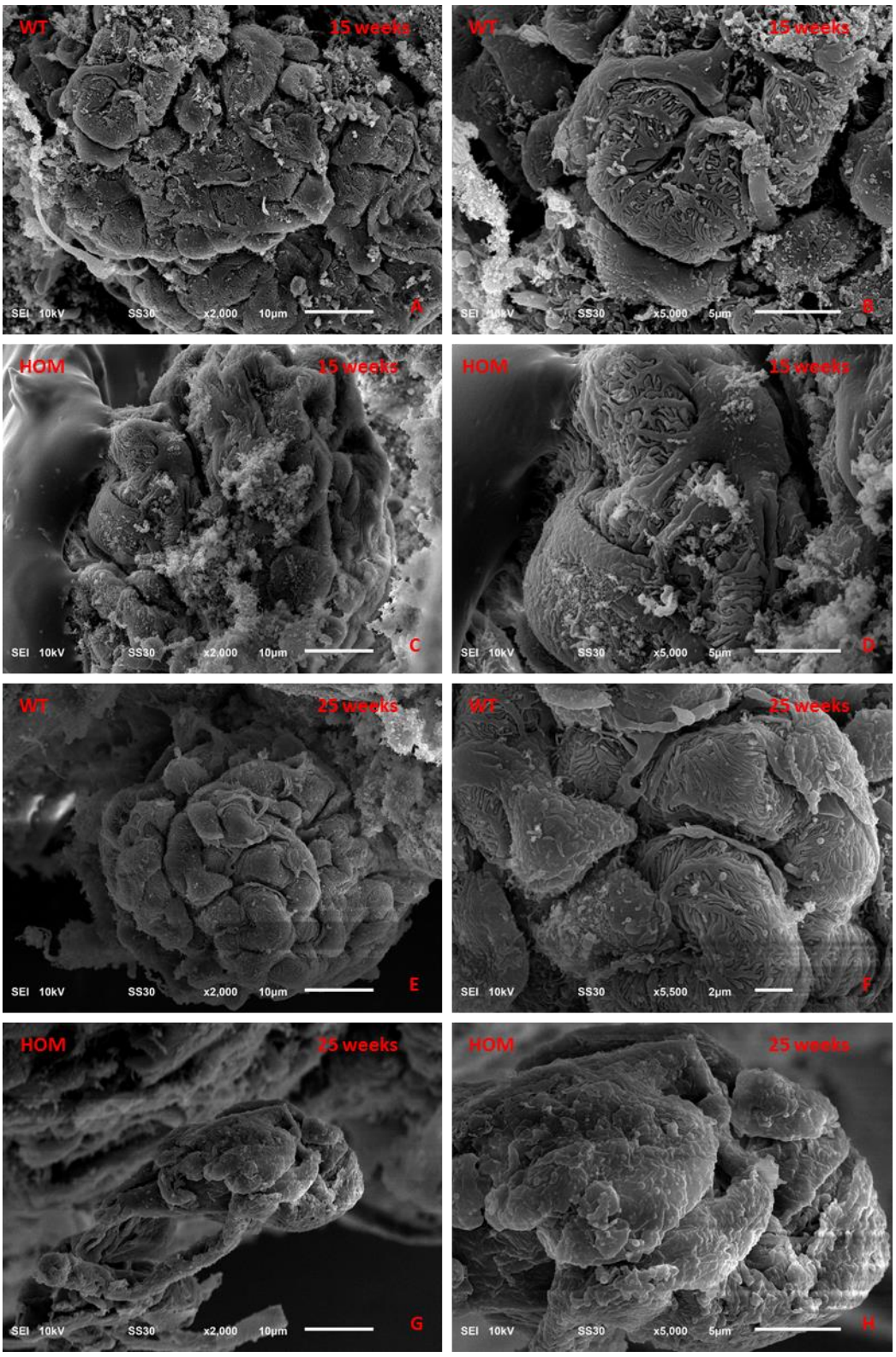

Figure 5.5. Results of SEM time course study on wild-type and B6-*Lama5*$^{E884G/E884G}$ kidneys. A normal podocyte body, primary processes and interdigitate foot processes can be observed in wild type mice at 15 (**A** and **B**) and 25 weeks (**E** and **F**), and in homozygous mice at 15 weeks (**C** and **D**). Foot process effacement, with loss of any interdigital structure, is present in homozygotes at 25 weeks of age, confirming the TEM data (**G** and **H**).

5.2 Laminin Distribution in the Glomerular Basement Membrane

The presence of LAMA5 is essential for the normal development and function of the glomerulus. *In vitro* analysis of laminin α5 expression showed that the E884G mutation affected the ability of HEK293 cells stably expressing *LAMB1* and *LAMC1* to secrete normally LAMA5. Indeed, the amount of mutated construct was dramatically reduced of almost fourfold (WT 90.6% ± 7.9 vs E884G 22.7% ± 0.9).

Since the B6-*Lama5*$^{E884G/E884G}$ mice are viable and develop normally, I investigated the expression of the laminin α5 chain and its trimer partner laminin β2 chain in the kidneys of affected mice and unaffected controls at 15 and 25 weeks (Figure 5.6 A and B). Both expression and distribution of LAMA5 and LAMB2 did not vary between in samples collected from homozygous and littermate control mice at 15 and 25 weeks. This confirms that the point mutation results in a hypomorphic allele.

As mutations in other components of the GBM such as collagen type IV proteins and laminin β2 chains result in the aberrant expression and localization of other laminin chains, I also looked at the expression of LAMB1, which can form a trimer with laminin α5 chain and laminin γ1 chain (laminin-511), but its expression is limited to the mesangium. The expression of LAMB1 in the mutants did not differ from the wild-type controls (Figure 5.6 C).

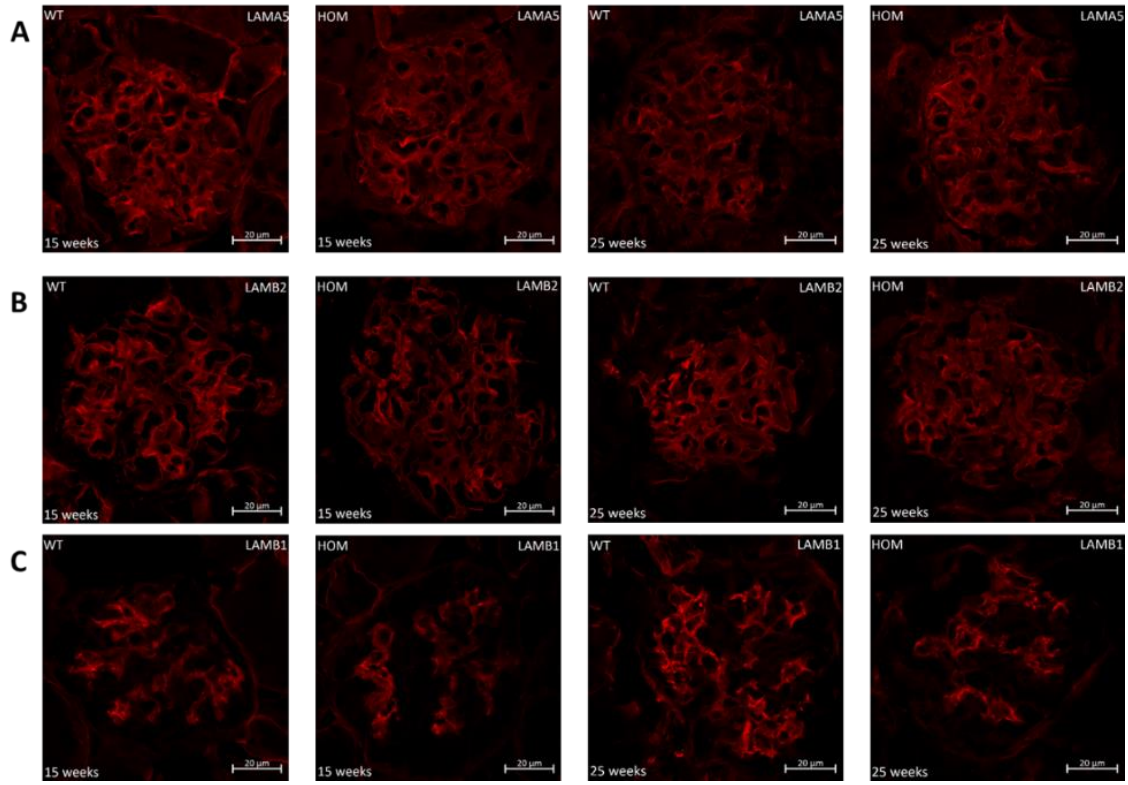

Figure 5.6. Representative immunofluorescence images of wild-type and homozygous mice, at 15 and 25 weeks, stained with anti-LAMA5 (**A**). anti-LAMB2 (**B**) and anti-LAMB1 (**C**). The mutant LAMA5 protein and its trimer partner LAMB2 are normally distributed in the homozygous sample suggesting a normal secretion and incorporation into the GBM. LAMB1 is expressed solely in the mesangium, demonstrating the absence of aberrant localization.

These immunofluorescence results are in contrast with the *in vitro* analysis of laminin α5 secretion and a different approach would be then needed to confirm the expression of laminin α5 in the GBM.

5.3 Protein Studies

The complex composition of the GBM (insoluble and highly cross-linked) represents a challenge for routine biochemical analysis. Given the nature of its protein, normal biochemical analysis such as immunoaffinity-based approaches is very complicated, time-consuming and likely to be inconclusive as they rely on the antibody affinity and antigen accessibility. Transcriptome analysis with RNA sequencing gives a global quantification of the gene expression. Nevertheless, mRNA quantification cannot be always used as a substitute for protein expression, especially in the case of ECM proteins that have a long half-life. Proteomics analysis is, therefore, the best option to study the GBM composition and identify possible pathways involved. Mass spectrometry (MS) is a technique that enables a global protein analysis.

As a result of their complexity and protein-rich nature, biological samples are often analysed with tandem MS (MS/MS), since peptides derived from protein digestion have more chance to have assigned a unique identification for an easier detection and quantification. In MS/MS the peptides are first selected and analysed to determine their exact mass. Then the peptides are fragmented into ions so the final mass spectrometric measurements are carried out in the gas phase on ionized analytes to generate fragment ion spectra [240].

I carried out an extensive proteomics analysis in collaboration with the Wellcome Trust Centre for Cell-Matrix Research (University of Manchester) to study the GBM composition and signalling in B6-*Lama5*$^{E884G/E884G}$. The experiment has been carried at 15 weeks, when proteinuria is detectable but very mild and there is no presence of foot processes effacement or irregular GBM, and at 25 weeks, when the mice exhibit severe

proteinuria, foot processes effacement and focal thickening of the GBM. In choosing these two time points, I hoped to be able to detect early changes and determine if additional changes occurred once the disease is established.

5.3.1 Glomerular Isolation and Protein Extraction

To study protein composition and molecular bases of disease, glomeruli were isolated to avoid contamination from other renal structures.

Sieving techniques have been successfully used to isolate human and rat glomeruli, but it has been difficult to adapt this procedure in mice because of the small diameter of murine glomeruli, very similar to their tubules. I, therefore, used dynabeads containing iron which accumulate in the glomerular vessels and collected the pure B6-*Lama5*$^{+/E884G}$ and B6-*Lama5*$^{E884G/E884G}$ glomeruli with a magnet. The original published protocol [228] was modified to exclude the incubation step with collagenase A, to preserve the composition of the GBM.

Proteins from the isolated glomeruli were extracted using a fractionation approach to enrich the otherwise insoluble ECM component, and preparing protein fractions of the different cell structures (i.e. cellular components and nuclear protein). Immunoblotting confirmed the ECM enrichment and absence of the proteins from another compartment in the ECM fraction (Figure 5.7).

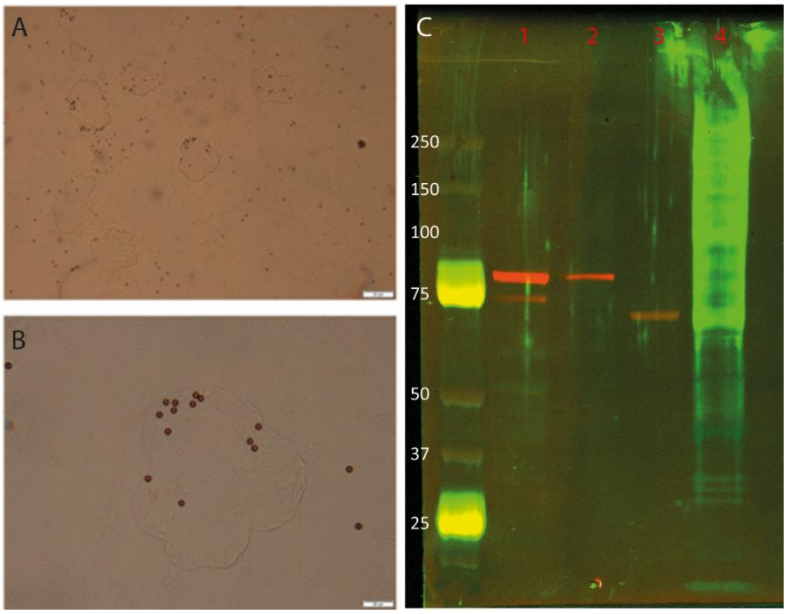

Figure 5.7. A, B: Glomeruli isolated with Dynabeads perfusion and magnetic collection. Dynabeads are visible inside the glomerular tufts as small brown dots (**A** and **B**). Scale bar represents 20 µm. **C**: The successful protein fractionation extraction was confirmed by immunoblotting: nephrin (in red, observed band size: ~85 kDa) is enriched in the two cellular fractions (lane 1 and lane 2); pan-collagen type IV (in green) is only expressed in the ECM enriched fraction (lane 4). An unspecific band (in red) is present in the nuclear fraction (lane 3) and the first cellular fraction (lane 1).

The samples so obtained were prepared for proteomics analysis by the service core of the Wellcome Trust Centre for Cell-Matrix Research.

5.3.2 Renal Extracellular Matrix Proteomics

The abundance of the ECM proteins identified by MS was quantified using Progenesis LCMS (Non Linear Dynamics Ltd) and calculated form the sum of all unique normalised peptide ion abundance for a specific protein on each run. Of all the 1141 proteins identified in all samples, quantification analysis was only carried out on the ones with at least three unique peptides (485).

To highlight the possible different ECM composition in a genotype- and time-dependent manner, a two network maps (one for each time point) were generated. The nodes of the network represent the proteins identified and the different colours represent a protein that is enriched in control samples (blue) or in mutated samples (red) (Figure 5.8).

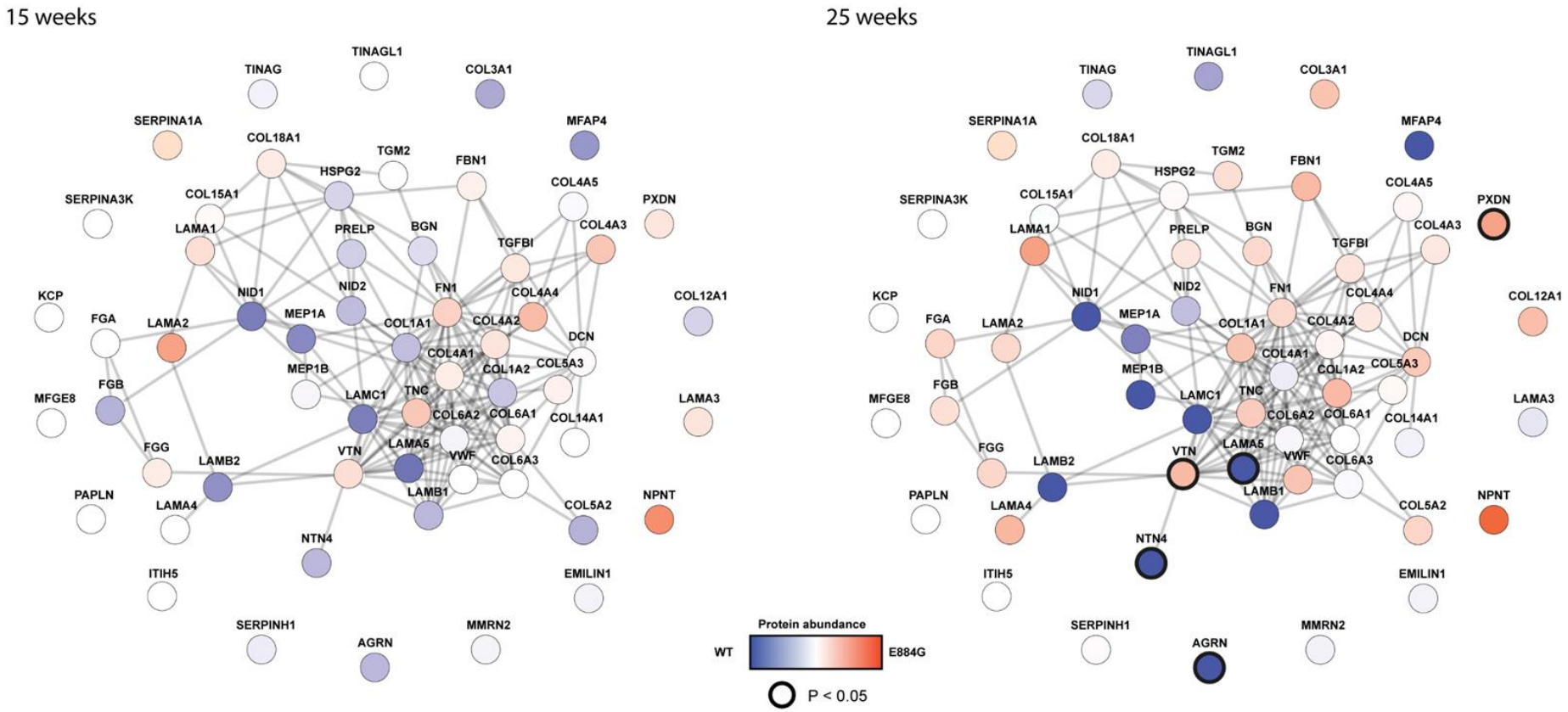

Figure 5.8. Protein interaction network constructed from enriched glomerular ECM proteins identified by MS. The nodes, circles, represent the proteins identified and the edges, lines, represent a reported protein-protein interaction. Nodes are coloured according to the protein abundance, blue if enriched in the wild-type samples and red if enriched in the mutant samples. Darker circles around the nodes indicate statistical significance (two-way ANOVA with Bonferroni post-hoc test $p < 0.05$). Netrin-4 and agrin are enriched in wild-type samples at 25 weeks, laminin α5 is enriched in wild-type samples at 25 weeks, peroxidasin is enriched in mutant samples at 25 weeks. Quantification and network analysis performed by Dr Michael Randles.

Network analysis showed a statistically significant reduction of the abundance of the laminin alpha α5 chain in B6-*Lama5*$^{E884G/E884G}$ samples at 25 weeks. Other laminins that form a trimer with laminin α5 such as laminin β2, laminin β1 and laminin γ1 seem to be more abundant in the wild-type samples meaning that there is a reduction of the laminin networks as a whole. The lower expression of laminin-521 corroborates the hypothesis that the mutation results in a hypomorphic protein since the complete absence of laminin alpha 5 would have resulted in a lethal phenotype.

In addition to the reduced laminin-521, I found a decreased expression at 25 weeks of proteins strictly related to this network: agrin (AGRN) and netrin-4 (NTN4). Agrin, the most abundant HSPG in the GBM [27], is expressed in its full length only in the GBM while isoforms lacking the C-terminal epitopes are localised in the other kidney BMs [241]. Agrin N-terminal end binds laminin γ1 coiled coil via hydrophobic and ionic interactions, while its C-terminal end binds to cell surface receptor-like integrin [242-245]. Although neither agrin nor the other HSPGs of the GBM is essential to maintaining a normal renal function [246], their role is essential for the normal activity of factor H which inactivates the bound of C3b to the GBM [247]. The absence or reduction of HSPGs triggers the local amplification of the C3 activation worsening or exacerbating glomerular lesions, as in glomerulopathies mediated by immunocomplexes (i.e. membranous nephritis and lupus nephritis) or FSGS, where glomerular deposition of C3 and IgM are a common finding [59, 247]. Segmental and reduced expression or absence of HSPGs is reported in several kidney diseases such as membranous nephropathy, minimal change disease and diabetic nephropathy, but not in Alport syndrome or IgA nephropathy [248, 249].

Netrin-4 is a protein of the laminin-related netrin family, with a structure related to laminin β chains and expressed widely especially in the kidney [250]. As agrin, netrin-4

interacts with laminin γ1 forming a high-affinity complex: the strong bond between the LN domains of both proteins prevents the polymerization of the laminin trimers and disrupts the pre-existing laminin network in a non-enzymatic manner [251].

In addition to GBM components, the ECM also contains a number of enzymes required for the post-translational modification of said components [252]. Peroxidasin, enriched in the mutants at 25 weeks, stabilises the collagen IV network catalysing the formation of a sulfilimine bond between the alpha chains [253]. Increased peroxidasin expression is been found in a mouse model of renal fibrosis suggesting that it promotes the formation of ECM during injury, but its role in pathogenesis remains unknown [254].

Lastly, vitronectin (VTN), an ECM glycoprotein also known as complement S protein, is more abundant in homozygous ECM at 25 weeks. Vitronectin is synthesized mostly in the liver and circulates in the bloodstream, however controversial production by the podocytes has been also reported [255, 256]. In the kidney, vitronectin is expressed in the glomerulus and an increased accumulation is detected in many patients with glomerular diseases in both glomeruli [257] and urine [258] suggesting a deleterious role in the progression of glomerulopathies. Indeed, *Vtn*$^{-/-}$ mice showed less glomerular fibrosis and milder proteinuria in a model of experimental nephrotoxic nephritis, possibly due to a decreased deposition of plasminogen activator inhibitor-1 (PAI-1) leading to a more facilitated fibrin clearance because of a greater activation of plasminogen activator activity [259]. The major vitronectin receptor is integrin αVβ3, expressed on the podocyte cell surface and the activation of which has been reported to be the cause of proteinuria, especially when acting as a mediator of the urokinase receptor (uPAR) and soluble urokinase receptor (suPAR) (Nature Medicine papers). Therefore, the role of vitronectin in the pathogenesis of glomerular diseases is still poorly understood.

5.3.3 Renal Cellular Component Proteomics

A similar analysis performed on the glomerular matrisome was also performed to investigate the expression of the proteins involved in focal adhesion (Figure 5.9).

Most of the adhesion proteins expressed in the cellular fractions did not show any significant difference. The only two proteins whose expression were significantly downregulated are kindlin-2 (FERMT2) and integrin α6 (ITGA6).

Integrin α6 forms a heterodimer with integrin β4 and integrin β1 and together they are expressed in podocytes. Indeed, laminin α6 can bind integrin β4 and β1 through binding site present in the LG C-terminal domains and LN n-terminal domain. Although integrin α6 is expressed in the kidney, *Itga6* knockout mice do not show any renal phenotype and double Itga3/Itga6 knockout mice showed the same phenotype of *Itgα3*$^{-/-}$ mice meaning that integrin α6 is dispensable for a proper kidney function [146, 260, 261]. Nonetheless, integrin α6β4 plays a role in regulating the anchoring of the podocytes to the GBM and it is possible that integrin containing the α6 subunit are associated with the development of fibrotic kidney disease [262].

Kindlin-2 is one of the proteins that mediate mechanical signals through the integrin-laminin pathway. *In vivo* and *in vitro* studies have shown that its role is crucial for the normal architecture of podocytes and their foot processes indirectly promoting the activation of Rac1.

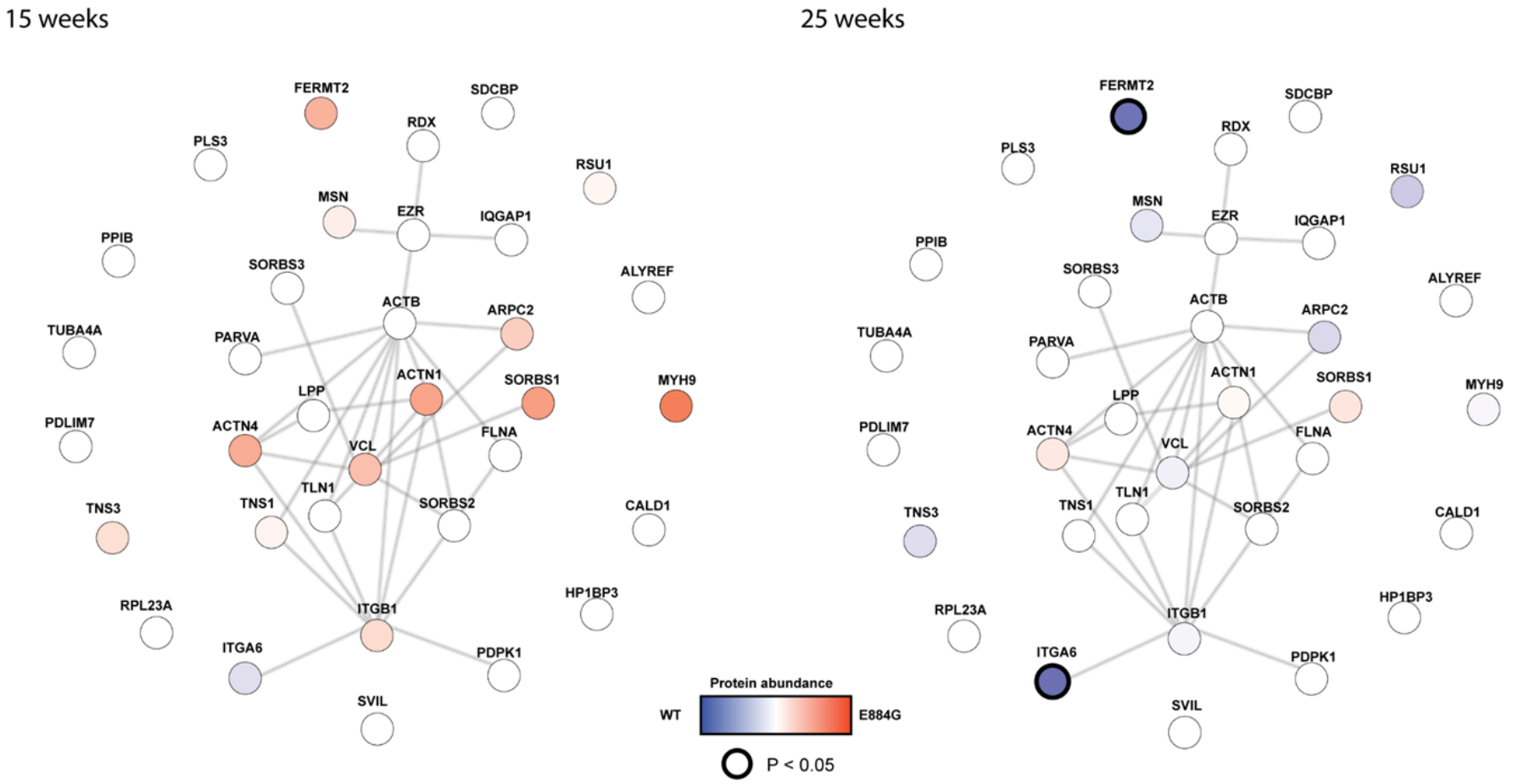

Figure 5.9. Protein interaction network constructed from enriched glomerular cellular proteins identified by MS. The nodes, circles, represent the proteins identified and the edges, lines, represent a reported protein-protein interaction. Nodes are coloured according to the protein abundance, blue if enriched in the wild-type samples and red if enriched in the mutant samples. Darker circles around the nodes indicate statistical significance (two-way ANOVA with Bonferroni post-hoc test $p < 0.05$). Kindlin-2 and integrin α6 are enriched in the wild-type samples. Quantification and network analysis performed by Dr Michael Randles.

Since adhesion proteins can be still present in an insoluble state, their abundance was analysed in the ECM fraction as well (Figure 5.10). Again, all the proteins analysed at 15 weeks and most of the ones analysed at 25 weeks did not show any statistically significant difference, with the exception of supervillin (SVIL) and integrin β1 (ITGB1).

Not much is known about supervillin, especially in relation to its role in maintaining GFB architecture. However, it is known that SVIL modulates focal adhesion involving thyroid receptor–interacting protein 6 (TRIP6) and lipoma-preferred partner (LPP). Expression of LPP was detected in both the cell fraction and ECM fraction but its abundance was not different in B6-*Lama5*$^{E884G/E884G}$ samples compared to wild types.

Integrin β1 is possibly the most important laminin-binding integrin in regards to kidney disease. Increased abundance of ITGB1 at 25 weeks coincides with the previous mRNA expression results carried out on the C3H-*Lama5* line. However, the protein abundance gives an indication of the total protein expression. More analysis would be needed to look at the level of activation of integrin β1.

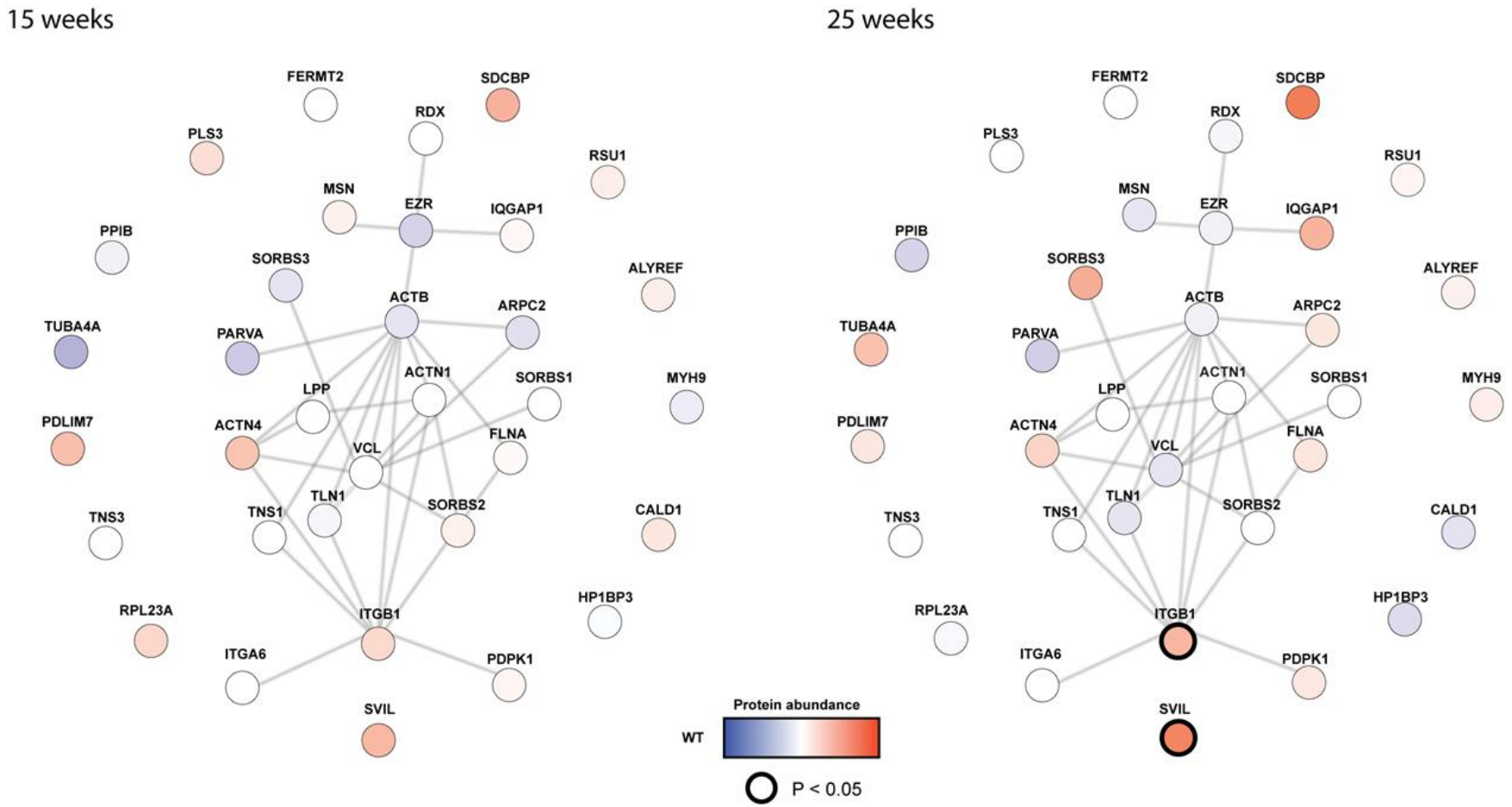

Figure 5.10. Protein interaction network constructed from enriched glomerular ECM proteins identified by MS. The nodes, circles, represent the proteins identified and the edges, lines, represent a reported protein-protein interaction. Nodes are coloured according to the protein abundance, blue if enriched in the wild-type samples and red if enriched in the mutant samples. Darker circles around the nodes indicate statistical significance (two-way ANOVA with Bonferroni post-hoc test $p < 0.05$). Integrin β1 and supervillin are enriched in the mutant samples at 25 weeks. Quantification and network analysis performed by Dr Michael Randles.

The abundance of other proteins involved in focal adhesion complexes but not included in the network analysis, such as ILK, FAK and talin1, was also analysed and no difference was detected between wild-type and B6-*Lama5*$^{E884G/E884G}$ (Figure 5.11).

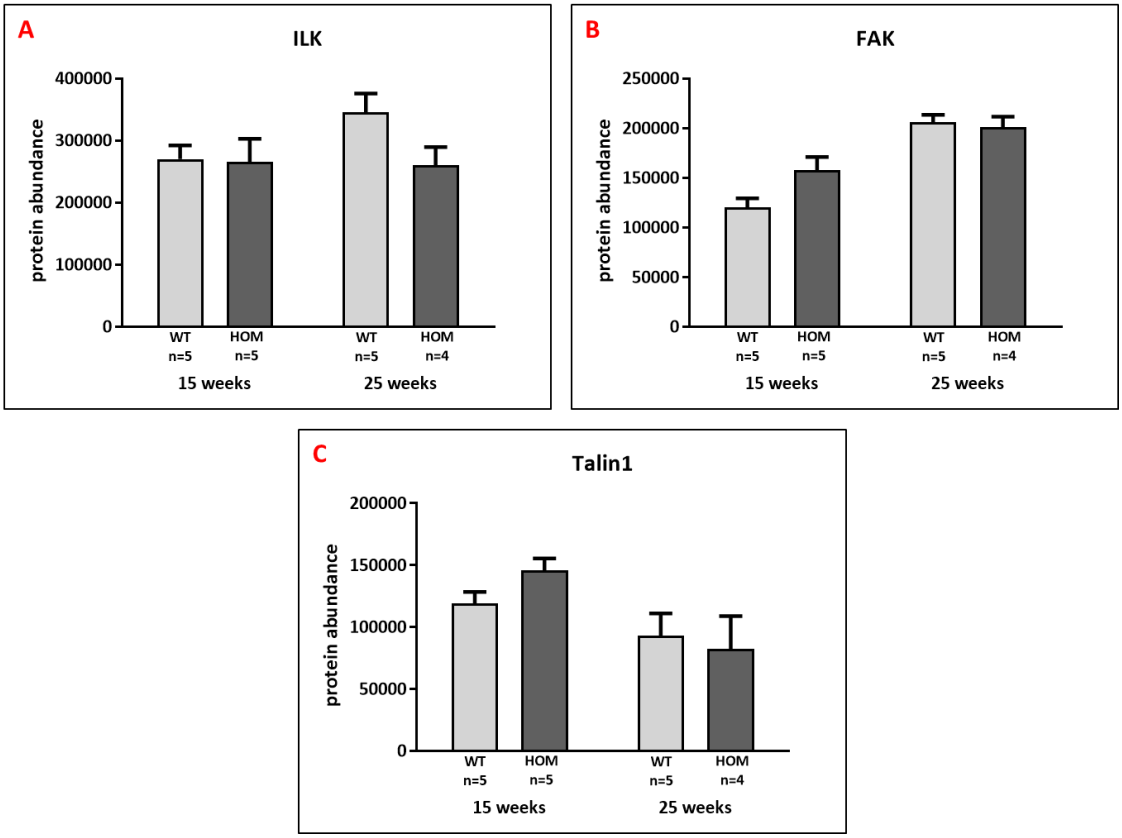

Figure 5.11. Results of the protein abundance of ILK (**A**), FAK (**B**) and talin1 (**C**) in wild-type and B6-*Lama5*$^{E884G/E884G}$ mice. The expression of these proteins, involved in the formation of focal adhesion complexes, in homozygotes appears to be normal when compared to littermate controls.

Lastly, abundance of the protein endoplasmin, also known as heat shock protein 90β1 (HSP90B1) and glucose-regulated protein 94 (GRP94), was increased in homozygous samples at 25 weeks (Figure 5.12). Endoplasmin is the most abundant glycoprotein in the ER, it participates in chaperoning the folding of proteins and it is involved in the ER-associated degradation (ERAD) assisting the targeting of misfolded proteins [263]. Endoplasmin is a selective chaperon and has as clients proteins such as

histocompatibility class I (MHC-I), insulin-like growth factor (IGF) II and integrins [263, 264], but it has also affinity to laminin chains and it has been indicated as a possible chaperone involved in chain assembly [265].

In case of abnormal protein misfolding and/or accumulation of unfolded proteins, ER stress occurs triggering the activation of an adaptive mechanism, the unfolded protein response (UPR), in the patent of increasing the folding capacity and degrading misfold proteins so to restore homeostasis. Endoplasmin is involved in UPR response and it is upregulated during ER stress to increase the efficiency of the folding preventing the activation of apoptotic pathways by the UPR [263, 264].

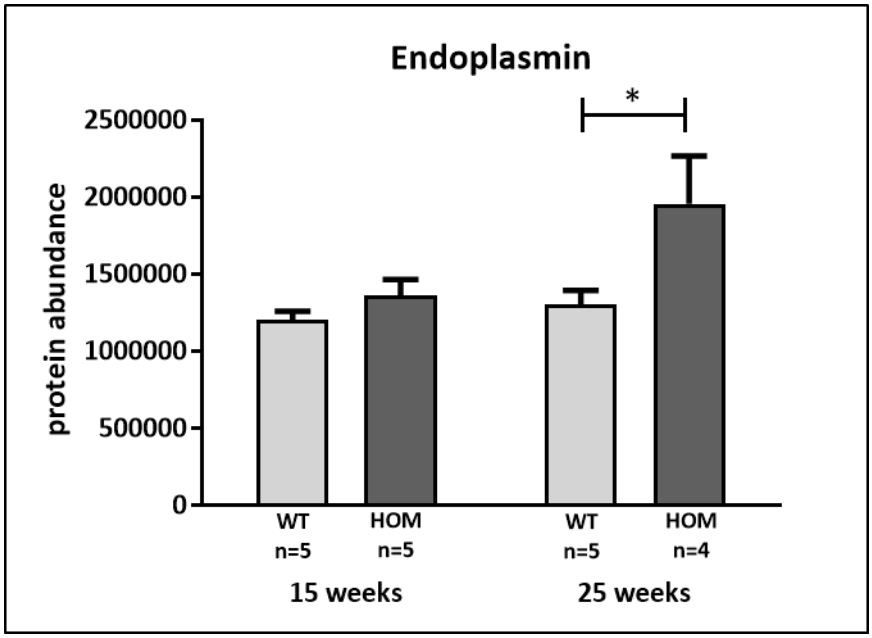

Figure 5.12. Results of the protein abundance of endoplasmin in wild-type and B6-*Lama5*$^{E884G/E884G}$ mice. Mutant samples showed increased abundance at 25 weeks suggesting ER stress and activation of the UPR. The values shown are means ± SEM. Two-way ANOVA with Bonferroni post-hoc test *p <0.05.

5.4 Integrin Activation

Integrin α3β1 is the most highly expressed integrin in the podocytes and binds directly laminin α5. Its importance it has been described in several studies on both laminins and integrins. Up- and downregulation during kidney diseases have both been reported. In models and studies of diabetic nephropathy, downregulation of integrin α3β1 expression in podocytes is thought to be associated with podocyte detachment [266-268]. However, upregulation of α3β1 in podocytes in early stages of diabetic nephropathy has also been reported, as well as in case of reduction of laminin α5 expression [107, 269]. The latter seems to be the case also in this model of *Lama5*-related nephrotic syndrome since the reduction of laminin α5 results in increased expression of integrin β1 in homozygous mice. Moreover, the upregulation of ITGB1 was detected in both C3pde-*Lama5*^{E884G} and B6-*Lama5*^{E884G} lines.

Integrin αVβ3 is not a laminin-binding integrin, it binds vitronectin and fibronectin and it is expressed on the podocyte foot process surface [262]. The αVβ3 dimer, and in particular of integrin β3, has been associated with damage pathway leading to proteinuria and FSGS. In particular, integrin β3 is a mediator of the urokinase receptor (uPAR) and soluble urokinase receptor (suPAR), through its activation [256, 270-272]. MS analysis revealed that in 25 weeks old B6-*Lama5*$^{E884G/E884G}$ mice abundance of vitronectin was increased. Since vitronectin binds integrin β3, and that the activation of the latter leads to proteinuria and FSGS, it could be possible that the more abundant vitronectin in mutant mice activates integrin β3, helping to exacerbate the nephrotic phenotype.

When activated, integrins physically change their conformation and it is possible to measure their activation using specific antibodies that detect epitopes exposed only after the conformational change. The antibody clones 9EG7[273] and HUTS-4[274] for integrin β1, and clones AP5[227] and WOW-1[226] for integrin β3, have been often been used in renal field to look at the activation of these integrins [163, 166, 256, 270, 271, 275-278].

Immunoblotting using the 9EG7 clone antibody was used to assess the activation of integrin β1 (Figure 5.13).

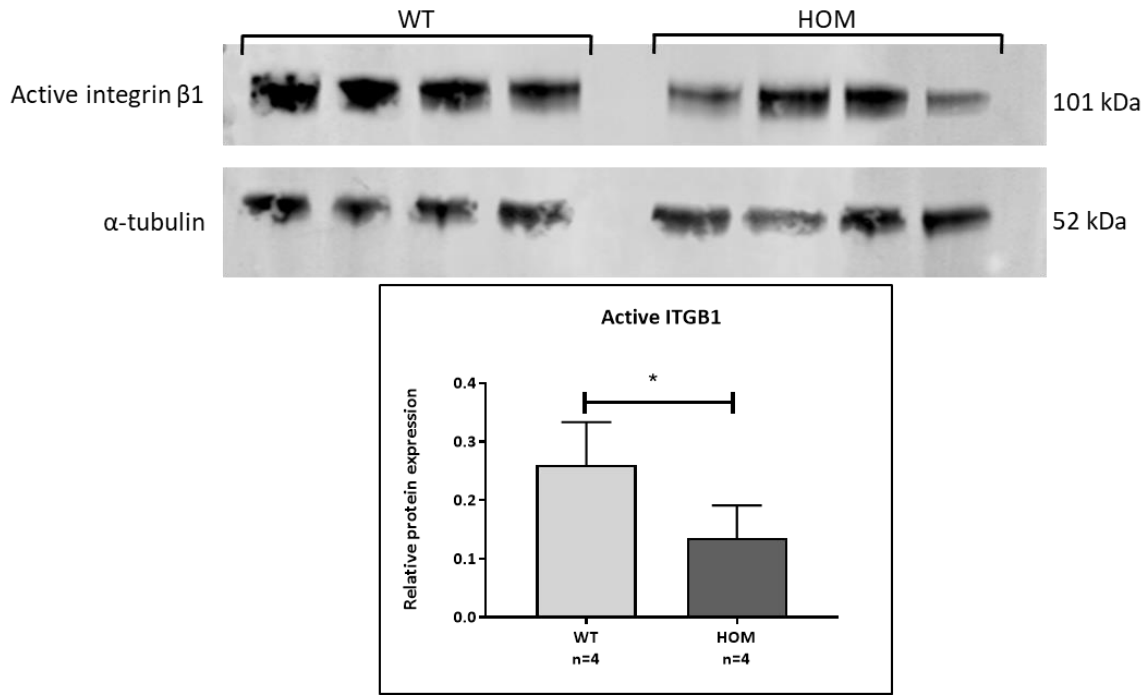

Figure 5.13. Results of the protein expression of active integrin β1 in wild-type and B6-*Lama5*$^{E884G/E884G}$ mice. Mutant samples showed reduced expression at 25 weeks suggesting decreased activation of ITGB1. The values shown are means ± SEM. Two-way ANOVA with Bonferroni post-hoc test *p <0.05.

This result would suggest that although total integrin β1 protein expression in increased in 25 weeks old B6-*Lama5*$^{E884G/E884G}$, the amount of protein that is activated changing its conformation is reduced.

Since vitronectin, increasingly abundant in homozygotes at 25 weeks of age, activates integrin β3, and that integrin β1 seems to be less activated, I decided to investigate whether an integrin signalling switch was occurring in B6-*Lama5*$^{E884G.E884G}$ mice. Using the antibody WOW-1 (kindly gifted by Prof S. Shattil), I looked at integrin β3 activation with immunofluorescence (Figure 5.14). In case of abnormal podocyte activation of integrin β3, WOW-1 should colocalise with slit diaphragm markers such as podocin. In B6-*Lama5*$^{E884G/E884G}$ samples, WOW-1 localisation does not vary from wild-type controls, remaining expressed in the mesangium. Same results were obtained using the antibody AP5 (kindly gifted by Dr P. Newman), another antibody that recognises integrin activation (data not shown).

Results on integrin activation seem to indicate that even if there is a downregulation of active integrin β1, a switch in integrin activation is not present.

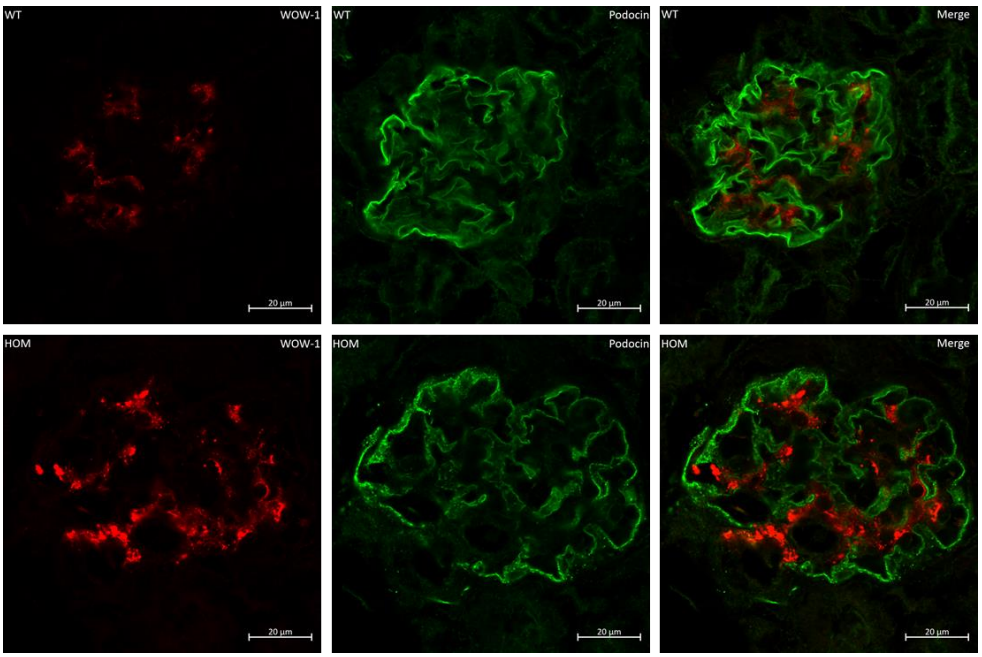

Figure 5.14. Representative immunofluorescence images of wild-type and homozygous mice, at 1 25 weeks, stained with anti-WOW-1 (red) anti-Podocin (green). WOW-1 is expressed solely in the mesangium in both wild-type and homozygotes, as demonstrated in the merge panel, suggesting the absence of abnormal activation of integrin β3 in the podocyte.

5.5 Kindlin-2 Downregulation

Kindlin -2 is one of the components of the focal adhesion of the podocytes. *In vitro* and *in vivo* studies have confirmed the importance of kindlin-2 expression in podocytes for normal cell attachment to the GBM and cell morphology, however, not much it is known about how its specific role. In podocyte-specific knockout mice, the lack of kindlin-2 results in a higher activation of Rac1 due to the reduced expression of one of its inhibitors, RhoGDIα [168]. In a very recent *in vitro* study associated with *in vivo* zebrafish and Drosophila models, the loss of kindlin-2 resulted in cortex destabilization and membrane blebbing due to a re-distrubution of actin filaments [167]. The expression of coronin-1C (CORO1C) and filamin A (FLNA), proteins of the cortical actin cytoskeleton, was reduced in knockout cells and RhoA more active (no difference was found in the activation of Rac1) [167].

Because kindlin-2 was less abundant in 25 weeks B6-*Lama5*$^{E884G/E884G}$ samples analysed by MS, I have looked at the expression of the proteins reported to be related with its decreased expression: coronin-1C, filamin A and RhoGDIα. No difference was detected in the abundance of these proteins between homozygous or control samples at both 15 and 25 weeks (Figure 5.15).

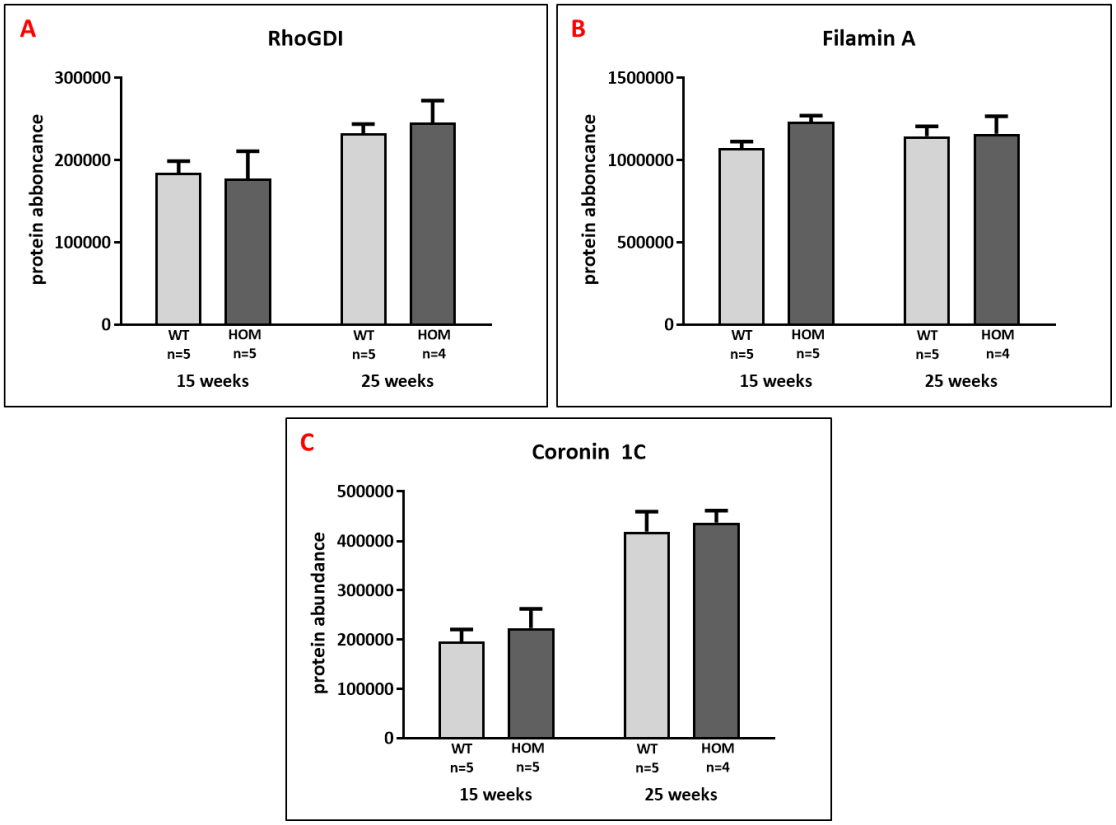

Figure 5.15. Results of the protein abundance of RhoGDI (**A**), filamin A (**B**) and coronin 1C (**C**) in wild-type and B6-*Lama5*$^{E884G/E884G}$ mice. Downregulation of these proteins has been reported in podocytes lacking kindlin-2, but in *Lama5*$^{E884G/E884G}$ mice, their expression did not differ from wild-type glomeruli.

Expression of downstream proteins could exclude a role of kindlin-2 in the pathogenesis of *Lama5*-related nephrotic syndrome. Nonetheless, it could still possible that the decreased expression of kindlin-2 could have an effect on activation of GTPases. Unfortunately, given the high protein concentration needed for to perform the assay, the activation of the GTPases Rac1 and RhoA, could not be measured.

5.6 Chapter 5 Summary and Discussion

Congenic B6 mice homozygous for the E884G mutation still developed a nephrotic phenotype although much later than the original pedigree MPC-205 and C3pde-*Lama5*$^{E884g/E884G}$. If at 6 months of age, the MPC-205$^{E884/E884G}$ mice showed increased levels of urea and creatinine in plasma and C3pde-*Lama5*$^{E884g/E884G}$ had to be culled for welfare concerns, at the same age B6-*Lama5*$^{E884G/E884G}$ mice showed severe proteinuria, hypoalbuminaemia and hypercholesterolaemia but no elevated creatinine or histological lesions by light microscopy. Glomerular ultrastructure assessed by TEM revealed no foot process effacement and a normal-looking GBM at 5 and 15 weeks, but foot process fusion and irregular GBM at 25 weeks. Samples of 15 and 25 weeks old mice were also processed for SEM analysis confirming the healthy aspect of the podocytes at 15 weeks and the complete loss of the interdigitated appearance of the foot processes at 25 weeks.

Even though severe proteinuria correlates with foot process effacement as expected, at 15 weeks B6-*Lama5*$^{E884G/E884G}$ exhibited mild proteinuria but no difference in the podocyte or GBM appearance. Similar results were observed in *Lamb2* knockout mice, a murine model of Pierson syndrome. although the phenotype exhibited by these mice is much more aggressive, with homozygotes dying at one month of age from ESRD, P2 and P5 *Lamb2*$^{-/-}$ animals showed detectable proteinuria but no sign of foot process effacement [85]. The *Lamb2*-null model and now the results of the B6-*Lama5*$^{E884G/E884G}$, implicate a more active role of the GBM in acting as a barrier for albumin.

Proteomics analysis is particularly indicated to study large insoluble proteins such the ones that make up the GBM. Using this approach, I was able to look at the glomerular

GBM composition and a large number of proteins involved in focal adhesion. Indeed MS analysis detected reduced abundance of laminin α5 in mutant samples at 25 weeks that immunofluorescence analysis cannot reveal. Other proteins related to the laminin-521 trimer, such as agrin and netri-4, were less abundant in B6-*Lama5*$^{E884G/E884G}$ glomeruli at 25 weeks of age, while vitronectin abundance was increased in mutants at the same time point.

Proteomics studies on components of the focal adhesion complex revealed an upregulation of integrin β1 in 25 weeks mutant samples, backing up the results seen in the C3pde-*Lama5*$^{E884G/E884G}$samples, and a downregulation of kindlin-2 (FERMT2).

The expression of the RhoGDI, filamin and coronin 1C, reported to be downregulated in the podocyte lacking kindlin-2, maintained a normal level of abundance at both 15 and 25 weeks when compared to wild-type littermates. This result suggests that kindlin-2 is not involved in the mechanism of the pathogenesis of the nephrotic syndrome resulting from the E884G mutation, at least not through the pathways previously described. Both mechanisms suggested result in the over-activation of a GTPase protein, either RhoA or Rac1. The assessment of GTPases activation in B6-*Lama5*$^{E884G/E884G}$ mice could answer the question of a possible involvement of this pathway. Unfortunately, the technicality of the assay does not allow it to be performed on protein isolated from glomeruli.

Integrin β1 was upregulated in homozygous mice of both C3pde-*Lama5*^{E884G} and B6-*Lama5*^{E884G} lines. Nonetheless, the integrin activation was reduced in B6-*Lama5*^{E884G}. Considering the increased abundance of vitronectin, and that the activation of integrin β3, binding partner of vitronectin, is deleterious in podocytes, I have looked at its activation. The localization and expression of active β3 did not differ between controls

and affected, therefore switching in integrin activation seems not to be a factor in the pathogenesis of disease.

Focal adhesion proteomics analysis also indicated an increased abundance of supervillin, a protein member of the villin/gelsolin family that binds F-actin [279]. Overexpression of supervillin decreases cell adhesion to fibronectin and induces redistribution of lamellipodial increasing the numbers of F-actin punctae [280, 281]. Supervillin has not be described in relation to podocyte physiology or to foot process effacement.

Lastly, the reduced abundance of laminin α5 (and in minor extent of the other laminin of the trimer) in the ECM enriched fraction, correlates with the increased expression of the chaperone endoplasmin, or GPR94, a marker of UPR activation.

CHAPTER 6

Discussion and Conclusion

6. Discussion and Conclusion

6.1 Discussion

As part of a large-scale ENU mutagenesis program focused on identifying genes involved in age-related diseases, the Harwell ageing screen, a mutant line with a mutation in the gene coding laminin α5 chain showed kidney impairment and classic histological lesions attributable to CKD. Laminin α5 is a major component of the GBM and it is indispensable for a normal embryonic development.

The causative point mutation was identified as a change of a glutamic acid residue into a glycine in the globular L4a domain. Glutamic acid is a polar acidic amino acid while glycine is a non-polar amino acid, meaning that the mutation results in the change from a hydrophilic amino acid to a hydrophobic one. Moreover, glycine differs greatly in size being the smallest amino acid. *In silico* analysis, using a number of protein prediction algorithms indicated the missense variant as deleterious and likely resulting in disease. *In vitro* study showed that the E884G mutation results in a hypomorph that seems to affect protein secretion. Expression of mutated fragments of the short arm of laminin α5 chain in HEK293T cells resulted in complete absence of secretion, whilst expression of the full-length protein in association with other laminin chains partially rescued the phenotype, reducing the secretion by about 67%.

Phenotypically, homozygous mice showed typical signs of nephrotic syndrome such as severe proteinuria, hypoalbuminaemia and hypercholesterolaemia. The expression of the laminin α5 chain is necessary for a normal embryonic development. LAMA5 is the most abundant laminin α chain of the body and it is expressed almost ubiquitously,

hence the dramatic phenotype displayed by *Lama5* knockout mice. Even given this crucial role, the mutation E884G of laminin α5 ultimately leads only to nephrotic syndrome, without the presence of other obvious phenotypes. Similarly, mutation in collagen IV and laminin β2 sometimes only cause a renal symptomatology.

Kidneys, and in particular glomeruli, are subjected to a series of forces resulting from the filtration of the pre-urine that continuously apply pressure to the GFB. This alone could be the reason why mutations in widely expressed ECM proteins manifest with only kidney disease. Another explanation could lie in the strict composition of the GBM: some organs, such as lungs, express similar laminin and collagen networks to the GBM. However, in lungs, laminin-521 and collagen α3α4α5 are expressed concomitantly with other networks, therefore the lack of one of the components could be compensated with protein already normally present in the ECM. In the case of the GBM, the networks present are the only possible combination. Compensation for loss of one component could lead to the retention of embryonic forms of the given protein (such as collagen α1α1α2 or laminin β1) or to the accumulation of ectopic proteins (like laminin α2) that can change the resistance of the GBM to filtration forces and/or the signalling to the podocytes.

Nonetheless, disease progression was greatly affected by genetic background. Homozygous mice of the original MPC-205 pedigree that entered the pipeline of the Harwell Ageing Screen exhibited signs of kidney impairment at 6 months and had to be culled due welfare concerns around 9 months of age, presumably because of ESRD. C57BL/6J-C3H-C3pde6b+ mixed background mice exhibited proteinuria as early as 7 weeks of age, signs of kidney impairment at 15 weeks and eventually developed ESRD around 25 weeks. On the contrary, *Lama5*$^{E884G/E884G}$ congenic C57BL/6J mice developed

mild proteinuria at 15 weeks and severe proteinuria at 25 weeks, but this was not associated with impaired kidney function. The difference in disease progression is more than likely attributable to the different strain backgrounds of the lines. It is well reported that C57BL/6J is a protective strain for the development of fibrosis [233] and this greatly influences the progression of kidney diseases and hypertension. The percentage of C57BL/6J component in the different lines varies from 18.75% in the C3pde-*Lama5* line, to 62.5% in the original MPC-205 pedigree, and 100% in the congenic B6-*Lama5* line. The progression of the nephrotic phenotype was increasingly more severe in presence of the lower percentage of C57BL/6J.

The effect of different strains influences the onset and progression also of Alport syndrome, another GBM disease. The cause of Alport syndrome is mutations in the genes coding for the α3α4α5 collagen type IV network. In C57BL/6J mice, the upregulation of *Col4a6* and the expression of the α5α5α6 network has been identified as a possible mechanism to compensate the loss of the α3α4α5 network ameliorating disease in models of autosomal recessive Alport syndrome [235]. However, in a more recent study the role of the α5α5α6 as compensatory role has been disproved suggesting the existence of other genes that act as modifiers [282]. In an attempt to determine possible modifiers, Andrews *et al.* used age at ESRD as a quantitative trait to map the modifier as a quantitative trait loci (QTL), identifying possible markers on chromosomes 9 and 16 [283]. Unfortunately, no follow up studies have been carried out to confirm or disprove the presence of a modifier in these two chromosomes.

The reason why C57BL/6J are less susceptible to the development of proteinuria, glomerulosclerosis and hypertension is not clear yet. The activation of the renin-angiotensin-aldosterone system (RAAS) is an important factor in the onset of CKD. Mice

are polymorphic for the number of renin genes, some murine strains such as C57BL/6J, only have one gene (*Ren-1*), while other strains more susceptible to develop renal phenotypes such as 129SvJ have two genes (*Ren-1* and *Ren-2*) [284, 285]. The presence of only one renin gene leads to a decreased activation of the RAAS, slowing down the development of CKD, as demonstrated in a study of glomerularsclerosis and hypertension induced by deoxycorticosterone acetate salt [234]. However, if the difference in the number of renin genes can be a factor in C57BL/6J vs 129SvJ comparison, it should not influence the development of CKD on C3H-C3pde6b+mice, that have only one gene like C57BL/6J mice [285]. Using a model of albumin overload, Ishola *et al.* observed a strain difference in proteinuria and renal inflammatory response which were not due to a difference in renal morphology after the BSA treatment, but more likely due to differences in glomerular protein permeability [286]. Indeed, protein composition and organization of the glomerular ECM varies depending on the genetic background. Global proteomics analysis on the glomerular matrisome found that proteins such as netrin-4 and fibroblast growth factor 2 were enriched in FVB glomeruli (susceptible strain) and proteins such as tenascin C and type I collagen enriched in C57BL/6J glomeruli.

The effect of the susceptible/protective mouse strain disruption of different components of the GFB seems to be consistent, independent of whether mutations affect the GBM, as in the case of Alport syndrome [235] or laminin-521 [105], or by mutations in genes associated with focal adhesion complexes, such as CD151 [157].

The strain effect on renal phenotypes should be considered when choosing the mouse as a model of kidney diseases. C57BL/6 mice are widely used as the background for murine models of disease, but kidney phenotypes might be mild and with late onset

because of the slow development of renal fibrosis or complete absence. Renal phenotypes could be exacerbated by challenging C57BL/6 mice through the administration of deoxycorticosterone acetate/high-salt treatments [236] or by unilateral nephrectomy [287]. On the contrary, susceptible murine strains such as 129SvJ develop a more aggressive phenotype, making dissection of the disease progression challenging.

In humans, studies on the epidemiology of CKD revealed a prevalence of disease varies by sex, race and age [288]. For example, two risk alleles in *APOL1* found in individuals of West African descent have been identified as being a modifier that increases the risk of developing CKD of 3-5 fold [72]. The identifications of modifiers in murine models of renal diseases and their possible translation to patients could be a useful tool to identify new risk alleles deleterious to human health.

More in-depth histological and ultrastructural studies on B6-*Lama5*$^{E884G/E884G}$ revealed the absence of lesions by light microscopy. On electron microscopy, both TEM and SEM, foot process effacement was visible at 25 weeks but not at 15 weeks, the time of proteinuria onset. Given these findings and based on histopathological criteria of classification of nephrotic syndrome, B6-*Lama5*$^{E884G/E884}$ seem to develop MCD since they showed normal-appearing glomeruli on light microscopy but foot process fusion on electron microscopy. Severe proteinuria is the cornerstone symptom of nephrotic syndrome and it is usually the first manifestation of disease and triggers most of the other nephrotic symptoms such as hypoalbuminaemia, oedema and hypercholesterolaemia.

In vitro studies have shown the toxic effect of albumin on both podocytes, inducing inflammatory response [289], and tubular cells, with upregulation of TGF-β1 and inducing ER stress [290, 291]. The effect of albumin overload is reproducible *in vivo*, where it causes

foot process effacement, upregulation of TGF-β1 and COX-2, and reorganization of the actin cytoskeleton [292-295]. In a model of Alport syndrome, the lack of circulating albumin (obtained by generating a *Col4a3* and albumin -*Alb*- double knockout) dramatically improved lifespan of *Col4a3*$^{-/-}$ mice, that developed elevated urea just around one year of age [296]. Mice lacking *Lamb2*, used as model of Pierson syndrome, develop proteinuria before any sign of foot process effacement [85]. B6-*Lama5*$^{E884G/E884G}$ mice exhibit the same phenotype showing proteinuria at 15 weeks but maintaining a normal glomerular ultrastructure until 25 weeks of age. This result suggests a much more active role of the GBM in preventing the passage of albumin through the GFB to the pre-urine. How the GBM plays a role in the filtration of plasma is still unclear. A popular hypothesis is that the deposition of ectopic laminins such as LAMA1, LAMA2 and LAMB1 leads to a change of the usual gel properties and porosity of the GBM [85]. Accumulation of ectopic laminins indeed occurs not only in the case of LAMB2-related disease, but also in Alport syndrome, where deposition of the laminin α2 chain in GBM causes an increased phosphorylation of FAK [194]. However, B6-*Lama5*$^{E884G/E884G}$ samples did not show increased abundance or staining of ectopic laminins suggesting that the filtration role of the GBM does not depend solely on the aberrant presence of constituent proteins. Nonetheless, proteinuria is unlikely to be the only cause of podocyte effacement. The absence of albumin in *Col4a3-Alb* double knock out mice did not completely rescue the phenotype, and there is evidence that podocyte morphology can be maintained in the presence of proteinuria [296, 297]. How much proteinuria affects podocyte health is a causality dilemma very hard to solve. Unfortunately, due to time constrictions, it was not possible to age the B6-*Lama5*$^{E884G/E884G}$ mice long enough to establish the possible onset of kidney impairment, or if these mice would not show any signs of reduced GFR

at all. However, they could prove a very useful tool to study the effect of proteinuria on podocyte health and physiology.

With the aim to dissect the possible pathways and mechanisms of diseases, molecular studies have been performed on both C3pde-*Lama5*^{E884G} and B6-*Lama5*^{E884G} mouse lines. The ultimate role of laminin α5 is to maintain and stabilise the F-actin bundles that make up the cytoskeleton of the foot processes, providing scaffolding and signalling to the podocytes. Laminin α5 regulates actin cytoskeleton through two pathways: integrin, mainly α3β1, signalling pathway and agrin-utrophin pathway. Integrin α3β1 is the main receptor of the laminin α5 chain, its activation leads to clustering and a change of conformation of the dimer, and the recruitment of proteins to form focal adhesion complexes. The podocyte-specific knockout of integrin α3 or β1 results in proteinuria in mice [146]. In addition, reduced activation of integrin β1, but not reduction of total integrin β1 protein, has been reported after lipopolysaccharide-induced podocytopathy and overexpression of B7-1 (also known as CD80) induction of which is associated with nephrotic syndrome by preventing the binding of talin with integrin β1 [298, 299].

Agrin binds laminin-521 coiled coil[245] and together they interact with α and β dystroglycans stabilising the actin cytoskeleton via utrophin [300, 301]. Although the importance of this pathways in podocytes has not been a focus of studies yet, it is very well described in muscles in relation to congenital muscular dystrophy resulting from mutations in *LAMA2* [302]. Interestingly, *LAMA2* mutations found in patients affected by congenital muscular dystrophy are clustered in the short arm [303], just like the ones identified patients affected by *LAMB2*- and *LAMA5*-related nephrotic syndrome and the one described in this thesis. In fact, both pathways seems to be involved in the pathogenesis of the *Lama5*^{E884G} phenotype.

Preliminary study on mixed background mice was performed using gene expression and protein expression analysis. Upregulation of mRNA levels of integrin α3 and β1 and protein levels of integrin β1 suggested a possible response to *Lama5*^{E884G} that compromises the interface podocyte-GBM via the regulation of focal adhesion complexes. This theory was corroborated by the upregulation of genes coding chemical mediators of integrin signals, such as ILK and paxillin, however, protein levels remained unchanged with the only exclusion of total RhoA.

Even though preliminary data looked promising, a better approach to study GBM composition and possible pathways involved was needed. Analysis of the matrisome on ECM fractions extracted from isolated glomeruli was chosen as the best tool to look at the ECM composition, and proteomics analysis of cellular fractions was used to look at any possible variation in cell response between homozygotes and wild-type controls at 15 and 25 weeks of age. This methodology allowed the study of scaffolding proteins that are otherwise very difficult to approach given the complexity of their structure and their limited solubility.

Matrisome analysis confirmed a reduction in laminin α5 protein abundance at 25 weeks of age, backing up the *in vitro* experiment results. Decreased concentration of laminin α5 was not visible with immunofluorescence (possibly due to the position of the epitope or because insufficient sensitivity) proving that MS is a much more sensitive and precise technique. Reduction of wild-type laminin α5 has previously been investigated by Shannon *et al.* who described a more severe phenotype than the one outlined in this thesis [104]. The compound heterozygous animals, used to validate the causative mutation in this thesis, displayed a more severe phenotype than the *Lama5*$^{E884G/E884G}$ animals, although milder than the one described by Shannon *et al*. In addition, *Lama5*$^{+/-}$

animals, with a theoretical 50% reduction in protein levels, do not develop any phenotypes. Taken together, these results produce an allelic series demonstrating various degrees of reduction in LAMA5 and suggests that there may be a threshold level for reduced protein levels before renal phenotypes are observed, and below which there is a relationship between level of LAMA5 and severity of disease.

Reduced secretion has been observed in laminin β2-related nephrotic syndrome, in particular due to mutations, such as R246Q [89] and C321R [90], causing mild symptoms of the Pierson syndrome-spectrum (i.e. milder nephrotic syndrome and absence of extra-renal manifestations). The authors of the i*n vitro* studies on and mouse models of *Lamb2*^{C321R} attributed the nephrotic phenotype to the ER stress resulting from the retention of unfolded laminin β2 and did not explore other modifications that could take part in disease pathogenesis. Similar to *Lamb2*^{C321R}, *Lama5*^{E884G} causes retention of unfolded/misfolded laminin α5 that results in activation of the UPR, as demonstrated by the increased protein abundance of endoplasmin in 25 weeks old homozygotes detected with MS analysis, but the disease mechanism seems to be much more complex than just ER stress.

In addition to the direct effect that unfolded/misfolded laminin α5 has on the activation of the UPR and ER stress, there seem to be two possible pathways involved in the pathogenesis of *Lama5*^{E884G}-dependent nephrotic syndrome which result in actin cytoskeleton regulation.

Laminin α5-binding integrin β1 signalling is a well-characterised pathway since through the activation of ITGB1 focal adhesion complexes are formed. Upregulation of integrin β1 gene and protein was found in both mouse lines under study, but its activation was reduced in B6-*Lama5*$^{E884G/E884G}$ mice. Similar results were seen in a talin 1 knockout

model [163] but no difference in talin 1 abundance was detected in this study. Whether the reduced activation of integrin β1 depends directly on the mutation or just on the reduction of specific substrate, is hard to tell and further investigation would be needed to answer these questions.

Laminin α5 regulates actin cytoskeleton also through the interaction with agrin via dystroglycans-utrophin. Indeed, agrin concentration is reduced in 25 weeks old B6-*Lama5*$^{E884G/E884G}$, concomitant with the reduction of laminin α5. As for integrin β1 activation, it is difficult to attribute the lower protein abundance directly to the effect of E884G on the structure of LAMA5, or if it is simply due to less available trimer available for agrin to interact with. In conclusion, we can, therefore, hypothesise that the mutations affect the actin cytoskeleton regulation through disruption/misregulation of both possible pathways.

Lastly, this study has identified a potential novel role of the protein supervillin in maintaining a stable actin cytoskeleton in podocytes. Podocytes extend numerous lamellipodia that branch into the primary, secondary and foot processes [304], so the redistribution triggered by the overexpression of supervillin seen *in vitro* could have a role in the pathogenesis of foot process effacement [281].

In summary, this study helped to characterise the effect of a deleterious point mutation in a domain with an unknown function of the protein laminin α5. The mutation results in a reduction of laminin α5, reduced activation of integrin β1 and reduction of agrin, as well as upregulation of supervillin, a possible novel protein involved in podocyte pathophysiology. Phenotypically, homozygous mice for the E884G mutation showed nephrotic syndrome, onset and progression of which was greatly modified by the genetic background of the lines under investigation.

6.1.1 Implications for the Field of Renal Research

Recent identification of mutations in *LAMA5* in paediatric patients affected by nephrotic syndrome indicated that this gene is indeed important in human health and it should be screened as a candidate in case of nephrotic patients with no other diagnosis.

Two of the three families understudy carried mutations in the laminin α5 short arm, one of which resulted in the change of a glutamic acid into a glycine in the L4a domain. Although it is not in the exact same position, the mutation identified in the Harwell Ageing Screen it is the first murine model of a point mutation in laminin α5. It could serve as a useful tool to dissect disease mechanisms and could be a good line to test new treatments to alleviate symptoms.

6.2 Future Directions

Even if this study gives an insight into the effect of the mutation on the laminin α5 protein, the work completed so far raises many questions, which could not be answered given time and technical limitations.

Firstly, I demonstrated that the E884G mutation affects laminin α5 secretion but it is not clear whether the phenotype results from the overall reduction of LAMA5 in the GBM or if it is due to the direct effect of the mutation on cell binding or cell signalling.

Secondly, different approaches could be used to try to rescue the phenotype possibly to eventuality identify treatments that could be applicable to humans.

6.2.1 The effect of *Lama5*^{E884G} on the Actin Cytoskeleton

The ECM is not just an agglomeration of scaffold proteins that support cells, it is instead an active component of the GFB involved in pathway signalling.

The laminin α5 chain regulates the actin cytoskeleton of the podocyte foot processes through the integrin α3β1 pathway or the agrin-dystroglycan pathway. The study of actin cytoskeleton in tissues is very challenging, so I suggest two approaches, *in vitro* and *ex vivo*, to study the effect of the E884G mutation. The ultimate aim of the experiments would be to assess the shape and distribution of F-actin bundles and shape/distribution of focal adhesion complexes in a similar fashion to the study of Tian *et al.* on talin 1 [163]. Both approaches would require the use of cultured podocytes, which are a notoriously hard to culture cell line. Human [305] and murine [306] immortalised cell lines are available, and widely used, and should provide consistency for technical and biological replicates.

Moreover, the use of exclusively wild-type cells would eliminate the ER stress factor resulting from the retention of unsecreted LAMA5, so any eventual result would be depending solely on the effect of the E884G mutation on signalling.

In vivo approach. Even in presence of the E884G mutation, LAMA5 is still secreted *in vivo*, although to a severely reduced extent. The protein could therefore be purified and adhesion assays and assessment of the actin cytoskeleton performed by growing podocytes on recombinant LAMA5-coated coverslips.

Since to be secreted laminin α5 has to be part of a trimer, a cell line expressing a β and γ chain is necessary. HEK293 cells stably transfected with laminins are a popular option and have already been used in this project. Another option would be the use of cells that produce their own ECM such as the PFHR-9 cell line, an epithelial adherent line isolated from mouse embryonal carcinoma [307], and already used to study another component of the GBM, collagen type IV [308, 309]. PFHR-9 cells are not easy to transfect, so the CRISPR-Cas9 gene editing technology could be used to induce the E884G to create a cell line stably expressing mutated laminin α5.

Even though *in vitro* production of recombinant proteins does not include the complexity of the components of the GBM, especially after the modifications occurring during disease, this approach is relatively quick and could be used to screen different mutations found in patients in both *LAMA5* and *LAMB2*. Moreover, the coverslips could be coated with the same concentration of wild-type and mutant laminin α5, in this way I could distinguish between the effect of the mutation and the reduced expression of LAMA5. If the actin cytoskeleton and/or the focal adhesion complexes looked variated, the phenotype could be ascribed to the direct effect of E884G.

Ex vivo approach. Multiples studies have demonstrated the possibility of using ECM from organs as a scaffold for downstream applications. Methods of decellularization have been described using organs from animals and humans, and with regards to renal diseases, kidneys have been used to create ECM scaffold to study Alport syndrome or to find new approaches for renal transplant [310-312]. Following published protocols [312], it is possible to decellularise and isolate glomeruli. Podocytes can then be seeded on the glomeruli, which work as a new scaffold since they maintain the same intricate architecture of macromolecules [313].

This approach would be more laborious and animals carrying the E884G mutation would be required. However, the podocyte response would be a better representation of what happens *in vivo* with the benefit of allowing study of the actin cytoskeleton more easily. Other interesting measurements, such as time of colonization of the scaffold glomeruli and cell binding and proteomics analysis, could also help to elucidate the direct effect that this point mutation has on podocytes.

6.2.2 Rescue of the Phenotype

Considering that the effect of the ENU-induced E884G mutation on the laminin α5 structure leads to a defect in secretion, probably resulting in protein misfolding, a way to facilitate LAMA5 release from the cell could be a target to ameliorate disease. Chemical chaperones, in particular tauroursodeoxycholic acid (TUDCA), have been used *in vitro* and *in vivo* to rescue defective trafficking of potentially functional proteins. TUDCA treatment has been successfully used in nephrogenic diabetes insipidus [314], Fabry's disease [315], cystic fibrosis [316], and proved to protect the kidney in a model of

ischaemia/reperfusion-induced acute kidney injury [317]. The use of TUDCA also enhanced the secretion of LAMB2^{C321R} *in vitro* [90].

Consequently, the treatment of *Lama5*$^{E884G/E884G}$ mice with TUDCA could be a good trial to attempt rescue of the nephrotic phenotype or at least delay the disease onset.

It remains unclear whether the phenotype is the direct result of the E884G mutation on the function of the L4a domain, or a result of decreased deposition of laminin α5 in the GBM. It may be possible to determine which of these is the cause of the phenotype by transgenically overexpressing LAMA5^{E884G} in podocytes. This would be done by pronuclear injection of a vector containing the laminin α5 gene under the control of the podocin promoter (*Nphs2*), resulting in podocyte specific overexpression of LAMA5^{E884G}. Theoretically this method would restore laminin α5 protein in the GBM to levels comparable to, or greater than, wild-type animals. If the phenotype is a result of reduced laminin α5 protein levels in the GBM, this approach should rescue it. However, if the phenotype is a direct result of the E884G mutation on the function of the L4a domain, overexpression of LAMA5 is unlikely to significantly alter the development of disease. A considerable caveat to this is that it does not take into account the effect of the misfolded protein on the ER. If the overexpressed protein is unable to be secreted from the podocytes it may lead to a more severe phenotype due to ER stress.

6.2.3 Murine Models of *LAMA5* Mutations Found in Patients

The use of CRISPR-Cas9 technology based on the adaptive immune system that prokaryotic cells use against plasmids and phage, has recently revolutionised gene-editing techniques [318]. This technique uses RNA-guides and the Cas9, an RNA-guided

DNA endonuclease to edit DNA target sequence complementary to the RNA-guides and recognised by a nucleotide motif (PAM – protospacer adjacent motif) downstream of the target sequence [319]. The gene editing so described can be used on cells for *in vitro* studies, or to create animal models injecting the RNA guides and Cas9 in embryos [320, 321].

CRISPR-Cas9 technology can be used to generate animals carrying disease-causing point mutation, it could be then used to create murine models of the mutations recently identified in laminin α5 [118]. The study of different mutations could help to confirm the pathogenicity of the mutations as cause of the nephrotic syndrome. Models of different mutations can also help elucidate the role of laminin α5 and the function of uncharacterised domains in kidney diseases, especially of L4a domain that carries the mutation described in this thesis and one of the disease-causing mutation described by Braun *et al*.

6.3 Concluding Remarks

Using the combination of ENU-mutagenesis and extensive phenotyping pipeline across 18 months, I have been able to identify the first point mutation (E884G) in the gene *Lama5* encoding laminin α5, a major and vital component of the GBM. The mutation results in nephrotic syndrome and is the first model of *Lama5*-related dysfunction where the animals survive to adulthood.

The data I have generated leads me to suggest that defect in protein folding and secretion resulting from the mutation described leads to disease not just triggering ER

stress and UPR, but also influencing the regulation of the actin cytoskeleton via downregulation of agrin and reduced activation of integrin β1.

In conclusion, *Lama5*^{E884G} represents not only a novel mouse model of LAMA5 related nephrotic syndrome, recently identified also in paediatric patients, but could also work as a tool to investigate the role of the entire laminin-521 network, as mutations in LAMB2 lead to Pierson Syndrome and congenital nephrotic syndrome.

CHAPTER 7

Bibliography

7. References

1. Bertram, J.F., et al., *Human nephron number: implications for health and disease.* Pediatr Nephrol, 2011. **26**(9): p. 1529-33.
2. Scott, R.P. and S.E. Quaggin, *Review series: The cell biology of renal filtration.* J Cell Biol, 2015. **209**(2): p. 199-210.
3. Miner, J.H., *Organogenesis of the kidney glomerulus: focus on the glomerular basement membrane.* Organogenesis, 2011. **7**(2): p. 75-82.
4. Miner, J.H., *Glomerular basement membrane composition and the filtration barrier.* Pediatr Nephrol, 2011. **26**(9): p. 1413-7.
5. Haraldsson, B., J. Nystrom, and W.M. Deen, *Properties of the glomerular barrier and mechanisms of proteinuria.* Physiol Rev, 2008. **88**(2): p. 451-87.
6. Suh, J.H. and J.H. Miner, *The glomerular basement membrane as a barrier to albumin.* Nat Rev Nephrol, 2013. **9**(8): p. 470-7.
7. Bulger, R.E., et al., *Endothelial characteristics of glomerular capillaries in normal, mercuric chloride-induced, and gentamicin-induced acute renal failure in the rat.* J Clin Invest, 1983. **72**(1): p. 128-41.
8. Dane, M.J., et al., *A microscopic view on the renal endothelial glycocalyx.* Am J Physiol Renal Physiol, 2015. **308**(9): p. F956-66.
9. Miner, J.H., *Glomerular filtration: the charge debate charges ahead.* Kidney Int, 2008. **74**(3): p. 259-61.
10. Hynes, R.O., *The extracellular matrix: not just pretty fibrils.* Science, 2009. **326**(5957): p. 1216-9.
11. Menon, M.C., P.Y. Chuang, and C.J. He, *The glomerular filtration barrier: components and crosstalk.* Int J Nephrol, 2012. **2012**: p. 749010.
12. Zeisberg, M., et al., *Stage-specific action of matrix metalloproteinases influences progressive hereditary kidney disease.* PLoS Med, 2006. **3**(4): p. e100.
13. Hudson, B.G., S.T. Reeders, and K. Tryggvason, *Type IV collagen: structure, gene organization, and role in human diseases. Molecular basis of Goodpasture and Alport syndromes and diffuse leiomyomatosis.* J Biol Chem, 1993. **268**(35): p. 26033-6.
14. Khoshnoodi, J., et al., *Molecular recognition in the assembly of collagens: terminal noncollagenous domains are key recognition modules in the formation of triple helical protomers.* J Biol Chem, 2006. **281**(50): p. 38117-21.
15. Gubler, M.C., *Inherited diseases of the glomerular basement membrane.* Nat Clin Pract Nephrol, 2008. **4**(1): p. 24-37.
16. Hudson, B.G., et al., *Alport's syndrome, Goodpasture's syndrome, and type IV collagen.* N Engl J Med, 2003. **348**(25): p. 2543-56.
17. Hudson, B.G., *The molecular basis of Goodpasture and Alport syndromes: beacons for the discovery of the collagen IV family.* J Am Soc Nephrol, 2004. **15**(10): p. 2514-27.
18. Alport, A.C., *Hereditary Familial Congenital Haemorrhagic Nephritis.* Br Med J, 1927. **1**(3454): p. 504-6.
19. Yurchenco, P.D., *Basement membranes: cell scaffoldings and signaling platforms.* Cold Spring Harb Perspect Biol, 2011. **3**(2).
20. Nishiuchi, R., et al., *Ligand-binding specificities of laminin-binding integrins: a comprehensive survey of laminin-integrin interactions using recombinant alpha3beta1, alpha6beta1, alpha7beta1 and alpha6beta4 integrins.* Matrix Biol, 2006. **25**(3): p. 189-97.

21. Pierson, M., et al., *[an Unusual Congenital and Familial Congenital Malformative Combination Involving the Eye and Kidney].* J Genet Hum, 1963. **12**: p. 184-213.
22. Zenker, M., et al., *Human laminin beta2 deficiency causes congenital nephrosis with mesangial sclerosis and distinct eye abnormalities.* Hum Mol Genet, 2004. **13**(21): p. 2625-32.
23. Zenker, M., et al., *Demonstration of two novel LAMB2 mutations in the original Pierson syndrome family reported 42 years ago.* Am J Med Genet A, 2005. **138**(1): p. 73-4.
24. Hasselbacher, K., et al., *Recessive missense mutations in LAMB2 expand the clinical spectrum of LAMB2-associated disorders.* Kidney Int, 2006. **70**(6): p. 1008-12.
25. Costell, M., et al., *Perlecan maintains the integrity of cartilage and some basement membranes.* J Cell Biol, 1999. **147**(5): p. 1109-22.
26. Fox, J.W., et al., *Recombinant nidogen consists of three globular domains and mediates binding of laminin to collagen type IV.* EMBO J, 1991. **10**(11): p. 3137-46.
27. Groffen, A.J., et al., *Agrin is a major heparan sulfate proteoglycan in the human glomerular basement membrane.* J Histochem Cytochem, 1998. **46**(1): p. 19-27.
28. Goldberg, S., et al., *Glomerular filtration is normal in the absence of both agrin and perlecan-heparan sulfate from the glomerular basement membrane.* Nephrol Dial Transplant, 2009. **24**(7): p. 2044-51.
29. Bader, B.L., et al., *Compound genetic ablation of nidogen 1 and 2 causes basement membrane defects and perinatal lethality in mice.* Mol Cell Biol, 2005. **25**(15): p. 6846-56.
30. Suleiman, H., et al., *Nanoscale protein architecture of the kidney glomerular basement membrane.* Elife, 2013. **2**: p. e01149.
31. Godel, M., et al., *Microtubule Associated Protein 1b (MAP1B) Is a Marker of the Microtubular Cytoskeleton in Podocytes but Is Not Essential for the Function of the Kidney Filtration Barrier in Mice.* PLoS One, 2015. **10**(10): p. e0140116.
32. Welsh, G.I. and M.A. Saleem, *The podocyte cytoskeleton--key to a functioning glomerulus in health and disease.* Nat Rev Nephrol, 2011. **8**(1): p. 14-21.
33. Hu, G., *Mechanism of podocyte detachment: Targeting transmembrane molecules between podocytes and glomerular basement membrane.* Biomedicine & Aging Pathology, 2013. **3**(1): p. 36-42.
34. Faul, C., et al., *Actin up: regulation of podocyte structure and function by components of the actin cytoskeleton.* Trends Cell Biol, 2007. **17**(9): p. 428-37.
35. Neal, C.R., *Podocytes ... What's Under Yours? (Podocytes and Foot Processes and How They Change in Nephropathy).* Front Endocrinol (Lausanne), 2015. **6**: p. 9.
36. Dressler, G.R., *The cellular basis of kidney development.* Annu Rev Cell Dev Biol, 2006. **22**: p. 509-29.
37. Schlondorff, D., *The glomerular mesangial cell: an expanding role for a specialized pericyte.* FASEB J, 1987. **1**(4): p. 272-81.
38. Soriano, P., *Abnormal kidney development and hematological disorders in PDGF beta-receptor mutant mice.* Genes Dev, 1994. **8**(16): p. 1888-96.
39. Leveen, P., et al., *Mice deficient for PDGF B show renal, cardiovascular, and hematological abnormalities.* Genes Dev, 1994. **8**(16): p. 1875-87.
40. Lindahl, P., et al., *Paracrine PDGF-B/PDGF-Rbeta signaling controls mesangial cell development in kidney glomeruli.* Development, 1998. **125**(17): p. 3313-22.
41. Stockand, J.D. and S.C. Sansom, *Glomerular mesangial cells: electrophysiology and regulation of contraction.* Physiol Rev, 1998. **78**(3): p. 723-44.
42. Gruden, G., et al., *Interaction of angiotensin II and mechanical stretch on vascular endothelial growth factor production by human mesangial cells.* J Am Soc Nephrol, 1999. **10**(4): p. 730-7.
43. Riser, B.L., et al., *Cyclic stretching force selectively up-regulates transforming growth factor-beta isoforms in cultured rat mesangial cells.* Am J Pathol, 1996. **148**(6): p. 1915-23.

44. Riser, B.L., et al., *Regulation of connective tissue growth factor activity in cultured rat mesangial cells and its expression in experimental diabetic glomerulosclerosis.* J Am Soc Nephrol, 2000. **11**(1): p. 25-38.
45. Jefferson, J.A., S.J. Shankland, and R.H. Pichler, *Proteinuria in diabetic kidney disease: a mechanistic viewpoint.* Kidney Int, 2008. **74**(1): p. 22-36.
46. Schlondorff, D. and B. Banas, *The mesangial cell revisited: no cell is an island.* J Am Soc Nephrol, 2009. **20**(6): p. 1179-87.
47. Suzuki, H., et al., *IgA1-secreting cell lines from patients with IgA nephropathy produce aberrantly glycosylated IgA1.* J Clin Invest, 2008. **118**(2): p. 629-39.
48. Moeller, M.J. and V. Tenten, *Renal albumin filtration: alternative models to the standard physical barriers.* Nat Rev Nephrol, 2013. **9**(5): p. 266-77.
49. Rodewald, R. and M.J. Karnovsky, *Porous substructure of the glomerular slit diaphragm in the rat and mouse.* J Cell Biol, 1974. **60**(2): p. 423-33.
50. Ryan, G.B. and M.J. Karnovsky, *Distribution of endogenous albumin in the rat glomerulus: role of hemodynamic factors in glomerular barrier function.* Kidney Int, 1976. **9**(1): p. 36-45.
51. Smithies, O., *Why the kidney glomerulus does not clog: a gel permeation/diffusion hypothesis of renal function.* Proc Natl Acad Sci U S A, 2003. **100**(7): p. 4108-13.
52. Eppel, G.A., et al., *The return of glomerular-filtered albumin to the rat renal vein.* Kidney Int, 1999. **55**(5): p. 1861-70.
53. Russo, L.M., et al., *The normal kidney filters nephrotic levels of albumin retrieved by proximal tubule cells: retrieval is disrupted in nephrotic states.* Kidney Int, 2007. **71**(6): p. 504-13.
54. Hausmann, R., et al., *Electrical forces determine glomerular permeability.* J Am Soc Nephrol, 2010. **21**(12): p. 2053-8.
55. Hausmann, R., et al., *The glomerular filtration barrier function: new concepts.* Curr Opin Nephrol Hypertens, 2012. **21**(4): p. 441-9.
56. Moeller, M.J. and G.A. Tanner, *Reply: podocytes are key-although albumin never reaches the slit diaphragm.* Nat Rev Nephrol, 2014. **10**(3): p. 180.
57. Vaziri, N.D., *Disorders of lipid metabolism in nephrotic syndrome: mechanisms and consequences.* Kidney Int, 2016. **90**(1): p. 41-52.
58. de Seigneux, S. and P.Y. Martin, *Management of patients with nephrotic syndrome.* Swiss Med Wkly, 2009. **139**(29-30): p. 416-22.
59. Kodner, C., *Nephrotic syndrome in adults: diagnosis and management.* Am Fam Physician, 2009. **80**(10): p. 1129-34.
60. Waldman, M., et al., *Adult minimal-change disease: clinical characteristics, treatment, and outcomes.* Clin J Am Soc Nephrol, 2007. **2**(3): p. 445-53.
61. Rosenberg, A.Z. and J.B. Kopp, *Focal Segmental Glomerulosclerosis.* Clin J Am Soc Nephrol, 2017. **12**(3): p. 502-517.
62. Lai, W.L., et al., *Membranous nephropathy: a review on the pathogenesis, diagnosis, and treatment.* J Formos Med Assoc, 2015. **114**(2): p. 102-11.
63. Jalanko, H., *Congenital nephrotic syndrome.* Pediatr Nephrol, 2009. **24**(11): p. 2121-8.
64. Lennon, R., M.J. Randles, and M.J. Humphries, *The importance of podocyte adhesion for a healthy glomerulus.* Front Endocrinol (Lausanne), 2014. **5**: p. 160.
65. Kestila, M., et al., *Positionally cloned gene for a novel glomerular protein--nephrin--is mutated in congenital nephrotic syndrome.* Mol Cell, 1998. **1**(4): p. 575-82.
66. Preston, R., H.M. Stuart, and R. Lennon, *Genetic testing in steroid-resistant nephrotic syndrome: why, who, when and how?* Pediatr Nephrol, 2017.
67. Weber, S., et al., *NPHS2 mutation analysis shows genetic heterogeneity of steroid-resistant nephrotic syndrome and low post-transplant recurrence.* Kidney Int, 2004. **66**(2): p. 571-9.

68. Bierzynska, A., et al., *Genomic and clinical profiling of a national nephrotic syndrome cohort advocates a precision medicine approach to disease management.* Kidney Int, 2017. **91**(4): p. 937-947.
69. Lipska, B.S., et al., *Genotype-phenotype associations in WT1 glomerulopathy.* Kidney Int, 2014. **85**(5): p. 1169-78.
70. Dreyer, S.D., et al., *Mutations in LMX1B cause abnormal skeletal patterning and renal dysplasia in nail patella syndrome.* Nat Genet, 1998. **19**(1): p. 47-50.
71. Boyer, O., et al., *LMX1B mutations cause hereditary FSGS without extrarenal involvement.* J Am Soc Nephrol, 2013. **24**(8): p. 1216-22.
72. Beckerman, P., et al., *Transgenic expression of human APOL1 risk variants in podocytes induces kidney disease in mice.* Nat Med, 2017. **23**(4): p. 429-438.
73. Yu, H., et al., *A role for genetic susceptibility in sporadic focal segmental glomerulosclerosis.* J Clin Invest, 2016. **126**(4): p. 1603.
74. Cohen, A.H., *Collagen Type III Glomerulopathies.* Adv Chronic Kidney Dis, 2012. **19**(2): p. 101-6.
75. Ryan, J.J., et al., *Sequence analysis of the 'Goodpasture antigen' of mammals.* Nephrol Dial Transplant, 1998. **13**(3): p. 602-7.
76. Salama, A.D., et al., *Goodpasture's disease.* Lancet, 2001. **358**(9285): p. 917-20.
77. Ishimoto, I., et al., *Fibronectin glomerulopathy.* Clin Kidney J, 2013. **6**(5): p. 513-5.
78. Deltas, C., A. Pierides, and K. Voskarides, *The role of molecular genetics in diagnosing familial hematuria(s).* Pediatr Nephrol, 2012. **27**(8): p. 1221-31.
79. Zhang, X., et al., *Structure of the human type IV collagen COL4A6 gene, which is mutated in Alport syndrome-associated leiomyomatosis.* Genomics, 1996. **33**(3): p. 473-9.
80. van der Loop, F.T., et al., *Autosomal dominant Alport syndrome caused by a COL4A3 splice site mutation.* Kidney Int, 2000. **58**(5): p. 1870-5.
81. Longo, I., et al., *COL4A3/COL4A4 mutations: from familial hematuria to autosomal-dominant or recessive Alport syndrome.* Kidney Int, 2002. **61**(6): p. 1947-56.
82. Kfoury, H. and M. Arafah, *The pathological spectrum associated with the ultrastructural finding of thin glomerular basement membrane: A tertiary medical city experience and review of the literature.* Ultrastruct Pathol, 2017. **41**(1): p. 51-54.
83. Noakes, P.G., et al., *The renal glomerulus of mice lacking s-laminin/laminin beta 2: nephrosis despite molecular compensation by laminin beta 1.* Nat Genet, 1995. **10**(4): p. 400-6.
84. Noakes, P.G., et al., *Aberrant differentiation of neuromuscular junctions in mice lacking s-laminin/laminin beta 2.* Nature, 1995. **374**(6519): p. 258-62.
85. Jarad, G., et al., *Proteinuria precedes podocyte abnormalities inLamb2-/- mice, implicating the glomerular basement membrane as an albumin barrier.* J Clin Invest, 2006. **116**(8): p. 2272-9.
86. Kagan, M., et al., *A milder variant of Pierson syndrome.* Pediatr Nephrol, 2008. **23**(2): p. 323-7.
87. Lehnhardt, A., et al., *Pierson syndrome in an adolescent girl with nephrotic range proteinuria but a normal GFR.* Pediatr Nephrol, 2012. **27**(5): p. 865-8.
88. Mohney, B.G., et al., *A novel mutation of LAMB2 in a multigenerational mennonite family reveals a new phenotypic variant of Pierson syndrome.* Ophthalmology, 2011. **118**(6): p. 1137-44.
89. Chen, Y.M., Y. Kikkawa, and J.H. Miner, *A missense LAMB2 mutation causes congenital nephrotic syndrome by impairing laminin secretion.* J Am Soc Nephrol, 2011. **22**(5): p. 849-58.
90. Chen, Y.M., et al., *Laminin beta2 gene missense mutation produces endoplasmic reticulum stress in podocytes.* J Am Soc Nephrol, 2013. **24**(8): p. 1223-33.
91. Bull, K.R., et al., *Next-generation sequencing to dissect hereditary nephrotic syndrome in mice identifies a hypomorphic mutation in Lamb2 and models Pierson's syndrome.* J Pathol, 2014. **233**(1): p. 18-26.

92. Matejas, V., et al., *Mutations in the human laminin beta2 (LAMB2) gene and the associated phenotypic spectrum.* Hum Mutat, 2010. **31**(9): p. 992-1002.
93. Purvis, A. and E. Hohenester, *Laminin network formation studied by reconstitution of ternary nodes in solution.* J Biol Chem, 2012. **287**(53): p. 44270-7.
94. Caroline Spenlé, P.S.A., Gertraud Orend, Jeffrey H. Miner, *Laminin α5 guides tissue patterning and organogenesis.* Cell Adhesion & Migration, 2013. **7**(1): p. 1-11.
95. Miner, J., *Laminins and Their Roles in Mammals.* Microscopy research and Techique, 2008. **71**: p. 349-356.
96. Timpl, R., et al., *Laminin--a glycoprotein from basement membranes.* J Biol Chem, 1979. **254**(19): p. 9933-7.
97. Chung, A.E., et al., *Properties of a basement membrane-related glycoprotein synthesized in culture by a mouse embryonal carcinoma-derived cell line.* Cell, 1979. **16**(2): p. 277-87.
98. Miner, J.H., R.M. Lewis, and J.R. Sanes, *Molecular cloning of a novel laminin chain, alpha 5, and widespread expression in adult mouse tissues.* J Biol Chem, 1995. **270**(48): p. 28523-6.
99. Garbe, J.H., et al., *Complete sequence, recombinant analysis and binding to laminins and sulphated ligands of the N-terminal domains of laminin alpha3B and alpha5 chains.* Biochem J, 2002. **362**(Pt 1): p. 213-21.
100. Miner, J.H., *Building the glomerulus: a matricentric view.* J Am Soc Nephrol, 2005. **16**(4): p. 857-61.
101. Davidson, A.J., *Mouse kidney development*, in *StemBook*. 2008: Cambridge (MA).
102. Abrahamson, D.R., et al., *Cellular origins of type IV collagen networks in developing glomeruli.* J Am Soc Nephrol, 2009. **20**(7): p. 1471-9.
103. Miner, J.H. and C. Li, *Defective glomerulogenesis in the absence of laminin alpha5 demonstrates a developmental role for the kidney glomerular basement membrane.* Dev Biol, 2000. **217**(2): p. 278-89.
104. Shannon, M.B., et al., *A hypomorphic mutation in the mouse laminin alpha5 gene causes polycystic kidney disease.* J Am Soc Nephrol, 2006. **17**(7): p. 1913-22.
105. Goldberg, S., et al., *Maintenance of glomerular filtration barrier integrity requires laminin alpha5.* J Am Soc Nephrol, 2010. **21**(4): p. 579-86.
106. Nguyen, N.M., et al., *Laminin alpha 5 is required for lobar septation and visceral pleural basement membrane formation in the developing mouse lung.* Dev Biol, 2002. **246**(2): p. 231-44.
107. Nguyen, N.M., et al., *Epithelial laminin alpha5 is necessary for distal epithelial cell maturation, VEGF production, and alveolization in the developing murine lung.* Dev Biol, 2005. **282**(1): p. 111-25.
108. Mahoney, Z.X., T.S. Stappenbeck, and J.H. Miner, *Laminin alpha 5 influences the architecture of the mouse small intestine mucosa.* J Cell Sci, 2008. **121**(Pt 15): p. 2493-502.
109. Simon-Assmann, P., et al., *The role of the basement membrane as a modulator of intestinal epithelial-mesenchymal interactions.* Prog Mol Biol Transl Sci, 2010. **96**: p. 175-206.
110. Fukumoto, S., et al., *Laminin alpha5 is required for dental epithelium growth and polarity and the development of tooth bud and shape.* J Biol Chem, 2006. **281**(8): p. 5008-16.
111. Wegner, J., et al., *Laminin alpha5 in the keratinocyte basement membrane is required for epidermal-dermal intercommunication.* Matrix Biol, 2016. **56**: p. 24-41.
112. Pouliot, N., N.A. Saunders, and P. Kaur, *Laminin 10/11: an alternative adhesive ligand for epidermal keratinocytes with a functional role in promoting proliferation and migration.* Exp Dermatol, 2002. **11**(5): p. 387-97.
113. Sampaolo, S., et al., *Identification of the first dominant mutation of LAMA5 gene causing a complex multisystem syndrome due to dysfunction of the extracellular matrix.* J Med Genet, 2017. **54**(10): p. 710-720.

114. Maselli, R.A., et al., *Presynaptic congenital myasthenic syndrome with a homozygous sequence variant in LAMA5 combines myopia, facial tics, and failure of neuromuscular transmission.* Am J Med Genet A, 2017. **173**(8): p. 2240-2245.
115. Chatterjee, R., et al., *Targeted exome sequencing integrated with clinicopathological information reveals novel and rare mutations in atypical, suspected and unknown cases of Alport syndrome or proteinuria.* PLoS One, 2013. **8**(10): p. e76360.
116. Gast, C., et al., *Collagen (COL4A) mutations are the most frequent mutations underlying adult focal segmental glomerulosclerosis.* Nephrol Dial Transplant, 2016. **31**(6): p. 961-70.
117. Miner, J.H., *Mutation in LAMA5 in patients affected bby FSFGS*, S. Falcone, Editor. 2017.
118. Braun, D.A., et al., *Genetic variants in the LAMA5 gene in pediatric nephrotic syndrome.* Nephrol Dial Transplant, 2018.
119. Yurchenco, P.D. and B.L. Patton, *Developmental and pathogenic mechanisms of basement membrane assembly.* Curr Pharm Des, 2009. **15**(12): p. 1277-94.
120. Hussain, S.A., F. Carafoli, and E. Hohenester, *Determinants of laminin polymerization revealed by the structure of the alpha5 chain amino-terminal region.* EMBO Rep, 2011. **12**(3): p. 276-82.
121. Nomizu, M., et al., *Identification of homologous biologically active sites on the N-terminal domain of laminin alpha chains.* Biochemistry, 2001. **40**(50): p. 15310-7.
122. Kikkawa, Y., et al., *Identification of laminin alpha5 short arm peptides active for endothelial cell attachment and tube formation.* J Pept Sci, 2017. **23**(7-8): p. 666-673.
123. Nielsen, P.K. and Y. Yamada, *Identification of cell-binding sites on the Laminin alpha 5 N-terminal domain by site-directed mutagenesis.* J Biol Chem, 2001. **276**(14): p. 10906-12.
124. Katagiri, F., et al., *Identification of active sequences in the L4a domain of laminin alpha5 promoting neurite elongation.* Biochemistry, 2012. **51**(24): p. 4950-8.
125. Sasaki, T. and R. Timpl, *Domain IVa of laminin alpha5 chain is cell-adhesive and binds beta1 and alphaVbeta3 integrins through Arg-Gly-Asp.* FEBS Lett, 2001. **509**(2): p. 181-5.
126. Yu, H. and J.F. Talts, *Beta1 integrin and alpha-dystroglycan binding sites are localized to different laminin-G-domain-like (LG) modules within the laminin alpha5 chain G domain.* Biochem J, 2003. **371**(Pt 2): p. 289-99.
127. Ido, H., et al., *Molecular dissection of the alpha-dystroglycan- and integrin-binding sites within the globular domain of human laminin-10.* J Biol Chem, 2004. **279**(12): p. 10946-54.
128. Kikkawa, Y., et al., *The LG1-3 tandem of laminin alpha5 harbors the binding sites of Lutheran/basal cell adhesion molecule and alpha3beta1/alpha6beta1 integrins.* J Biol Chem, 2007. **282**(20): p. 14853-60.
129. Kikkawa, Y., et al., *Identification of the binding site for the Lutheran blood group glycoprotein on laminin alpha 5 through expression of chimeric laminin chains in vivo.* J Biol Chem, 2002. **277**(47): p. 44864-9.
130. Moulson, C.L., C. Li, and J.H. Miner, *Localization of Lutheran, a novel laminin receptor, in normal, knockout, and transgenic mice suggests an interaction with laminin alpha5 in vivo.* Dev Dyn, 2001. **222**(1): p. 101-14.
131. Rahuel, C., et al., *Genetic inactivation of the laminin alpha5 chain receptor Lu/BCAM leads to kidney and intestinal abnormalities in the mouse.* Am J Physiol Renal Physiol, 2008. **294**(2): p. F393-406.
132. Kikkawa, Y. and J.H. Miner, *Molecular dissection of laminin alpha 5 in vivo reveals separable domain-specific roles in embryonic development and kidney function.* Dev Biol, 2006. **296**(1): p. 265-77.
133. Kikkawa, Y., I. Virtanen, and J.H. Miner, *Mesangial cells organize the glomerular capillaries by adhering to the G domain of laminin alpha5 in the glomerular basement membrane.* J Cell Biol, 2003. **161**(1): p. 187-96.

134. Hynes, R.O., *Integrins: bidirectional, allosteric signaling machines.* Cell, 2002. **110**(6): p. 673-87.
135. Humphries, M.J., *Insights into integrin-ligand binding and activation from the first crystal structure.* Arthritis Res, 2002. **4 Suppl 3**: p. S69-78.
136. Humphries, J.D., A. Byron, and M.J. Humphries, *Integrin ligands at a glance.* J Cell Sci, 2006. **119**(Pt 19): p. 3901-3.
137. Calderwood, D.A., et al., *The integrin alpha1 A-domain is a ligand binding site for collagens and laminin.* J Biol Chem, 1997. **272**(19): p. 12311-7.
138. Tulla, M., et al., *Selective binding of collagen subtypes by integrin alpha 1I, alpha 2I, and alpha 10I domains.* J Biol Chem, 2001. **276**(51): p. 48206-12.
139. Frelinger, A.L., 3rd, et al., *Selective inhibition of integrin function by antibodies specific for ligand-occupied receptor conformers.* J Biol Chem, 1990. **265**(11): p. 6346-52.
140. Askari, J.A., et al., *Linking integrin conformation to function.* J Cell Sci, 2009. **122**(Pt 2): p. 165-70.
141. Mould, A.P. and M.J. Humphries, *Regulation of integrin function through conformational complexity: not simply a knee-jerk reaction?* Curr Opin Cell Biol, 2004. **16**(5): p. 544-51.
142. Shen, B., M.K. Delaney, and X. Du, *Inside-out, outside-in, and inside-outside-in: G protein signaling in integrin-mediated cell adhesion, spreading, and retraction.* Curr Opin Cell Biol, 2012. **24**(5): p. 600-6.
143. Sterk, L.M., et al., *Glomerular extracellular matrix components and integrins.* Cell Adhes Commun, 1998. **5**(3): p. 177-92.
144. Fassler, R. and M. Meyer, *Consequences of lack of beta 1 integrin gene expression in mice.* Genes Dev, 1995. **9**(15): p. 1896-908.
145. Fassler, R., et al., *Lack of beta 1 integrin gene in embryonic stem cells affects morphology, adhesion, and migration but not integration into the inner cell mass of blastocysts.* J Cell Biol, 1995. **128**(5): p. 979-88.
146. Pozzi, A., et al., *Beta1 integrin expression by podocytes is required to maintain glomerular structural integrity.* Dev Biol, 2008. **316**(2): p. 288-301.
147. Kanasaki, K., et al., *Integrin beta1-mediated matrix assembly and signaling are critical for the normal development and function of the kidney glomerulus.* Dev Biol, 2008. **313**(2): p. 584-93.
148. Kreidberg, J.A., et al., *Alpha 3 beta 1 integrin has a crucial role in kidney and lung organogenesis.* Development, 1996. **122**(11): p. 3537-47.
149. Sachs, N., et al., *Kidney failure in mice lacking the tetraspanin CD151.* J Cell Biol, 2006. **175**(1): p. 33-9.
150. Has, C., et al., *Integrin alpha3 mutations with kidney, lung, and skin disease.* N Engl J Med, 2012. **366**(16): p. 1508-14.
151. Nicolaou, N., et al., *Gain of glycosylation in integrin alpha3 causes lung disease and nephrotic syndrome.* J Clin Invest, 2012. **122**(12): p. 4375-87.
152. Yauch, R.L., et al., *Highly stoichiometric, stable, and specific association of integrin alpha3beta1 with CD151 provides a major link to phosphatidylinositol 4-kinase, and may regulate cell migration.* Mol Biol Cell, 1998. **9**(10): p. 2751-65.
153. Zhang, F., et al., *Tetraspanin CD151 maintains vascular stability by balancing the forces of cell adhesion and cytoskeletal tension.* Blood, 2011. **118**(15): p. 4274-84.
154. Sincock, P.M., G. Mayrhofer, and L.K. Ashman, *Localization of the transmembrane 4 superfamily (TM4SF) member PETA-3 (CD151) in normal human tissues: comparison with CD9, CD63, and alpha5beta1 integrin.* J Histochem Cytochem, 1997. **45**(4): p. 515-25.
155. Karamatic Crew, V., et al., *CD151, the first member of the tetraspanin (TM4) superfamily detected on erythrocytes, is essential for the correct assembly of human basement membranes in kidney and skin.* Blood, 2004. **104**(8): p. 2217-23.
156. Wright, M.D., et al., *Characterization of mice lacking the tetraspanin superfamily member CD151.* Mol Cell Biol, 2004. **24**(13): p. 5978-88.

157. Baleato, R.M., et al., *Deletion of CD151 results in a strain-dependent glomerular disease due to severe alterations of the glomerular basement membrane.* Am J Pathol, 2008. **173**(4): p. 927-37.
158. Yamada, M. and K. Sekiguchi, *Molecular Basis of Laminin-Integrin Interactions.* Curr Top Membr, 2015. **76**: p. 197-229.
159. Tadokoro, S., et al., *Talin binding to integrin beta tails: a final common step in integrin activation.* Science, 2003. **302**(5642): p. 103-6.
160. Gingras, A.R., et al., *Structural and dynamic characterization of a vinculin binding site in the talin rod.* Biochemistry, 2006. **45**(6): p. 1805-17.
161. Gingras, A.R., et al., *Structural determinants of integrin binding to the talin rod.* J Biol Chem, 2009. **284**(13): p. 8866-76.
162. Zhang, X., et al., *Talin depletion reveals independence of initial cell spreading from integrin activation and traction.* Nat Cell Biol, 2008. **10**(9): p. 1062-8.
163. Tian, X., et al., *Podocyte-associated talin1 is critical for glomerular filtration barrier maintenance.* J Clin Invest, 2014. **124**(3): p. 1098-113.
164. Malinin, N.L., E.F. Plow, and T.V. Byzova, *Kindlins in FERM adhesion.* Blood, 2010. **115**(20): p. 4011-7.
165. Montanez, E., et al., *Kindlin-2 controls bidirectional signaling of integrins.* Genes Dev, 2008. **22**(10): p. 1325-30.
166. Qu, H., et al., *Kindlin-2 regulates podocyte adhesion and fibronectin matrix deposition through interactions with phosphoinositides and integrins.* J Cell Sci, 2011. **124**(Pt 6): p. 879-91.
167. Yasuda-Yamahara, M., et al., *FERMT2 links cortical actin structures, plasma membrane tension and focal adhesion function to stabilize podocyte morphology.* Matrix Biology.
168. Sun, Y., et al., *Kindlin-2 Association with Rho GDP-Dissociation Inhibitor alpha Suppresses Rac1 Activation and Podocyte Injury.* J Am Soc Nephrol, 2017. **28**(12): p. 3545-3562.
169. Otey, C.A. and O. Carpen, *Alpha-actinin revisited: a fresh look at an old player.* Cell Motil Cytoskeleton, 2004. **58**(2): p. 104-11.
170. Feng, D., C. DuMontier, and M.R. Pollak, *The role of alpha-actinin-4 in human kidney disease.* Cell Biosci, 2015. **5**: p. 44.
171. Kaplan, J.M., et al., *Mutations in ACTN4, encoding alpha-actinin-4, cause familial focal segmental glomerulosclerosis.* Nat Genet, 2000. **24**(3): p. 251-6.
172. Yao, J., et al., *Alpha-actinin-4-mediated FSGS: an inherited kidney disease caused by an aggregated and rapidly degraded cytoskeletal protein.* PLoS Biol, 2004. **2**(6): p. e167.
173. Weins, A., et al., *Mutational and Biological Analysis of alpha-actinin-4 in focal segmental glomerulosclerosis.* J Am Soc Nephrol, 2005. **16**(12): p. 3694-701.
174. Dandapani, S.V., et al., *Alpha-actinin-4 is required for normal podocyte adhesion.* J Biol Chem, 2007. **282**(1): p. 467-77.
175. Bays, J.L. and K.A. DeMali, *Vinculin in cell-cell and cell-matrix adhesions.* Cell Mol Life Sci, 2017. **74**(16): p. 2999-3009.
176. Hemmings, L., et al., *Talin contains three actin-binding sites each of which is adjacent to a vinculin-binding site.* J Cell Sci, 1996. **109 (Pt 11)**: p. 2715-26.
177. Bakolitsa, C., et al., *Structural basis for vinculin activation at sites of cell adhesion.* Nature, 2004. **430**(6999): p. 583-6.
178. Carisey, A., et al., *Vinculin regulates the recruitment and release of core focal adhesion proteins in a force-dependent manner.* Curr Biol, 2013. **23**(4): p. 271-81.
179. Lausecker, F., et al., *Vinculin is required to maintain glomerular barrier integrity.* Kidney Int, 2017.
180. Deakin, N.O. and C.E. Turner, *Paxillin comes of age.* J Cell Sci, 2008. **121**(Pt 15): p. 2435-44.
181. Lopez-Colome, A.M., et al., *Paxillin: a crossroad in pathological cell migration.* J Hematol Oncol, 2017. **10**(1): p. 50.

182. Koukouritaki, S.B., A. Tamizuddin, and E.A. Lianos, *Enhanced expression of the cytoskeleton-associated proteins paxillin and focal adhesion kinase in glomerular immune injury.* J Lab Clin Med, 1999. **134**(2): p. 173-9.
183. Hannigan, G.E., et al., *Regulation of cell adhesion and anchorage-dependent growth by a new beta 1-integrin-linked protein kinase.* Nature, 1996. **379**(6560): p. 91-6.
184. Nikolopoulos, S.N. and C.E. Turner, *Actopaxin, a new focal adhesion protein that binds paxillin LD motifs and actin and regulates cell adhesion.* J Cell Biol, 2000. **151**(7): p. 1435-48.
185. Widmaier, M., et al., *Integrin-linked kinase at a glance.* J Cell Sci, 2012. **125**(Pt 8): p. 1839-43.
186. Sakai, T., et al., *Integrin-linked kinase (ILK) is required for polarizing the epiblast, cell adhesion, and controlling actin accumulation.* Genes Dev, 2003. **17**(7): p. 926-40.
187. El-Aouni, C., et al., *Podocyte-specific deletion of integrin-linked kinase results in severe glomerular basement membrane alterations and progressive glomerulosclerosis.* J Am Soc Nephrol, 2006. **17**(5): p. 1334-44.
188. Kretzler, M., et al., *Integrin-linked kinase as a candidate downstream effector in proteinuria.* FASEB J, 2001. **15**(10): p. 1843-5.
189. Guo, L., et al., *The distribution and regulation of integrin-linked kinase in normal and diabetic kidneys.* Am J Pathol, 2001. **159**(5): p. 1735-42.
190. Schaller, M.D., et al., *pp125FAK a structurally distinctive protein-tyrosine kinase associated with focal adhesions.* Proc Natl Acad Sci U S A, 1992. **89**(11): p. 5192-6.
191. Frame, M.C., et al., *The FERM domain: organizing the structure and function of FAK.* Nat Rev Mol Cell Biol, 2010. **11**(11): p. 802-14.
192. Ma, H., et al., *Inhibition of podocyte FAK protects against proteinuria and foot process effacement.* J Am Soc Nephrol, 2010. **21**(7): p. 1145-56.
193. Ilic, D., et al., *Reduced cell motility and enhanced focal adhesion contact formation in cells from FAK-deficient mice.* Nature, 1995. **377**(6549): p. 539-44.
194. Delimont, D., et al., *Laminin alpha2-mediated focal adhesion kinase activation triggers Alport glomerular pathogenesis.* PLoS One, 2014. **9**(6): p. e99083.
195. Mouawad, F., H. Tsui, and T. Takano, *Role of Rho-GTPases and their regulatory proteins in glomerular podocyte function.* Can J Physiol Pharmacol, 2013. **91**(10): p. 773-82.
196. Boureux, A., et al., *Evolution of the Rho family of ras-like GTPases in eukaryotes.* Mol Biol Evol, 2007. **24**(1): p. 203-16.
197. Spiering, D. and L. Hodgson, *Dynamics of the Rho-family small GTPases in actin regulation and motility.* Cell Adh Migr, 2011. **5**(2): p. 170-80.
198. Scott, R.P., et al., *Podocyte-specific loss of Cdc42 leads to congenital nephropathy.* J Am Soc Nephrol, 2012. **23**(7): p. 1149-54.
199. Togawa, A., et al., *Progressive impairment of kidneys and reproductive organs in mice lacking Rho GDIalpha.* Oncogene, 1999. **18**(39): p. 5373-80.
200. Boulter, E., et al., *Regulation of Rho GTPase crosstalk, degradation and activity by RhoGDI1.* Nat Cell Biol, 2010. **12**(5): p. 477-83.
201. Akilesh, S., et al., *Arhgap24 inactivates Rac1 in mouse podocytes, and a mutant form is associated with familial focal segmental glomerulosclerosis.* J Clin Invest, 2011. **121**(10): p. 4127-37.
202. Shibata, S., et al., *Modification of mineralocorticoid receptor function by Rac1 GTPase: implication in proteinuric kidney disease.* Nat Med, 2008. **14**(12): p. 1370-6.
203. Yu, H., et al., *Rac1 activation in podocytes induces rapid foot process effacement and proteinuria.* Mol Cell Biol, 2013. **33**(23): p. 4755-64.
204. McCaffrey, J.C., et al., *Glucocorticoid therapy regulates podocyte motility by inhibition of Rac1.* Sci Rep, 2017. **7**(1): p. 6725.
205. Babelova, A., et al., *Activation of Rac-1 and RhoA contributes to podocyte injury in chronic kidney disease.* PLoS One, 2013. **8**(11): p. e80328.

206. Wang, L., et al., *Mechanisms of the proteinuria induced by Rho GTPases.* Kidney Int, 2012. **81**(11): p. 1075-85.
207. Zhu, L., et al., *Activation of RhoA in podocytes induces focal segmental glomerulosclerosis.* J Am Soc Nephrol, 2011. **22**(9): p. 1621-30.
208. Russell, W.L., et al., *Specific-locus test shows ethylnitrosourea to be the most potent mutagen in the mouse.* Proc Natl Acad Sci U S A, 1979. **76**(11): p. 5818-9.
209. Justice, M.J., et al., *Mouse ENU mutagenesis.* Hum Mol Genet, 1999. **8**(10): p. 1955-63.
210. Acevedo-Arozena, A., et al., *ENU mutagenesis, a way forward to understand gene function.* Annu Rev Genomics Hum Genet, 2008. **9**: p. 49-69.
211. Brown, S.D. and P.M. Nolan, *Mouse mutagenesis-systematic studies of mammalian gene function.* Hum Mol Genet, 1998. **7**(10): p. 1627-33.
212. Hrabe de Angelis, M. and R. Balling, *Large scale ENU screens in the mouse: genetics meets genomics.* Mutat Res, 1998. **400**(1-2): p. 25-32.
213. Soewarto, D., et al., *The large-scale Munich ENU-mouse-mutagenesis screen.* Mamm Genome, 2000. **11**(7): p. 507-10.
214. Gondo, Y., et al., *ENU-based gene-driven mutagenesis in the mouse: a next-generation gene-targeting system.* Exp Anim, 2010. **59**(5): p. 537-48.
215. Goldsworthy, M.E. and P.K. Potter, *Modelling age-related metabolic disorders in the mouse.* Mamm Genome, 2014. **25**(9-10): p. 487-96.
216. Hrabe de Angelis, M.H., et al., *Genome-wide, large-scale production of mutant mice by ENU mutagenesis.* Nat Genet, 2000. **25**(4): p. 444-7.
217. Aigner, B., et al., *Screening for increased plasma urea levels in a large-scale ENU mouse mutagenesis project reveals kidney disease models.* Am J Physiol Renal Physiol, 2007. **292**(5): p. F1560-7.
218. Rieger, A., et al., *Missense Mutation of POU Domain Class 3 Transcription Factor 3 in Pou3f3L423P Mice Causes Reduced Nephron Number and Impaired Development of the Thick Ascending Limb of the Loop of Henle.* PLoS One, 2016. **11**(7): p. e0158977.
219. Kumar, S., et al., *Standardized, systemic phenotypic analysis reveals kidney dysfunction as main alteration of Kctd1 (I27N) mutant mice.* J Biomed Sci, 2017. **24**(1): p. 57.
220. Arnold, C.N., et al., *Rapid identification of a disease allele in mouse through whole genome sequencing and bulk segregation analysis.* Genetics, 2011. **187**(3): p. 633-41.
221. Helmering, J., et al., *A mutation in Ampd2 is associated with nephrotic syndrome and hypercholesterolemia in mice.* Lipids Health Dis, 2014. **13**: p. 167.
222. Potter, P.K., et al., *Novel gene function revealed by mouse mutagenesis screens for models of age-related disease.* Nat Commun, 2016. **7**: p. 12444.
223. McKee, K.K., et al., *Role of laminin terminal globular domains in basement membrane assembly.* J Biol Chem, 2007. **282**(29): p. 21437-47.
224. Miner, J.H., et al., *The laminin alpha chains: expression, developmental transitions, and chromosomal locations of alpha1-5, identification of heterotrimeric laminins 8-11, and cloning of a novel alpha3 isoform.* J Cell Biol, 1997. **137**(3): p. 685-701.
225. Sasaki, T., et al., *Domain IV of mouse laminin beta1 and beta2 chains.* Eur J Biochem, 2002. **269**(2): p. 431-42.
226. Pampori, N., et al., *Mechanisms and consequences of affinity modulation of integrin alpha(V)beta(3) detected with a novel patch-engineered monovalent ligand.* J Biol Chem, 1999. **274**(31): p. 21609-16.
227. Honda, S., et al., *Topography of ligand-induced binding sites, including a novel cation-sensitive epitope (AP5) at the amino terminus, of the human integrin beta 3 subunit.* J Biol Chem, 1995. **270**(20): p. 11947-54.
228. Takemoto, M., et al., *A new method for large scale isolation of kidney glomeruli from mice.* Am J Pathol, 2002. **161**(3): p. 799-805.
229. Randles, M.J., et al., *Genetic Background is a Key Determinant of Glomerular Extracellular Matrix Composition and Organization.* J Am Soc Nephrol, 2015. **26**(12): p. 3021-34.

230. Illumina. *Mouse MD Linkage Panel*. 2018 2015]; Available from: https://emea.illumina.com/?langsel=/gb/.
231. Wittwer, C.T., et al., *High-resolution genotyping by amplicon melting analysis using LCGreen.* Clin Chem, 2003. **49**(6 Pt 1): p. 853-60.
232. Astarita, J.L., S.E. Acton, and S.J. Turley, *Podoplanin: emerging functions in development, the immune system, and cancer.* Front Immunol, 2012. **3**: p. 283.
233. Walkin, L., et al., *The role of mouse strain differences in the susceptibility to fibrosis: a systematic review.* Fibrogenesis Tissue Repair, 2013. **6**(1): p. 18.
234. Hartner, A., et al., *Strain differences in the development of hypertension and glomerular lesions induced by deoxycorticosterone acetate salt in mice.* Nephrol Dial Transplant, 2003. **18**(10): p. 1999-2004.
235. Kang, J.S., et al., *Loss of alpha3/alpha4(IV) collagen from the glomerular basement membrane induces a strain-dependent isoform switch to alpha5alpha6(IV) collagen associated with longer renal survival in Col4a3-/- Alport mice.* J Am Soc Nephrol, 2006. **17**(7): p. 1962-9.
236. Sachs, N., et al., *Blood pressure influences end-stage renal disease of Cd151 knockout mice.* J Clin Invest, 2012. **122**(1): p. 348-58.
237. Farhan, H. and C. Rabouille, *Signalling to and from the secretory pathway.* J Cell Sci, 2011. **124**(Pt 2): p. 171-80.
238. Dalton, A.C. and W.A. Barton, *Over-expression of secreted proteins from mammalian cell lines.* Protein Sci, 2014. **23**(5): p. 517-25.
239. Randles, M.J., et al., *Three-dimensional electron microscopy reveals the evolution of glomerular barrier injury.* Sci Rep, 2016. **6**: p. 35068.
240. Aebersold, R. and M. Mann, *Mass spectrometry-based proteomics.* Nature, 2003. **422**(6928): p. 198-207.
241. Raats, C.J., et al., *Differential expression of agrin in renal basement membranes as revealed by domain-specific antibodies.* J Biol Chem, 1998. **273**(28): p. 17832-8.
242. Martin, P.T. and J.R. Sanes, *Integrins mediate adhesion to agrin and modulate agrin signaling.* Development, 1997. **124**(19): p. 3909-17.
243. Denzer, A.J., et al., *Electron microscopic structure of agrin and mapping of its binding site in laminin-1.* EMBO J, 1998. **17**(2): p. 335-43.
244. Kammerer, R.A., et al., *Interaction of agrin with laminin requires a coiled-coil conformation of the agrin-binding site within the laminin gamma1 chain.* EMBO J, 1999. **18**(23): p. 6762-70.
245. Mascarenhas, J.B., et al., *Mapping of the laminin-binding site of the N-terminal agrin domain (NtA).* EMBO J, 2003. **22**(3): p. 529-36.
246. Harvey, S.J. and J.H. Miner, *Revisiting the glomerular charge barrier in the molecular era.* Curr Opin Nephrol Hypertens, 2008. **17**(4): p. 393-8.
247. Borza, D.B., *Glomerular basement membrane heparan sulfate in health and disease: A regulator of local complement activation.* Matrix Biol, 2017. **57-58**: p. 299-310.
248. van den Born, J., et al., *Distribution of GBM heparan sulfate proteoglycan core protein and side chains in human glomerular diseases.* Kidney Int, 1993. **43**(2): p. 454-63.
249. Groffen, A.J., et al., *Recent insights into the structure and functions of heparan sulfate proteoglycans in the human glomerular basement membrane.* Nephrol Dial Transplant, 1999. **14**(9): p. 2119-29.
250. Yin, Y., J.R. Sanes, and J.H. Miner, *Identification and expression of mouse netrin-4.* Mech Dev, 2000. **96**(1): p. 115-9.
251. Reuten, R., et al., *Structural decoding of netrin-4 reveals a regulatory function towards mature basement membranes.* Nat Commun, 2016. **7**: p. 13515.
252. Borza, C.M., et al., *Cell Receptor-Basement Membrane Interactions in Health and Disease: A Kidney-Centric View.* Curr Top Membr, 2015. **76**: p. 231-53.
253. Vanacore, R., et al., *A sulfilimine bond identified in collagen IV.* Science, 2009. **325**(5945): p. 1230-4.

254. Peterfi, Z., et al., *Peroxidasin is secreted and incorporated into the extracellular matrix of myofibroblasts and fibrotic kidney.* Am J Pathol, 2009. **175**(2): p. 725-35.
255. Seiffert, D., et al., *Detection of vitronectin mRNA in tissues and cells of the mouse.* Proc Natl Acad Sci U S A, 1991. **88**(21): p. 9402-6.
256. Wei, C., et al., *Modification of kidney barrier function by the urokinase receptor.* Nat Med, 2008. **14**(1): p. 55-63.
257. Bariety, J., et al., *Immunohistochemical study of complement S protein (Vitronectin) in normal and diseased human kidneys: relationship to neoantigens of the C5b-9 terminal complex.* Clin Exp Immunol, 1989. **75**(1): p. 76-81.
258. Takahashi, T., S. Inaba, and T. Okada, *[Vitronectin in children with renal disease--2. Examination of urinary vitronectin excretion].* Nihon Jinzo Gakkai Shi, 1995. **37**(4): p. 224-30.
259. Mesnard, L., et al., *Vitronectin dictates intraglomerular fibrinolysis in immune-mediated glomerulonephritis.* FASEB J, 2011. **25**(10): p. 3543-53.
260. Georges-Labouesse, E., et al., *Absence of integrin alpha 6 leads to epidermolysis bullosa and neonatal death in mice.* Nat Genet, 1996. **13**(3): p. 370-3.
261. De Arcangelis, A., et al., *Synergistic activities of alpha3 and alpha6 integrins are required during apical ectodermal ridge formation and organogenesis in the mouse.* Development, 1999. **126**(17): p. 3957-68.
262. Pozzi, A. and R. Zent, *Integrins in kidney disease.* J Am Soc Nephrol, 2013. **24**(7): p. 1034-9.
263. Eletto, D., D. Dersh, and Y. Argon, *GRP94 in ER quality control and stress responses.* Semin Cell Dev Biol, 2010. **21**(5): p. 479-85.
264. Zhu, G. and A.S. Lee, *Role of the unfolded protein response, GRP78 and GRP94 in organ homeostasis.* J Cell Physiol, 2015. **230**(7): p. 1413-20.
265. Kumagai, C. and Y. Kitagawa, *Potential molecular chaperones involved in laminin chain assembly.* Cytotechnology, 1997. **25**(1-3): p. 173-82.
266. Regoli, M. and M. Bendayan, *Alterations in the expression of the alpha 3 beta 1 integrin in certain membrane domains of the glomerular epithelial cells (podocytes) in diabetes mellitus.* Diabetologia, 1997. **40**(1): p. 15-22.
267. Chen, H.C., et al., *Altering expression of alpha3beta1 integrin on podocytes of human and rats with diabetes.* Life Sci, 2000. **67**(19): p. 2345-53.
268. Lin, S., et al., *Spironolactone ameliorates podocytic adhesive capacity via restoring integrin alpha 3 expression in streptozotocin-induced diabetic rats.* J Renin Angiotensin Aldosterone Syst, 2010. **11**(3): p. 149-57.
269. Sawada, K., et al., *Upregulation of alpha3beta1-Integrin in Podocytes in Early-Stage Diabetic Nephropathy.* J Diabetes Res, 2016. **2016**: p. 9265074.
270. Wei, C., et al., *Circulating urokinase receptor as a cause of focal segmental glomerulosclerosis.* Nat Med, 2011. **17**(8): p. 952-60.
271. Yoo, T.H., et al., *Sphingomyelinase-like phosphodiesterase 3b expression levels determine podocyte injury phenotypes in glomerular disease.* J Am Soc Nephrol, 2015. **26**(1): p. 133-47.
272. Huang, J., et al., *Urinary soluble urokinase receptor levels are elevated and pathogenic in patients with primary focal segmental glomerulosclerosis.* BMC Med, 2014. **12**: p. 81.
273. Driessens, M.H., et al., *Adhesion of lymphoma cells to fibronectin: differential use of alpha 4 beta 1 and alpha 5 beta 1 integrins and stimulation by the 9EG7 mAb against the murine beta 1 integrin subunit.* Cell Adhes Commun, 1995. **3**(4): p. 327-36.
274. Luque, A., et al., *Activated conformations of very late activation integrins detected by a group of antibodies (HUTS) specific for a novel regulatory region (355-425) of the common beta 1 chain.* J Biol Chem, 1996. **271**(19): p. 11067-75.
275. Reidy, K.J., et al., *Excess podocyte semaphorin-3A leads to glomerular disease involving plexinA1-nephrin interaction.* Am J Pathol, 2013. **183**(4): p. 1156-1168.

276. Veron, D., et al., *Acute podocyte vascular endothelial growth factor (VEGF-A) knockdown disrupts alphaVbeta3 integrin signaling in the glomerulus.* PLoS One, 2012. **7**(7): p. e40589.
277. Potla, U., et al., *Podocyte-specific RAP1GAP expression contributes to focal segmental glomerulosclerosis-associated glomerular injury.* J Clin Invest, 2014. **124**(4): p. 1757-69.
278. Ussar, S., et al., *Loss of Kindlin-1 causes skin atrophy and lethal neonatal intestinal epithelial dysfunction.* PLoS Genet, 2008. **4**(12): p. e1000289.
279. Pestonjamasp, K.N., et al., *Supervillin (p205): A novel membrane-associated, F-actin-binding protein in the villin/gelsolin superfamily.* J Cell Biol, 1997. **139**(5): p. 1255-69.
280. Takizawa, N., et al., *Supervillin modulation of focal adhesions involving TRIP6/ZRP-1.* J Cell Biol, 2006. **174**(3): p. 447-58.
281. Crowley, J.L., et al., *Supervillin reorganizes the actin cytoskeleton and increases invadopodial efficiency.* Mol Biol Cell, 2009. **20**(3): p. 948-62.
282. Murata, T., et al., *COL4A6 is dispensable for autosomal recessive Alport syndrome.* Sci Rep, 2016. **6**: p. 29450.
283. Andrews, K.L., et al., *Quantitative trait loci influence renal disease progression in a mouse model of Alport syndrome.* Am J Pathol, 2002. **160**(2): p. 721-30.
284. Sigmund, C.D. and K.W. Gross, *Structure, expression, and regulation of the murine renin genes.* Hypertension, 1991. **18**(4): p. 446-57.
285. Hansen, P.B., et al., *Plasma renin in mice with one or two renin genes.* Acta Physiol Scand, 2004. **181**(4): p. 431-7.
286. Ishola, D.A., Jr., et al., *In mice, proteinuria and renal inflammatory responses to albumin overload are strain-dependent.* Nephrol Dial Transplant, 2006. **21**(3): p. 591-7.
287. Eddy, A.A., et al., *Investigating mechanisms of chronic kidney disease in mouse models.* Pediatr Nephrol, 2012. **27**(8): p. 1233-47.
288. Stevens, L.A., et al., *Evaluation of the Chronic Kidney Disease Epidemiology Collaboration equation for estimating the glomerular filtration rate in multiple ethnicities.* Kidney Int, 2011. **79**(5): p. 555-62.
289. Okamura, K., et al., *Endocytosis of albumin by podocytes elicits an inflammatory response and induces apoptotic cell death.* PLoS One, 2013. **8**(1): p. e54817.
290. Cybulsky, A.V., *Endoplasmic reticulum stress in proteinuric kidney disease.* Kidney Int, 2010. **77**(3): p. 187-93.
291. Zhao, J., A. Tramontano, and S.P. Makker, *Albumin-stimulated TGFbeta-1 in renal tubular cells is associated with activation of MAP kinase.* Int Urol Nephrol, 2007. **39**(4): p. 1265-71.
292. Davies, D.J., et al., *Glomerular podocytic injury in protein overload proteinuria.* Pathology, 1985. **17**(3): p. 412-9.
293. Yoshida, S., et al., *Podocyte injury induced by albumin overload in vivo and in vitro: involvement of TGF-beta and p38 MAPK.* Nephron Exp Nephrol, 2008. **108**(3): p. e57-68.
294. Agrawal, S., et al., *Albumin-induced podocyte injury and protection are associated with regulation of COX-2.* Kidney Int, 2014. **86**(6): p. 1150-60.
295. Morigi, M., et al., *In response to protein load podocytes reorganize cytoskeleton and modulate endothelin-1 gene: implication for permselective dysfunction of chronic nephropathies.* Am J Pathol, 2005. **166**(5): p. 1309-20.
296. Jarad, G., et al., *Albumin contributes to kidney disease progression in Alport syndrome.* Am J Physiol Renal Physiol, 2016. **311**(1): p. F120-30.
297. van den Berg, J.G., et al., *Podocyte foot process effacement is not correlated with the level of proteinuria in human glomerulopathies.* Kidney Int, 2004. **66**(5): p. 1901-6.
298. Reiser, J., et al., *Induction of B7-1 in podocytes is associated with nephrotic syndrome.* J Clin Invest, 2004. **113**(10): p. 1390-7.
299. Yu, C.C., et al., *Abatacept in B7-1-positive proteinuric kidney disease.* N Engl J Med, 2013. **369**(25): p. 2416-23.

300. Vogtlander, N.P., et al., *Ligation of alpha-dystroglycan on podocytes induces intracellular signaling: a new mechanism for podocyte effacement?* PLoS One, 2009. **4**(6): p. e5979.
301. Raats, C.J., et al., *Expression of agrin, dystroglycan, and utrophin in normal renal tissue and in experimental glomerulopathies.* Am J Pathol, 2000. **156**(5): p. 1749-65.
302. Meinen, S., et al., *Linker molecules between laminins and dystroglycan ameliorate laminin-alpha2-deficient muscular dystrophy at all disease stages.* J Cell Biol, 2007. **176**(7): p. 979-93.
303. Yurchenco, P.D., *Integrating Activities of Laminins that Drive Basement Membrane Assembly and Function.* Curr Top Membr, 2015. **76**: p. 1-30.
304. Zhao, X., et al., *alpha-Actinin 4 potentiates nuclear factor kappa-light-chain-enhancer of activated B-cell (NF-kappaB) activity in podocytes independent of its cytoplasmic actin binding function.* J Biol Chem, 2015. **290**(1): p. 338-49.
305. Saleem, M.A., et al., *A conditionally immortalized human podocyte cell line demonstrating nephrin and podocin expression.* J Am Soc Nephrol, 2002. **13**(3): p. 630-8.
306. Mundel, P., et al., *Rearrangements of the cytoskeleton and cell contacts induce process formation during differentiation of conditionally immortalized mouse podocyte cell lines.* Exp Cell Res, 1997. **236**(1): p. 248-58.
307. Chung, A.E., et al., *Morphological and biochemical observations on cells derived from the in vitro differentiation of the embryonal carcinoma cell line PCC4-F.* Cancer Res, 1977. **37**(7 Pt 1): p. 2072-81.
308. McCall, A.S., et al., *Bromine is an essential trace element for assembly of collagen IV scaffolds in tissue development and architecture.* Cell, 2014. **157**(6): p. 1380-92.
309. Anazco, C., et al., *Lysyl Oxidase-like-2 Cross-links Collagen IV of Glomerular Basement Membrane.* J Biol Chem, 2016. **291**(50): p. 25999-26012.
310. Orlando, G., et al., *Discarded human kidneys as a source of ECM scaffold for kidney regeneration technologies.* Biomaterials, 2013. **34**(24): p. 5915-25.
311. Petrosyan, A., et al., *Decellularized Renal Matrix and Regenerative Medicine of the Kidney: A Different Point of View.* Tissue Eng Part B Rev, 2016. **22**(3): p. 183-92.
312. Petrosyan, A., et al., *A step towards clinical application of acellular matrix: A clue from macrophage polarization.* Matrix Biol, 2017. **57-58**: p. 334-346.
313. Peloso, A., et al., *Renal Extracellular Matrix Scaffolds From Discarded Kidneys Maintain Glomerular Morphometry and Vascular Resilience and Retains Critical Growth Factors.* Transplantation, 2015. **99**(9): p. 1807-16.
314. Morello, J.P., et al., *Pharmacological chaperones rescue cell-surface expression and function of misfolded V2 vasopressin receptor mutants.* J Clin Invest, 2000. **105**(7): p. 887-95.
315. Fan, J.Q., et al., *Accelerated transport and maturation of lysosomal alpha-galactosidase A in Fabry lymphoblasts by an enzyme inhibitor.* Nat Med, 1999. **5**(1): p. 112-5.
316. Powell, K. and P.L. Zeitlin, *Therapeutic approaches to repair defects in deltaF508 CFTR folding and cellular targeting.* Adv Drug Deliv Rev, 2002. **54**(11): p. 1395-408.
317. Gao, X., et al., *The nephroprotective effect of tauroursodeoxycholic acid on ischaemia/reperfusion-induced acute kidney injury by inhibiting endoplasmic reticulum stress.* Basic Clin Pharmacol Toxicol, 2012. **111**(1): p. 14-23.
318. Hsu, P.D., E.S. Lander, and F. Zhang, *Development and applications of CRISPR-Cas9 for genome engineering.* Cell, 2014. **157**(6): p. 1262-78.
319. Kim, H. and J.S. Kim, *A guide to genome engineering with programmable nucleases.* Nat Rev Genet, 2014. **15**(5): p. 321-34.
320. Inui, M., et al., *Rapid generation of mouse models with defined point mutations by the CRISPR/Cas9 system.* Sci Rep, 2014. **4**: p. 5396.
321. Williams, A., J. Henao-Mejia, and R.A. Flavell, *Editing the Mouse Genome Using the CRISPR-Cas9 System.* Cold Spring Harb Protoc, 2016. **2016**(2): p. pdb top087536.

CHAPTER 8

Appendix

8. Appendix

8.1 Antibody List

8.1.1 Primary Antibodies

Antibody specificity	Antibody description	Supplier/Source	Work dilution
6X His	Rabbit polyclonal, TA150031	Origene	1:1000 (WB)
Cdc42	Rabbit monoclonal, ab187643	Abcam	1:1000 (WB)
ILK	Rabbin monoclonal, ab52480	Abcam	1:1000 (WB)
Intergin β1	Rabbit monoclonal, ab179471	Abcam	1:1000 (WB)
Intergin β1, active	Rat monoclonal, 9EG7	BD Pharmingen	1:100 (WB)
Intergin β3, active	Mouse monoclonal, WOW-1	Prof S. Shattil	No dilution (IF)
Intergin β3, active	Mouse monoclonal, AP5	Dr P. Newman	1:500 (IF)
Laminin α5	Rabbit polyclonal, clone 1586	Prof J. Miner	1:200 (IF)
Laminin β1	Rabbit polyclonal, clone 1065	Prof J. Miner	1:200 (IF)
Laminin β2	Rabbit polyclonal, clone 1117	Prof J. Miner	1:200 (IF)
Nephrin	Rabbit polyclonal, ab58968	Abcam	1:1000 (WB)
Pan-Collagen type 4	Rabbit polyclonal, ab6586	Abcam	1:1000 (WB)
Paxillin	Rabbit monoclonal, ab32084	Abcam	1:2000 (WB)
Podocin	Rabbit monoclonal, ab50339	Abcam	1:500 (IF)
RhoA	Rabbit monoclonal, ab187027	Abcam	1:5000 (WB)
α-TUBULIN	Rabbit monoclonal, ab176560	Abcam	1:3000 (WB)
β-actin	Mouse monoclonal, ab8226	Abcam	1:3000 (WB)

WB: Western blot, IF: immunofluorescence.

8.1.2 Secondary Antibodies

Antibody specificity	Antibody description	Supplier/Source	Work dilution
Alexa fluor 488	Goat anti-rabbit IgG (H+L),	Invitrogen	1:1000 (IF)
Alexa fluor 568	Goat anti-mouse IgG (H+L),	Invitrogen	1:1000 (IF)
Alexa fluor 568	Goat anti-rabbit IgG (H+L),	Invitrogen	1:1000 (IF)
Anti Rabbit HRP	Goat anti-rabbit, W4011	Promega	1:5000 (WB)
IRDye® 680LT	Goat anti-mouse IgG (H+L), 926-68020	Li-Cor	1:15000 (WB)
IRDye® 680LT	Goat anti-rabbit IgG (H+L), 926-68021	Li-Cor	1:15000 (WB)
IRDye® 800LT	Goat anti-mouse IgG (H+L), 926-32211	Li-Cor	1:15000 (WB)
IRDye® 800LT	Goat anti-rabbit IgG (H+L), 926-32210	Li-Cor	1:15000 (WB)

WB: Western blot, IF: immunofluorescence.

8.2 Gene list

Gene Name	*Description*
Arfrp1	ADP-ribosylation factor related protein 1
Zgpat	zinc finger, CCCH-type with G patch domain
Lime1	Lck interacting transmembrane adaptor 1
Zbtb46	zinc finger and BTB domain containing 46
Abhd16b	abhydrolase domain containing 16B
Tpd52l2	tumor protein D52-like 2
Dnajc5	DnaJ (Hsp40) homolog, subfamily C, member 5
Uckl1	uridine-cytidine kinase 1-like 1
Znf512b	zinc finger protein 512B
Prpf6	PRP6 pre-mRNA splicing factor 6 homolog (yeast)
Bhlhe23	basic helix-loop-helix family, member e23
Ythdf1	YTH domain family 1
Birc7	baculoviral IAP repeat-containing 7 (livin)
Nkain4	Na+/K+ transporting ATPase interacting 4
Arfgap1	ADP-ribosylation factor GTPase activating protein 1
9230112E08Rik	RIKEN cDNA 9230112E08 gene
Col20a1	collagen, type XX, alpha 1
Chrna4	cholinergic receptor, nicotinic, alpha polypeptide 4
Kcnq2	potassium voltage-gated channel, subfamily Q, member 2
Eef1a2	eukaryotic translation elongation factor 1 alpha 2
Ppdpf	pancreatic progenitor cell differentiation and proliferation factor homolog (zebrafish)
Ptk6	PTK6 protein tyrosine kinase 6

Srms	src-related kinase lacking C-terminal regulatory tyrosine and N-terminal myristylation sites
BC051628	cDNA sequence BC051628
Helz2	helicase with zinc finger 2, transcriptional coactivator
Gmeb2	glucocorticoid modulatory element binding protein 2
Stmn3	stathmin-like 3
Rtel1	regulator of telomere elongation helicase 1
Adrm1	adhesion regulating molecule 1
Lama5	laminin, alpha 5
Rps21	ribosomal protein S21
Cables2	CDK5 and Abl enzyme substrate 2
Rbbp8nl	RBBP8 N-terminal like
Gata5	GATA binding protein 5
Slco4a1	solute carrier organic anion transporter family, member 4a1
Ntsr1	neurotensin receptor 1
Mrgbp	MRG/MORF4L binding protein
Ogfr	opioid growth factor receptor
Col9a3	collagen, type IX, alpha 3
Tcfl5	transcription factor-like 5 (basic helix-loop-helix)
Dido1	death inducer-obliterator 1
Gid8	GID complex subunit 8 homolog (S. cerevisiae)
Slc17a9	solute carrier family 17, member 9
Osbpl2	oxysterol binding protein-like 2
Hrh3	histamine receptor H3
Gtpbp5	GTP binding protein 5
Ss18l1	synovial sarcoma translocation gene on chromosome 18-like 1

Psma7	proteasome (prosome, macropain) subunit, alpha type 7
Lsm14b	LSM14 homolog B (SCD6, S. cerevisiae)
Taf4a	TAF4A RNA polymerase II, TATA box binding protein (TBP)-associated factor
Gm10711	predicted gene 10711
Gm14403	predicted gene 14403
Gm14406	predicted gene 14406
Gm14322	predicted gene 14322
Gm14325	predicted gene 14325
Gm14327	predicted gene 14327
C330013J21Rik	RIKEN cDNA C330013J21 gene
Gm14326	predicted gene 14326
Etohi1	ethanol induced 1
Zfp931	zinc finger protein 931
Phactr3	phosphatase and actin regulator 3
Sycp2	synaptonemal complex protein 2
Ppp1r3d	protein phosphatase 1, regulatory subunit 3D
Fam217b	family with sequence similarity 217, member B
Cdh26	cadherin-like 26
Cdh4	cadherin 4
Gm14420	predicted gene 14420
Gm14418	predicted gene 14418
Gm14412	predicted gene 14412
Gm14409	predicted gene 14409
Gm20721	predicted gene, 20721
Nelfcd	negative elongation factor complex member C/D, Th1l
Ctsz	cathepsin Z
Tubb1	tubulin, beta 1 class VI

Atp5e	ATP synthase, H+ transporting, mitochondrial F1 complex, epsilon subunit
Slmo2	slowmo homolog 2 (Drosophila)
Zfp831	zinc finger protein 831
Edn3	endothelin 3
Gm14444	predicted gene 14444
Gm14393	predicted gene 14393
Gm14399	predicted gene 14399
Gm14443	predicted gene 14443
Gm14391	predicted gene 14391
Gm14440	predicted gene 14440
Gm4631	predicted gene 4631
Gm4723	predicted gene 4723
Gm4724	predicted gene 4724
Gm8923	predicted gene 8923
Gm11007	predicted gene 11007
Gm4245	predicted gene 4245
Gm2007	predicted gene 2007
Gm14288	predicted gene 14288
Gm6710	predicted gene 6710
Gm8898	predicted gene 8898
Gm2026	predicted gene 2026
Gm2004	predicted gene 2004
2210418O10Rik	RIKEN cDNA 2210418O10 gene
Gm11009	predicted gene 11009
Gm14435	predicted gene 14435
Gm14434	predicted gene 14434
Gm14431	predicted gene 14431

Gm14308	predicted gene 14308
Gm14306	predicted gene 14306
Gm14305	predicted gene 14305
Gm14295	predicted gene 14295
Gm14408	predicted gene 14408
Gm14296	predicted gene 14296
Gm14419	predicted gene 14419
Gm14401	predicted gene 14401
Gm14410	predicted gene 14410
Cbln4	cerebellin 4 precursor protein
Mc3r	melanocortin 3 receptor
Fam210b	family with sequence similarity 210, member B
Aurka	aurora kinase A
Cstf1	cleavage stimulation factor, 3' pre-RNA, subunit 1
Cass4	Cas scaffolding protein family member 4
Rtfdc1	replication termination factor 2 domain containing 1
Gcnt7	glucosaminyl (N-acetyl) transferase family member 7
Fam209	family with sequence similarity 209
Tfap2c	transcription factor AP-2, gamma
Bmp7	bone morphogenetic protein 7
Spo11	SPO11 meiotic protein covalently bound to DSB homolog (S. cerevisiae)
Rae1	RAE1 RNA export 1 homolog (S. pombe)
Rbm38	RNA binding motif protein 38
Ctcfl	CCCTC-binding factor (zinc finger protein)-like
Pck1	phosphoenolpyruvate carboxykinase 1, cytosolic
Zbp1	Z-DNA binding protein 1
Pmepa1	prostate transmembrane protein, androgen induced 1

1700021F07Rik	RIKEN cDNA 1700021F07 gene
Ankrd60	ankyrin repeat domain 60
Rab22a	RAB22A, member RAS oncogene family
1700010B08Rik	RIKEN cDNA 1700010B08 gene
Vapb	vesicle-associated membrane protein, associated protein B and C
Stx16	syntaxin 16
Npepl1	aminopeptidase-like 1
Gnas	GNAS (guanine nucleotide binding protein, alpha stimulating) complex locus
Samd10	sterile alpha motif domain containing 10
Gm22502	predicted gene, 22502
Mir298	microRNA 298
Sox18	SRY-box containing gene 18
Mir124a-3	microRNA 124a-3
Tcea2	transcription elongation factor A (SII), 2
Gm25184	predicted gene, 25184
Mir1a-1	microRNA 1a-1
BX284639.1	
Gm25879	predicted gene, 25879
Gm22842	predicted gene, 22842
Rgs19	regulator of G-protein signaling 19
Mir133a-2	microRNA 133a-2
4930526D03Rik	RIKEN cDNA 4930526D03 gene
Oprl1	opioid receptor-like 1
Myt1	myelin transcription factor 1
Pcmtd2	protein-L-isoaspartate (D-aspartate) O-methyltransferase domain containing 2

Polr3k	polymerase (RNA) III (DNA directed) polypeptide K
Gm14496	predicted gene 14496
1700028P15Rik	RIKEN cDNA 1700028P15 gene
Gm14272	predicted gene 14272
Gm14641	predicted gene 14641
Gm14271	predicted gene 14271
Gm14274	predicted gene 14274
Gm14275	predicted gene 14275
Gm14273	predicted gene 14273
Gm14455	predicted gene 14455
Gm14303	predicted gene 14303
Gm20490	predicted gene 20490
Gm14453	predicted gene 14453
1300015D01Rik	RIKEN cDNA 1300015D01 gene
Gm14454	predicted gene 14454
Gm14642	predicted gene 14642
Ppp4r1l-ps	protein phosphatase 4, regulatory subunit 1-like, pseudogene
Gm14371	predicted gene 14371
Gm14336	predicted gene 14336
Gm14337	predicted gene 14337
Vamp7-ps	vesicle-associated membrane protein 7, pseudogene
Gm10714	predicted gene 10714
Nespas	neuroendocrine secretory protein antisense
Rpl30-ps5	ribosomal protein L30, pseudogene 5
Gm14385	predicted gene 14385
Vmn1r-ps1	vomeronasal 1 receptor, pseudogene 1
Gm14617	predicted gene 14617

Gm14618	predicted gene 14618
Gm14616	predicted gene 14616
Gm16354	predicted gene 16354
Gm14445	predicted gene 14445
Gm14439	predicted gene 14439
Gm14387	predicted gene 14387
Gm14392	predicted gene 14392
Gm16355	predicted gene 16355
Gm14442	predicted gene 14442
Gm14438	predicted gene 14438
Gm14298	predicted gene 14298
Gm14297	predicted gene 14297
Gm16359	predicted gene 16359
Gm16358	predicted gene 16358
Rps8-ps2	ribosomal protein S8, pseudogene 2
Gm2020	predicted gene 2020
Gm16356	predicted gene 16356
Gm11008	predicted gene 11008
Gm16357	predicted gene 16357
Gm6182	predicted gene 6182
Gm17258	predicted gene, 17258
Gm1980	predicted gene 1980
Gm16362	predicted gene 16362
Gm14307	predicted gene 14307
Gm14301	predicted gene 14301
Gm14390	predicted gene 14390
Gm14405	predicted gene 14405
Gm14296	predicted gene 14296

Gm14417	predicted gene 14417
Gm14402	predicted gene 14402
Gm14421	predicted gene 14421
Gm14407	predicted gene 14407
Gm14415	predicted gene 14415
Gm14411	predicted gene 14411
Gm14416	predicted gene 14416
Gm14413	predicted gene 14413
Gm14400	predicted gene 14400
Gm14404	predicted gene 14404
Gm14414	predicted gene 14414
Gm16363	predicted gene 16363
Gm14324	predicted gene 14324
Gm14429	predicted gene 14429
Gm14323	predicted gene 14323
Gm14428	predicted gene 14428
Gm14314	predicted gene 14314
Gm14292	predicted gene 14292
Gm14293	predicted gene 14293
Gm14294	predicted gene 14294
4930591A17Rik	RIKEN cDNA 4930591A17 gene
Gm14300	predicted gene 14300
4921531C22Rik	RIKEN cDNA 4921531C22 gene
Gm14299	predicted gene 14299
Gm17180	predicted gene 17180
Gm14318	predicted gene 14318
B230312C02Rik	RIKEN cDNA B230312C02 gene
Gm14343	predicted gene 14343

Gm14340	predicted gene 14340
Gm14342	predicted gene 14342
Gm14344	predicted gene 14344
Gm14339	predicted gene 14339
RP23-359C15.10	
Gm14341	predicted gene 14341
Gm14398	predicted gene 14398
Gm7645	predicted gene 7645
Slc2a4rg-ps	Slc2a4 regulator, pseudogene
Gm16119	predicted gene 16119
Gm14489	predicted gene 14489
Gm5466	predicted gene 5466
Gm22773	predicted gene, 22773
Gm24892	predicted gene, 24892
Mir3091	microRNA 3091
Mir296	microRNA 296
Gm22708	predicted gene, 22708
Gm22071	predicted gene, 22071

8.2 Gene homology

8.2.1 Laminin β1 chain alignment

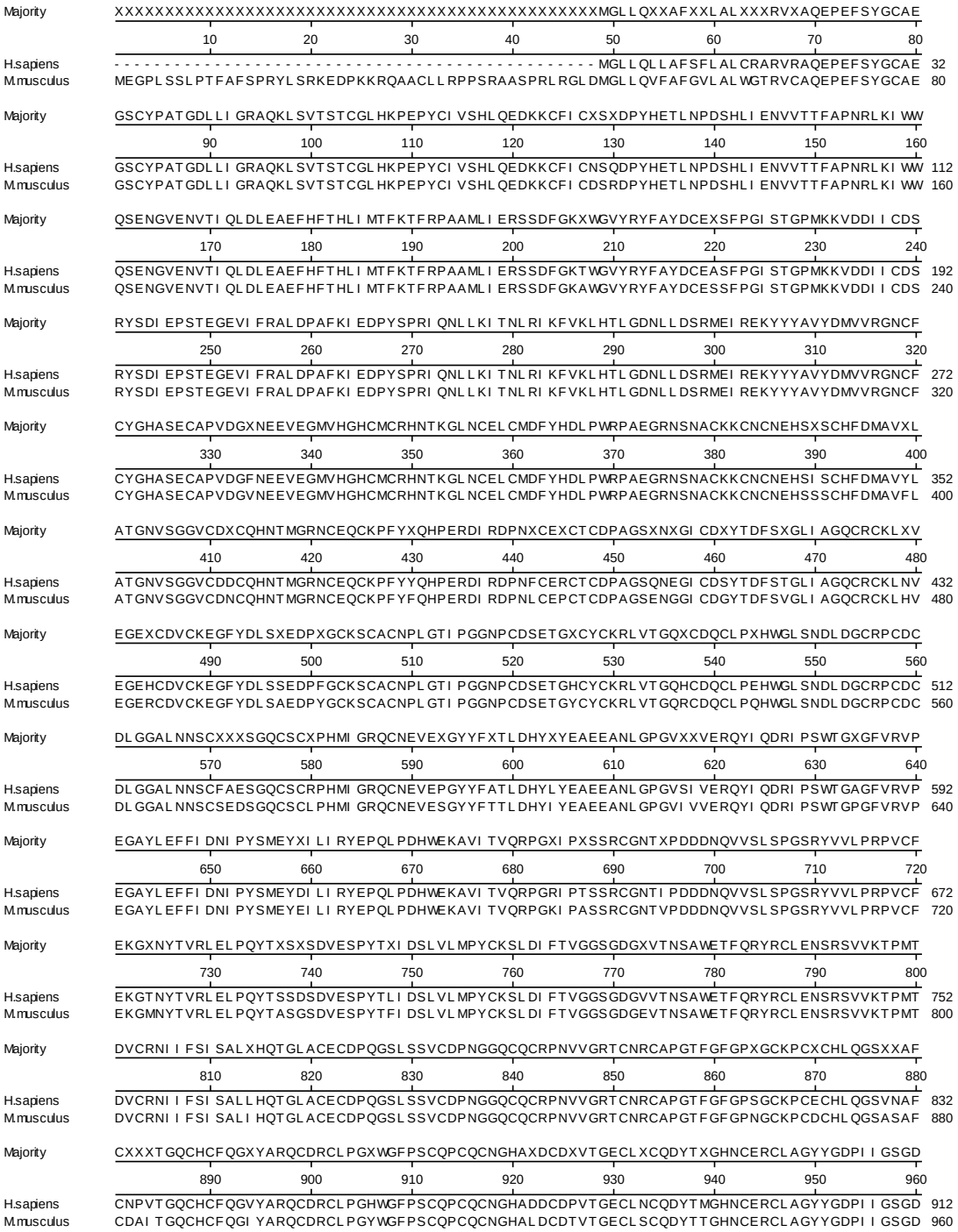

8.2.2 Laminin γ1 chain alignment

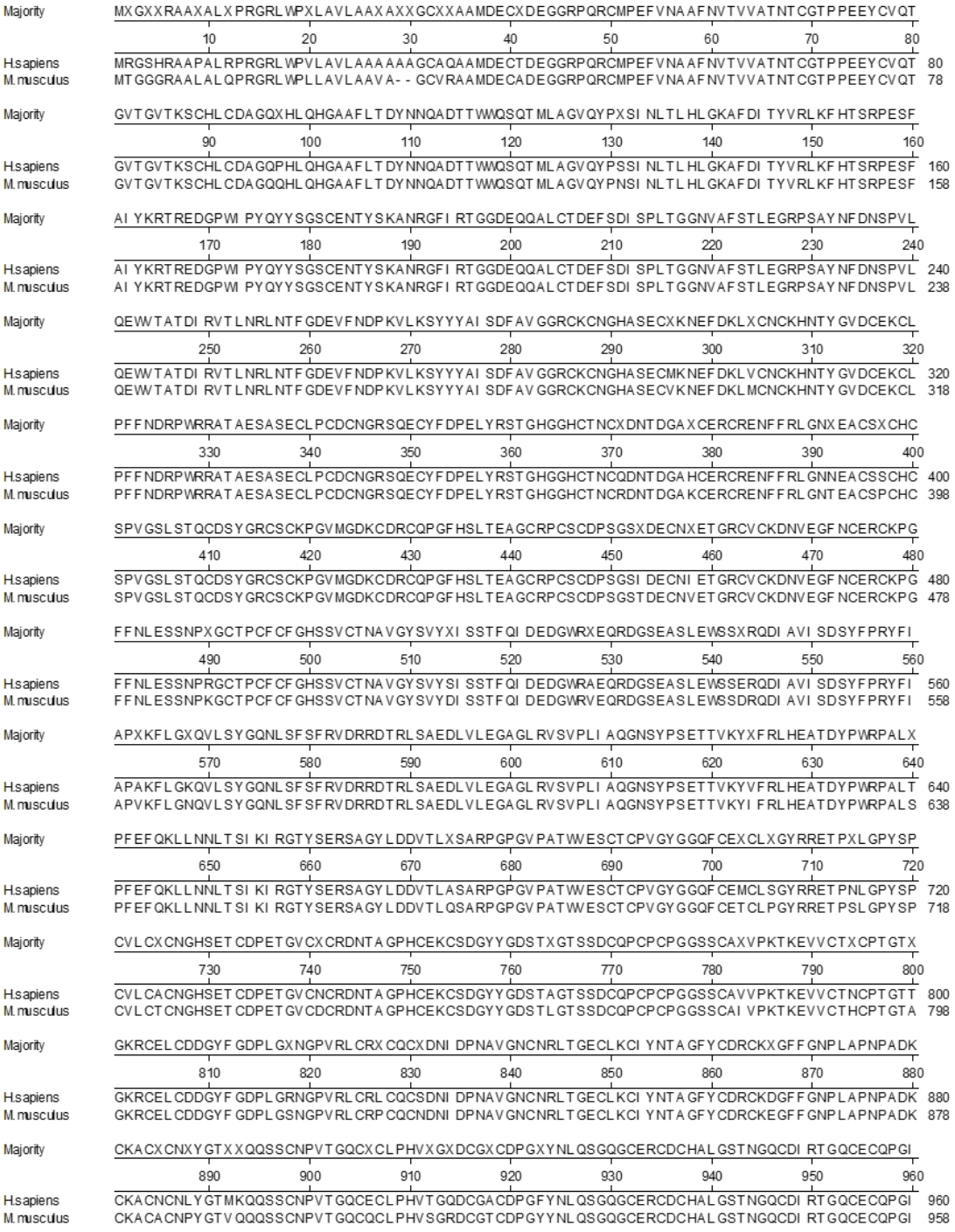

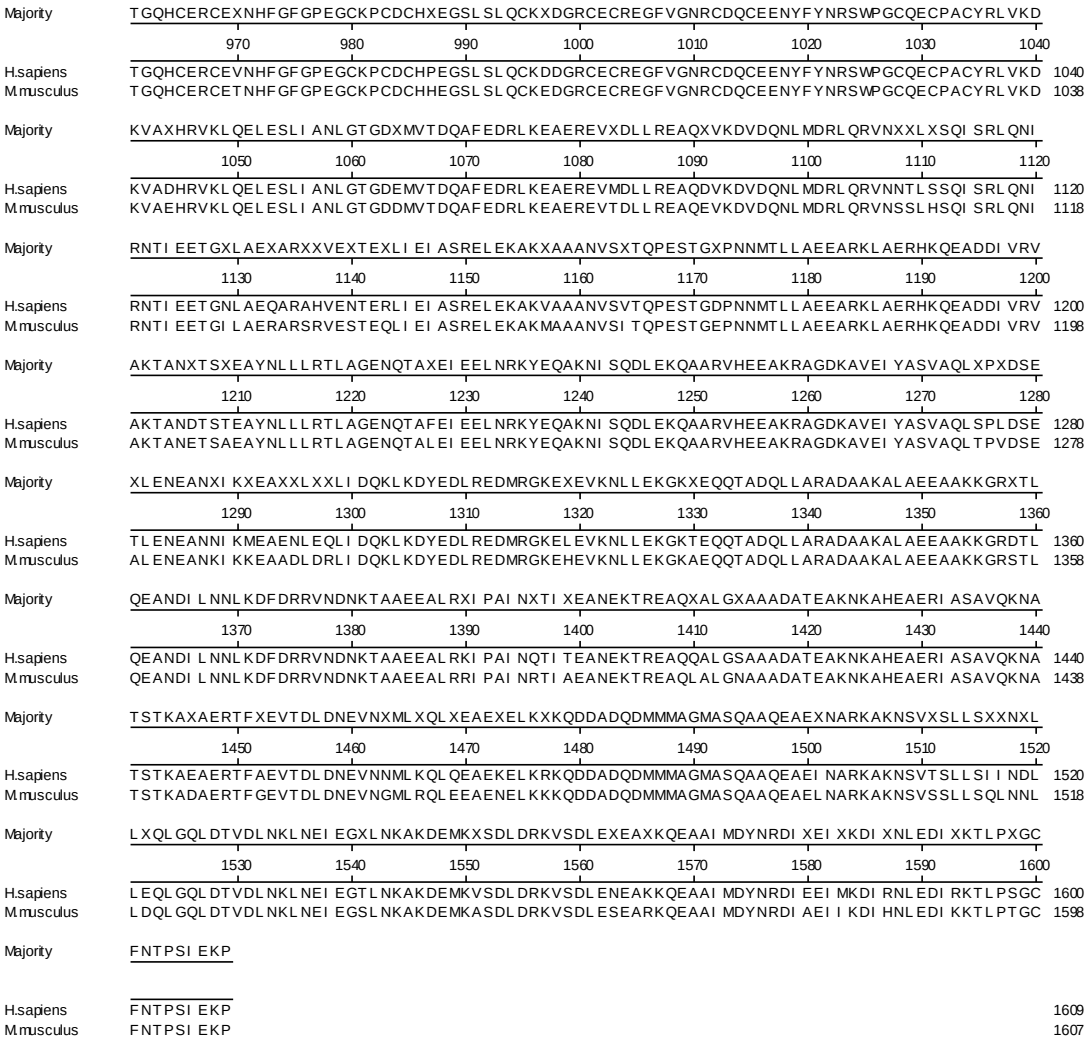
Majority TGQHCERCEXNHFGFGPEGCKPCDCHXEGSLSLQCKXDGRCECREGFVGNRCDQCEENYFYNRSWPGCQECPACYRLVKD
970 980 990 1000 1010 1020 1030 1040
H.sapiens TGQHCERCEVNHFGFGPEGCKPCDCHPEGSLSLQCKDDGRCECREGFVGNRCDQCEENYFYNRSWPGCQECPACYRLVKD 1040
M.musculus TGQHCERCETNHFGFGPEGCKPCDCHHEGSLSLQCKEDGRCECREGFVGNRCDQCEENYFYNRSWPGCQECPACYRLVKD 1038
Majority KVAXHRVKLQELESLIANLGTGDXMVTDQAFEDRLKEAEREVXDLLREAQXVKDVDQNLMDRLQRVNXXLXSQISRLQNI
1050 1060 1070 1080 1090 1100 1110 1120
H.sapiens KVADHRVKLQELESLIANLGTGDEMVTDQAFEDRLKEAEREVMDLLREAQDVKDVDQNLMDRLQRVNNTLSSQISRLQNI 1120
M.musculus KVAEHRVKLQELESLIANLGTGDDMVTDQAFEDRLKEAEREVTDLLREAQEVKDVDQNLMDRLQRVNSSLHSQISRLQNI 1118
Majority RNTIEETGXLAEXARXXVEXTEXLIEIASRELEKAKXAAANVSXTQPESTGXPNNMTLLAEEARKLAERHKQEADDIVRV
1130 1140 1150 1160 1170 1180 1190 1200
H.sapiens RNTIEETGNLAEQARAHVENTERLIEIASRELEKAKVAAANVSVTQPESTGDPNNMTLLAEEARKLAERHKQEADDIVRV 1200
M.musculus RNTIEETGILAERARSRVESTEQLIEIASRELEKAKMAAANVSITQPESTGEPNNMTLLAEEARKLAERHKQEADDIVRV 1198
Majority AKTANXTSXEAYNLLLRTLAGENQTAXEIEELNRKYEQAKNISQDLEKQAARVHEEAKRAGDKAVEIYASVAQLXPXDSE
1210 1220 1230 1240 1250 1260 1270 1280
H.sapiens AKTANDTSTEAYNLLLRTLAGENQTAFEIEELNRKYEQAKNISQDLEKQAARVHEEAKRAGDKAVEIYASVAQLSPLDSE 1280
M.musculus AKTANETSAEAYNLLLRTLAGENQTALEIEELNRKYEQAKNISQDLEKQAARVHEEAKRAGDKAVEIYASVAQLTPVDSE 1278
Majority XLENEANXIKXEAXXLXXLIDQKLKDYEDLREDMRGKEXEVKNLLEKGKXEQQTADQLLARADAAKALAEEAAKKGRXTL
1290 1300 1310 1320 1330 1340 1350 1360
H.sapiens TLENEANNIKMEAENLEQLIDQKLKDYEDLREDMRGKELEVKNLLEKGKTEQQTADQLLARADAAKALAEEAAKKGRDTL 1360
M.musculus ALENEANKIKKEAADLDRLIDQKLKDYEDLREDMRGKEHEVKNLLEKGKAEQQTADQLLARADAAKALAEEAAKKGRSTL 1358
Majority QEANDILNNLKDFDRRVNDNKTAAEEALRXIPAINXTIXEANEKTREAQXALGXAAADATEAKNKAHEAERIASAVQKNA
1370 1380 1390 1400 1410 1420 1430 1440
H.sapiens QEANDILNNLKDFDRRVNDNKTAAEEALRKIPAINQTITEANEKTREAQQALGSAAADATEAKNKAHEAERIASAVQKNA 1440
M.musculus QEANDILNNLKDFDRRVNDNKTAAEEALRRIPAINRTIAEANEKTREAQLALGNAAADATEAKNKAHEAERIASAVQKNA 1438
Majority TSTKAXAERTFXEVTDLDNEVNXMLXQLXEAEXELKXKQDDADQDMMMAGMASQAAQEAEXNARKAKNSVXSLLSXXNXL
1450 1460 1470 1480 1490 1500 1510 1520
H.sapiens TSTKAEAERTFAEVTDLDNEVNNMLKQLQEAEKELKRKQDDADQDMMMAGMASQAAQEAEINARKAKNSVTSLLSIINDL 1520
M.musculus TSTKADAERTFGEVTDLDNEVNGMLRQLEEAENELKKKQDDADQDMMMAGMASQAAQEAELNARKAKNSVSSLLSQLNNL 1518
Majority LXQLGQLDTVDLNKLNEIEGXLNKAKDEMKXSDLDRKVSDLEXEAXKQEAAIMDYNRDIXEIXKDIXNLEDIXKTLPXGC
1530 1540 1550 1560 1570 1580 1590 1600
H.sapiens LEQLGQLDTVDLNKLNEIEGTLNKAKDEMKVSDLDRKVSDLENEAKKQEAAIMDYNRDIEEIMKDIRNLEDIRKTLPSGC 1600
M.musculus LDQLGQLDTVDLNKLNEIEGSLNKAKDEMKASDLDRKVSDLESEARKQEAAIMDYNRDIAEIIKDIHNLEDIKKTLPTGC 1598
Majority FNTPSIEKP
H.sapiens FNTPSIEKP 1609
M.musculus FNTPSIEKP 1607